LEABHARLANN CHOLÁISTE NA TRÍONÓIDE, BAILE ÁTHA CLIATH | TRINITY COLLEGE LIBRARY DUBLIN
Ollscoil Átha Cliath | The University of Dublin

Terms and Conditions of Use of Digitised Theses from Trinity College Library Dublin

Copyright statement

All material supplied by Trinity College Library is protected by copyright (under the Copyright and Related Rights Act, 2000 as amended) and other relevant Intellectual Property Rights. By accessing and using a Digitised Thesis from Trinity College Library you acknowledge that all Intellectual Property Rights in any Works supplied are the sole and exclusive property of the copyright and/or other IPR holder. Specific copyright holders may not be explicitly identified. Use of materials from other sources within a thesis should not be construed as a claim over them.

A non-exclusive, non-transferable licence is hereby granted to those using or reproducing, in whole or in part, the material for valid purposes, providing the copyright owners are acknowledged using the normal conventions. Where specific permission to use material is required, this is identified and such permission must be sought from the copyright holder or agency cited.

Liability statement

By using a Digitised Thesis, I accept that Trinity College Dublin bears no legal responsibility for the accuracy, legality or comprehensiveness of materials contained within the thesis, and that Trinity College Dublin accepts no liability for indirect, consequential, or incidental, damages or losses arising from use of the thesis for whatever reason. Information located in a thesis may be subject to specific use constraints, details of which may not be explicitly described. It is the responsibility of potential and actual users to be aware of such constraints and to abide by them. By making use of material from a digitised thesis, you accept these copyright and disclaimer provisions. Where it is brought to the attention of Trinity College Library that there may be a breach of copyright or other restraint, it is the policy to withdraw or take down access to a thesis while the issue is being resolved.

Access Agreement

By using a Digitised Thesis from Trinity College Library you are bound by the following Terms & Conditions. Please read them carefully.

I have read and I understand the following statement: All material supplied via a Digitised Thesis from Trinity College Library is protected by copyright and other intellectual property rights, and duplication or sale of all or part of any of a thesis is not permitted, except that material may be duplicated by you for your research use or for educational purposes in electronic or print form providing the copyright owners are acknowledged using the normal conventions. You must obtain permission for any other use. Electronic or print copies may not be offered, whether for sale or otherwise to anyone. This copy has been supplied on the understanding that it is copyright material and that no quotation from the thesis may be published without proper acknowledgement.

Simulation of tissue differentiation during fracture healing

Damien Lacroix, Dipl. Ing., M.Sc.

A thesis submitted to the University of Dublin in partial fulfilment of the requirements for the degree of

Doctor in Philosophy

Department of Mechanical Engineering
Trinity College
Ireland

December 2000

Dr. P.J. Prendergast
Supervisor

Prof. dr. ir. R. Huiskes
External examiner

Prof. T.C. Lee
Internal examiner

TRINITY COLLEGE
06 JUN 2001
LIBRARY DUBLIN
Thesis
6191

A grand and almost untrodden field of inquiry will be opened, on the causes and laws of variation, on correlation of growth, on the effects of use and disuse, on the direct action of external conditions, and so forth.

Charles Darwin, *On the Origin of Species*, 1859

Declaration

I declare that I am the sole author of this thesis and that all the work presented in it, unless otherwise referenced, is my own. I also declare that this work has not been submitted, in whole or in part, to any other university or college for any degree or other qualification.

I authorise the library of the University of Dublin to lend this thesis.

Damien Lacroix

December 7, 2000

Acknowledgements

I am indebted to many people for their assistance throughout this thesis. Most particularly, I would like to thank Dr. Patrick Prendergast for his guidance throughout the thesis, his trust and encouragement during my years spent in Ireland, and for sharing his views on scientific objectives, ideas, and directions. Patrick has opened my mind to strive towards new ideas and developments in bioengineering and science. I am therefore very grateful to him.

I would like to thank Dr. Eamon Cahill and Dr. Martyn Field from Hitachi Europe Ltd. for their interest and support during this project. I am grateful to Martyn for his work on the development of a poroelastic code.

As in many cases, bioengineering is an interaction between engineers and practicians. I am thankful to Prof. David Marsh and Dr. Gang Li from Musgrave Park Hospital in Belfast, whose discussions on the biological processes during fracture healing have been very helpful.

Many thanks to Prof. Marjolein van der Meulen and Alicia Bailón-Plaza from Cornell University, NY, for accomodating me in their 'Ivy Buildings'. Their advice and experimentalist views are gratefully acknowledged.

Thanks to Willem van Driel from TNO for his help in DIANA and Dr. Alun Carr from University College Dublin for his help with LaTeX.

Much of my enjoyable stay in Ireland was due to the great atmosphere in the department. I would like to thank most particularly Alex, Bruce, Linda, Suzanne, John, Danny, Adriele, Framü, Mag, Seosamh and Richard for all the good laughs we had together and for making things easier when times were hard. From the department, I want to thank all the staff, technicians and

secretaries for their discussion and assistance through various times during this Ph.D. Prof. John Monaghan, head of the department, is thanked for his support during the 'French rebellion'.

Finally, my thanks go to those closest to me; my parents, Maud, and Laura without whose continual support, this thesis would never have been.

I acknowledge the funding of Hitachi Europe Ltd., The Trinity High Performance Computing Center, The Health Research Board, The Wellcome Trust, and The Trinity Trust.

Publications and presentations resulting from this study

D. Lacroix, P.J. Prendergast, D. Marsh, and G. Li. *'Royal Academy of Medicine in Ireland Bronze Medal'* A 3D finite element model of a tibia to simulate the regenerative and resorption phases during fracture healing. In *Proc. 12th Europ. Soc. Biomech.*, Dublin, Ireland, page 60, 2000 [Presented August 29, 2000, Dublin, Ireland].

D. Lacroix and P.J. Prendergast. Mechanotransduction during fracture healing: the effect of cell proliferation. In *Mechanotransduction 2000 - Materiaux et structures des sciences de l'ingénieur et du vivant.* Ed. GAMAC, France, pp. 39–46, 2000 [Presented May 17, 2000, Champs sur Marne, France].

D. Lacroix, P.J. Prendergast, D. Marsh, and G. Li. A model to simulate the regenerative and resorption phases of a long bone fracture healing. In *Trans. 46th Orthop. Res. Soc.*, Orlando, Fl., page 869, 2000 [Presented March 12, 2000, Orlando, Florida].

D. Lacroix and P.J. Prendergast. A homogenization procedure to prevent numerical instabilities in poroelastic tissue differentiation models. In *Proc. 8th Symp. Comput. Meth. Orthop. Biomech.*, Orlando, Fl., 2000 [Presented March 11, 2000, Orlando, Florida].

P.J. Prendergast and D. Lacroix. Mechanical regulation of fracture healing investigated using computer simulation: influence of loading and geometry.

Int. Symp. on Musculo-Skeletal Loading and its Implication for Clinical Practice, Berlin, Germany, 2000 [Presented February 11, 2000, Berlin, Germany].

D. Lacroix and P.J. Prendergast. Prediction of tissue differentiation during fracture healing – influence of mechanical loading. In *Proc. Am. Soc. Biomech.*, Pittsburgh, PA, page 276, 1999 [Presented October 23, 1999, Pittsburgh, Pennsylvania].

D. Lacroix and P.J. Prendergast. The influence of stem cell origin on fracture healing – a finite element analysis. *Ir. J. Med. Sci.,* 168:S4,5, 1999 [Presented June, 26, 1999, Limerick, Ireland].

D. Lacroix and P.J. Prendergast. Computational models of tissue differentiation – prediction of changes in mechanical stimuli (fluid flow and tissue microstrain) during cyclic loading. In *Trans. 9th Europ. Orthop. Res. Soc.*, Brussels, Belgium, 1999 [Presented June, 4, 1999, Brussels, Belgium].

D. Lacroix and P.J. Prendergast. Computer modelling of mechanical stimuli and cell migration in a fracture callus. *Ir. J. Med. Sci.,* 168:217, 1999 [Presented January 31, 1999, Blessington, Ireland].

Contents

Abstract

Fracture healing is a complex biological process during which, repair of the damaged tissues occurs so efficiently that the initial strength and anatomy of the bone are restored. Mechanical loading is believed to greatly influence the extent to which repair is accelerated or delayed.

An iterative algorithm based on a mechano-regulation concept was developed to simulate tissue differentiation during fracture healing. It is based on the calculation of two mechanical stimuli, octahedral shear strain and fluid flow, using a poroelastic finite element model. Proliferation of progenitor cells was accounted for. Depending on cell concentration and on predicted mechanical stimuli, cell differentiation was simulated for various fracture healing cases. Cell origin, load magnitude, fracture gap size, bending load, fracture type and a realistic 3D model were investigated.

The main phases observed during fracture healing were predicted. Fracture gap size and loading had a large influence on the healing patterns and mechanical stimuli. A bending load increased the amount of displacement and thereby delayed fracture healing. An oblique fracture was predicted to increase tissue shearing. A 3D fracture model showed the non-symmetric distribution of mechanical stimuli within the callus.

The model has successfully simulated tissue differentiation during fracture healing for various clinical cases. The stability of the algorithm and the use of fixed input parameters throughout the study, indicate that this concept may be applied to other problems in mechano-biology.

List of Figures

List of Tables

Nomenclature

Roman letters

c	Cell proliferation rate (m^2/s)
D	Hydrostatic stress (N/m^2)
E	Young's modulus (N/m^2)
e	Dilatational strain
I	Osteogenic index (N/m^2)
J	Deformation gradient
K	Compression modulus (N/m^2)
k	Fluid permeability (m^4/Ns)
n	Porosity (fluid volume fraction)
n_R	Porosity in the reference configuration
p	Fluid pore pressure (N/m^2)
Q	Biot material parameter (N/m^2)
S	Octahedral shear stress (N/m^2)
s	Specific matrix surface (m)
t	Time (s)

v Fluid flow (m/s)

Greek letters

Δ Increment in time

γ Octahedral shear strain

λ, μ Lamé constants (m^4/Ns)

ν Kinematic viscosity (m^2)

ρ Density (kg/m^3)

ρ_{cell} Cell density ($cell/m^2$)

ρ_{max} Maximum cell density ($cell/m^2$)

σ_i Principal stress (N/m^2)

τ Fluid shear stress (N/m^2)

Matrices (bold faced)

$\mathbf{I}$ Identity matrix

$\mathbf{k}$ Permeability tensor

$\mathbf{u}$ Displacement tensor

$\dot{\mathbf{u}}$ Velocity tensor

$\ddot{\mathbf{u}}$ Acceleration tensor

$\boldsymbol{\sigma}$ Total stress tensor

$\boldsymbol{\sigma}'$ Solid phase stress tensor

$\boldsymbol{\varepsilon}$ Strain tensor

∇ Gradient operator

Subscripts

f	fluid
s	solid

Chapter 1

Introduction

Contents

1.1 General introduction

Aristotle [1] wrote that "large animals need stronger and bigger and harder supports, especially those of them that are particularly violent in their habits". This shows that even in ancient times, the relationships between body size and activity level were appreciated. However, the correlation between mechanical loading and tissue architecture was only shown much later. Wolff suggested that the trabecular architecture of the femur corresponds to the stress trajectories [2]. The directions in which the trabeculae arrange depend mainly on the direction and magnitude of the applied loading. The geometrical disposition is obtained through a process of adaptation first understood by Roux [3]. Roux considered bone adaptation to be the result of a quantitative self-regulating mechanism for which a 'maximum-minimum design' principle is sought. Bones have different sizes and internal architecture to maximize efficiency and minimize the amount of tissue needed.

This process of mechanical adaptation is not only observed in bones but also in other tissues. Again, Aristotle [1] noted that cartilage acts as a pad to prevent the bones from rubbing against each other. Cartilage is found instead of bone where it is most advantageous; it is found in joints to improve motion, but also to better resist compression [4]. The evidence of cartilage at joints indicates that the initial mechanical stimuli play an important role in tissue differentiation during embryogenesis.

The body is therefore a biomechanical structure that is adapted, and continues to adapt, throughout life to external mechanical conditions. The external loading induces architectural and tissue phenotype changes due to a response of the cells. The macroscopic loading is transferred at a microscopic level through a sensing mechanism. In bone, it is believed that the osteocytes lying inside the extracellular matrix are the communicating agents. Local mechanical stimuli have a direct effect on the stimulation of cells and therefore on the tissue phenotype [4]. The advance of experimental methods has en-

abled the study of specific mechanical stimuli on cell cultures for investigation of how cell response to mechanical stimuli operates. Even though the precise mechanism of mechano-transduction has not yet been found, it is evident that the local mechanical stimuli transferred from the external loading influences the cell lineage of tissue differentiation [5].

1.2 Computer simulations in biomechanics

Knowing the mechanical stimuli regulating tissue differentiation is fundamental to many areas in biology. However, the potential of experimental science to answer questions about mechano-regulation has been limited by the complexity of cell behaviour and the multitude of biochemical factors governing cell/matrix interation. The full extent of biophysical stimuli has not been measured or calculated.

An alternative approach to the classical methods of scientific investigation (*i.e.* experimental and theoretical) is the 'third culture' [6]. It originates in the fast development of technology, especially in the advance of computational power. It creates tools that can explore domains, which were thought to be impossible to solve. The finite element (FE) technique is one of the key tool in the 'third culture' [7, 8]. It provides the capability for analysis of any structure knowing the geometry, loading, material properties and stress-strain law. However, due to computer limitations and incomplete information on loading and tissue properties, simplified assumptions must often be made. By applying an external load to a bone, for example, and by assuming bone as a solid linear elastic material, it is possible to relate strain at a cellular level to whole bone loading [9]. Moreover, the physical structure and behaviour of soft tissues (made of solid collagen matrix and interstitial fluid) can be modelled using commercial software [10, 11].

The approach taken by scientists usually requires the union of both experimental and theoretical methods by using the theory to understand the

experimental data, or the data to demonstrate the theory. The 'third culture' does not rely on either of these, but rather on dynamic computer simulation used in an exploratory way to establish an understanding of the problem. Such computer models have been developed in biomechanics. For example, it was used to predict bone remodelling [12], and to analyse implant designs [13].

1.3 Mechano-regulation during fracture healing

The importance of mechanical loading on fracture healing has been widely reported experimentally [14, 15, 16] and clinically [17, 18, 19]. Insufficient mechanical stimulation delays the initial stage of healing whereas excessive movement inhibits ossification and leads to a lack of stability.

Complex biological processes of tissue differentiation occur during fracture healing. The progenitor cells initially present in the fractured tissue can differentiate into fibroblast, chondrocyte or osteoblast cells leading respectively to fibrous tissue, cartilaginous tissue or bony tissue. The simulation of tissue differentiation during fracture healing is therefore a conceptual and technical difficulty, which makes it suitable for computer simulations.

Recently, dynamic simulations during fracture healing have been performed to predict realistic healing patterns [20, 21]. These simulations have shown the power of computational tools to investigate the process of tissue differentiation during fracture healing. However, these kind of simulations have remained limited and are, as the author will argue in the next chapter, often oversimplified. Other biomechanical analyses have simulated fracture patterns at fixed stages during the healing process and therefore have not fully established the actual causality-consequence of the hypotheses on which they are based [16, 22, 23, 24].

1.4 Challenges

The principal objective and challenge of this thesis is to simulate fracture healing from the initial phase of callus formation to the final resorption phase. Simulation of fracture healing using a mechano-regulation concept based on an iterative feed-back algorithm is proposed. If fracture healing is successfully simulated, this would further show the powerful tool that computer simulation can be when used to investigate mechano-regulation in biology. It would have applications as broad as tissue differentiation during embryology, growth and development, implant-bone interfaces, or tissue engineering.

Computer models can predict biological phenomena. However, it has been argued by many biologists (most passionately by Currey [25]), that good results are obtained through adjustments of the parameters needed to solve the problem. To counter this criticism, the mechano-regulation diagram developed independently by Huiskes *et al.* [26] is used (with the same model parameters) throughout the study. A good model should be able to predict different biological processes with different clinical settings without continuous manipulation of the model parameters. In this thesis, the material properties will not be tuned whatever the results are. It is believed that this approach will allow a more comprehensive assessment of the predictive power of the biphasic mechano-regulation concept.

Chapter 2

Literature review

Contents

2.1 Tissue differentiation during fracture healing

2.1.1 Fracture healing stages

There are two ways for fractures to heal: by primary fracture healing or by secondary fracture healing. Primary healing involves a direct attempt by the cortex to reestablish itself once it has become interrupted. When stabilisation is not adequate to permit primary healing, the abundant capillaries required for bone repair are constantly ruptured and secondary healing takes place. Secondary healing involves responses within the periosteum and external soft tissues and subsequent formation of an external callus. In addition to the classic classification of primary and secondary healing, Aro and Chao [14] distinguish between contact healing and gap healing for osteonal healing, both of which can occur with or without external callus formation. The majority of fractures heal by secondary healing, *i.e.* with formation of an external callus. Secondary fracture healing occurs in stages which are discussed below.

Inflammation

A fracture initially disrupts the local blood supply, causing hemorrhage, anoxia, death of cells, and an aseptic inflammatory response. This is followed by revascularisation, resorption of necrotic tissue, and the proliferation-differentiation of pluripotential cells in the periosteum, endosteum and marrow stroma. The function of the hematoma may be a source of signaling molecules that have the capacity to initiate the cascades of cellular events that are critical to fracture healing [27, 28].

Granulation tissue formation

Progenitor cells begin to produce new cells that differentiate and organise to provide new vessels, fibroblasts, intercellular materials, and supporting cells [28]. Collectively they form a soft granulation tissue.

Callus formation

Further cell proliferation, differentiation, and organisation begin to create new chondrocytes and osteoblasts in the granulation tissue in a manner analogous to that proposed by Caplan [5] during the mesengenic process (Fig. 2.1). Caplan proposed that progenitor cells (also called mesenchymal stem cells, MSCs) can enter the bone, cartilage, tendon, ligament, muscle, marrow, or connective tissue lineages. Once commited to a pathway, the cells begin to synthesise the extracellular organic matrices of tissues which may then mineralise. During fracture healing, mineralisation finishes some weeks later with the formation of a fracture callus.

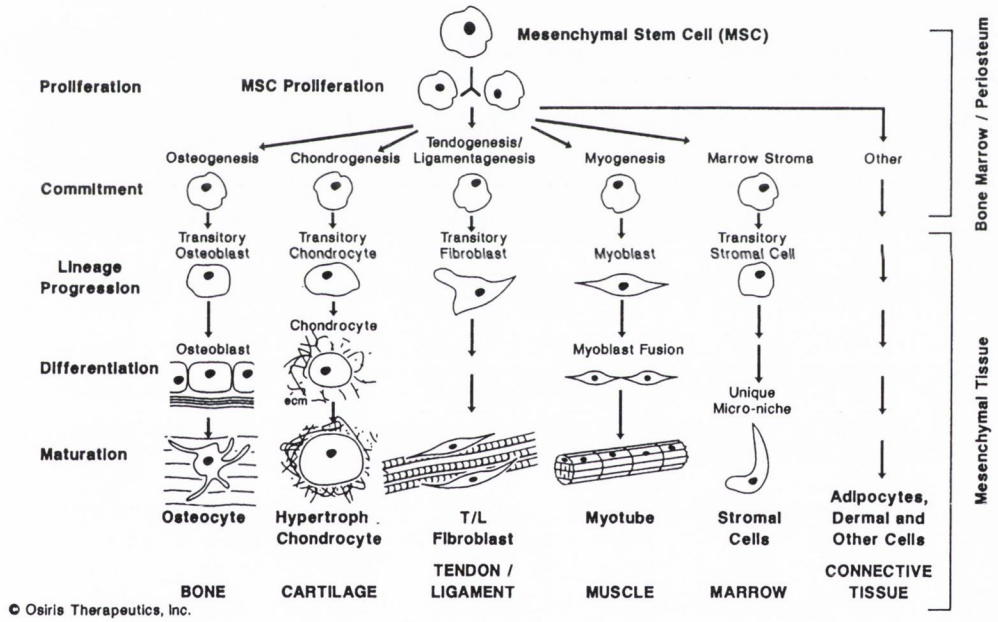

Figure 2.1. The mesengenic process, after Caplan and Boyan [29].

The external callus can be divided into two components: hard callus, where intramembranous ossification takes place, and soft callus, where the process of endochondral ossification proceeds (see review by Brand and Rubin [30]). According to Einhorn [27], the most important response in fracture healing is that of the periosteum under which intramembranous ossification occurs

within a few days after injury. The result is that the periosteum lifts off the bone surface and osteochondral progenitor cells proliferate underneath (see Fig. 2.2). Intramembranous bone is formed by progenitor cells that reside in the periosteum. After one or two weeks, there is an abundance of elongated proliferative chondrocytes that undergo mitosis and divide (see Fig. 2.3). Then cell proliferation declines and hypertrophic chondrocytes become the dominant cell type in the callus (see Fig. 2.4). Once the cartilage is calcified, it becomes a target for the ingrowth of blood vessels, and the calcified cartilage is resorbed by osteoclasts. The endochondral process ends with formation of an external callus made of woven bone (see Fig. 2.5).

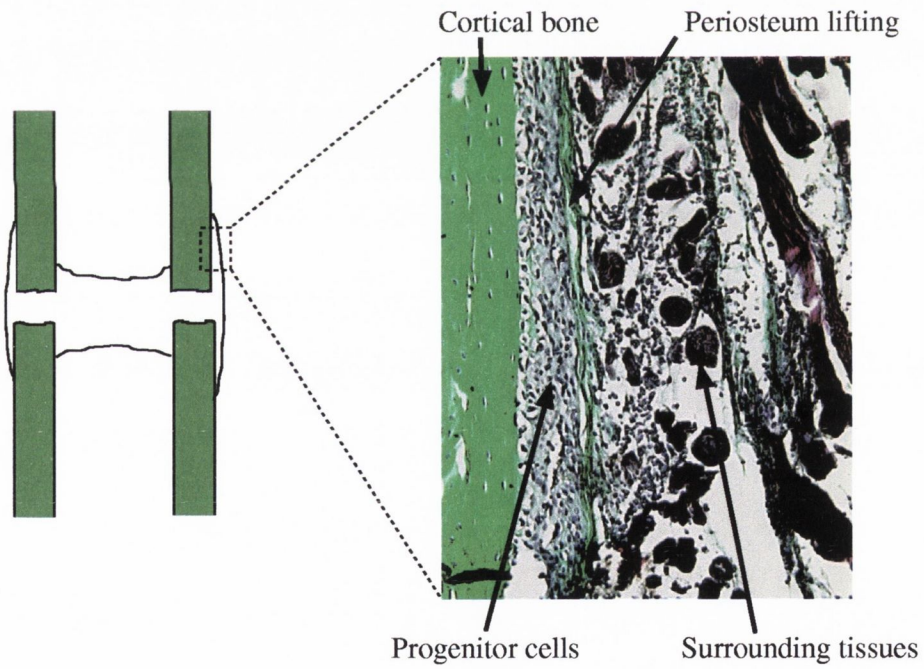

Figure 2.2. Early fracture healing histology of a mouse, day 2 [31]. The lifting of the periosteum is seen with an intense proliferation of progenitor cells. The large amount of surrounding tissues can also be observed. Courtesy of Prof. van der Meulen, Cornell University, NY.

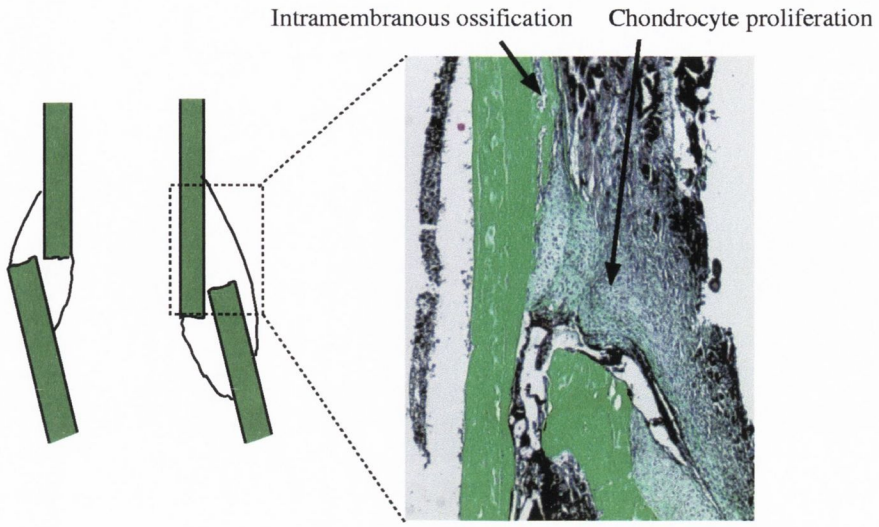

Figure 2.3. Fracture healing histology of a mouse, day 5 [31]. The intramembranous ossification can be seen further from the fracture site. Chondrocyte proliferation is observed in the remaining external callus. Courtesy of Prof. van der Meulen, Cornell University, NY.

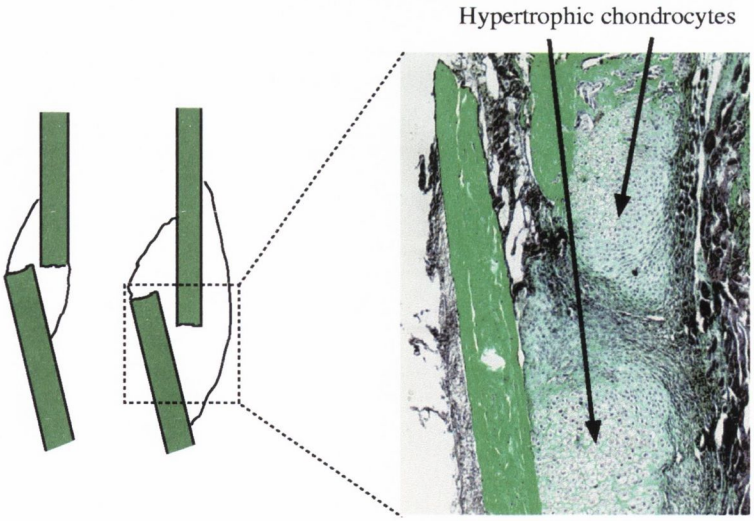

Figure 2.4. Fracture healing histology of a mouse, day 7 [31]. Hypertrophic chondrocytes are observed in most of the external callus. Chondrocytes close to the fracture gap are still in a phase of proliferation. Courtesy of Prof. van der Meulen, Cornell University, NY.

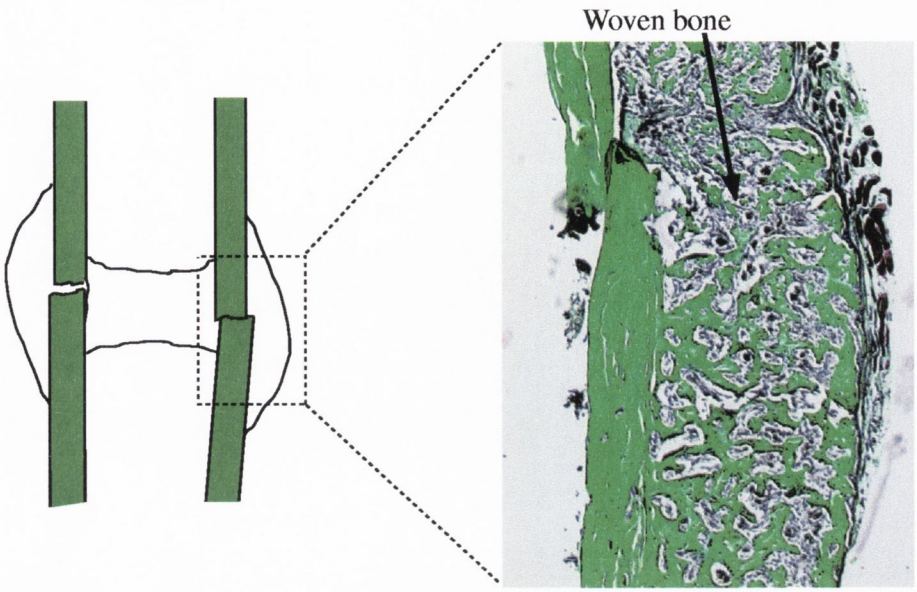

Figure 2.5. Fracture healing histology of a mouse, day 14 [31]. A large amount of woven bone is observed. Courtesy of Prof. van der Meulen, Cornell University, NY.

Remodelling stage

The remodelling stage has four functions [28]:

- To replace any mineralised cartilage with woven bone by endochondral ossification.
- To replace any woven bone with packets of new lamellar bone.
- To replace any callus between the fracture ends with new secondary osteons forming lamellar bone that aligns to the load direction.
- To remove any callus plugging the marrow cavity and restore the medullary cavity.

Modelling stage

During the remodelling stage and beyond (over a number of years), a process of modelling proceeds where the gross shape of compact bone is restored towards

normal without any scar.

2.1.2 The origin of the progenitor cells and their proliferation

Two origins of progenitor cells during fracture healing have been proposed. Bone marrow is believed by many to be a source of cells during fracture healing due to its high number of MSCs having the ability to differentiate into different cell types [32, 33, 34, 35, 36, 37]. Its contribution seems to occur during the early phase of healing [35]. The cells contained within the periosteum also play an important role during fracture healing [32, 34, 37, 38, 39]. Sandberg *et al.* [39] reported that the first chondrocytes are adjacent to cortical bone and therefore may be derived from the inner cambial layer of periosteum by differentiation.

It is unknown though if the cells originate from the cellular inner cambial layer of periosteum or from the external surrounding tissues. This has led to some controversy whether the progenitor cells are uncommited MSCs or commited osteochondral progenitor cells leading to differentiation of osteoblast or chondrocyte cells. Sandberg *et al.* [39] have suggested that growth cartilage occurs by differentiation of mesenchymal cells and less by proliferation of differentiated chondrocytes. Following a fracture, an extraosseous blood supply derived from the surrounding soft tissues develops very rapidly [40]. Although this may help to revascularise any necrotic cortex whose medullary supply has been affected, its main purpose appears to be the supply of external callus. It is therefore possible that if the vessels of external callus originate outside the bone, so also do the cells. On the other hand, Simmons [34] suggests that committed osteoprogenitor cells originate from the periosteum or surrounding tissues.

Iwaki *et al.* [38] have quantified the proliferation activity. They found that the highest cell proliferation activity is found initially in the periosteum (Fig. 2.6).

The distribution of proliferating cells and the degree of cell proliferation

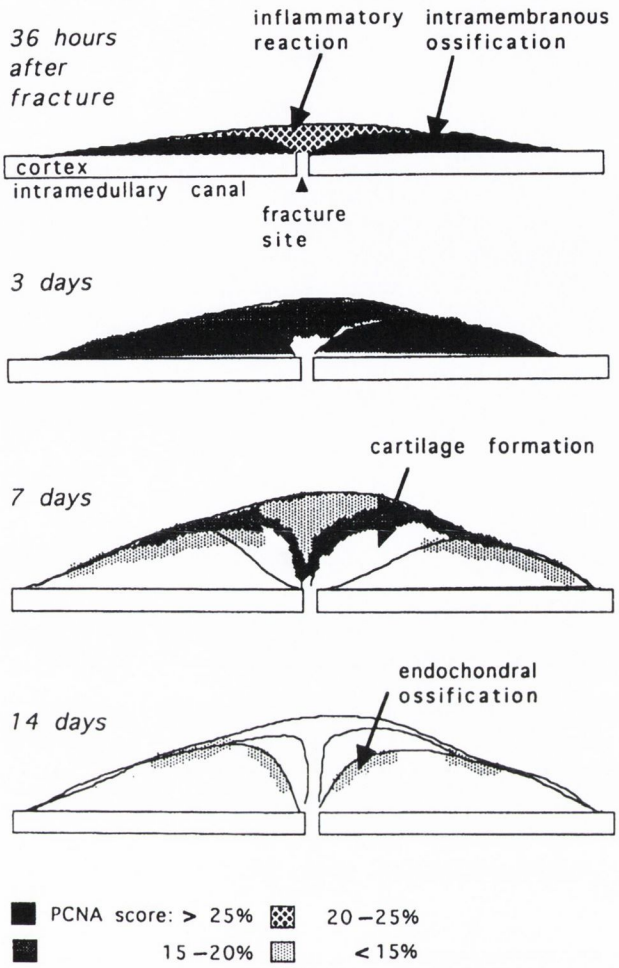

Figure 2.6. Distribution of proliferating cells during fracture repair on a rat model, after Iwaki *et al.* [38].

also vary according to the time lag after the fracture and may depend on growth factors [38]. The response of external soft tissues is also important. Soft tissue response involves rapid cellular activity and the development of an early bridging callus that stabilises the fracture fragments [27].

2.1.3 Angiogenesis during fracture healing

In the early stages of healing, only the periosteal callus has extensive microvasculature, allowing intramembranous ossification [35]. Since vascularisation of

cartilage is required for its replacement by bone during secondary healing fractures, angiogenesis has been suggested to be related to osteogenesis [36, 40, 41]. It was hypothesized that stimulation of cartilage antiangiogenic activity or inhibition of angiogenic factors could prolong the existence of cartilage.

Microangiography was used extensively by Rhinelander [40] and Trueta [41] to provide information on the presence of blood vessels during fracture healing. When the cortex is intact, the direction of cortical blood flow appears to be entirely centrifugal, *i.e.* from medulla to periosteum [40]. The three primary components of the normal blood supply (medullary artery, metaphyseal arteries, and periosteal arterioles) become enhanced as required for fracture repair (Fig. 2.7). In addition, healing bone receives a new external blood supply that derives from extraosseous arterial systems. The extraosseous blood supply of healing bone starts to develop immediately after fracture and becomes very extensive as healing of a fracture progresses [40]. It persists until the normal centrifugal blood flow is restored.

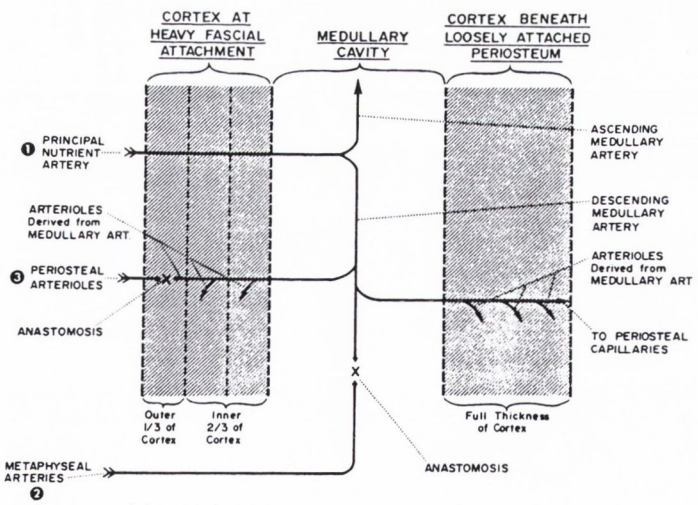

Figure 2.7. Diagram showing the distribution of the afferent vascular system on a mature long bone. The three primary components of the blood supply are (1) medullary artery, (2) metaphyseal arteries, (3) periosteal arterioles. After Rhinelander [40].

Since vasculature seems necessary for bone development, Brighton and Krebs [42], and Heppenstall *et al.* [43] measured oxygen tensions during fracture healing. Their results indicate that both cartilage and bone are formed in areas of low oxygen tension. Low oxygen tension in fracture callus persisted throughout and beyond the period of mechanical restoration of bone continuity and low oxygen tensions persisted well into the stage of callus reorganisation and medullary canal reconstitution. It seems paradoxal therefore that, if angiogenesis is related to osteogenesis, oxygen tension is low in well healed fractures. Brighton and Krebs, and Heppenstal *et al.* suggested that even though there is a great increase in vascularity at the fracture site, there is an even greater increase in cellularity and that the majority of these cells are at such a distance from a capillary that a state of relative anoxia exists throughout most of the callus. Once the fracture has healed, the medullary cavity is reconstituted, vascularity catches up with cellularity, and oxygen tension in the bone produced during fracture repair is increased to normal diaphyseal levels.

2.2 Clinical factors influencing fracture healing

Fracture healing is influenced by many clinical factors. Since these factors will be investigated using computer simulation later in this thesis, they will be reviewed in this section.

2.2.1 Fracture motion

Motion of the fracture ends has a determining influence on fracture healing. Excessive motion in highly unstable fractures does not allow soft-tissue healing and periosteal revascularisation, leading inevitably to non-union. Inhibition of motion, either by immobilising the limb in functionless plaster or by rigid fixation also inhibits healing. The movement of the limb brings about bioelectrical phenomena, interstitial fluid flow, release of biochemical mediators, and

provides greater vascular response [44].

Several experimental and clinical studies have tried to elucidate an optimal motion for fracture healing. Goodship and Kenwright [17] showed that a significant improvement in healing was associated with controlled micromovement. On a tibial osteotomy in sheep, a daily controlled dynamic loading of 360 N during 17 minutes at 0.5 Hz improved fracture healing significantly compared with a rigid fixation. Kenwright and Goodship [45] varied the parameters of the applied stimulus and found that the healing process is acutely sensitive to small periods of daily axial loading within the first two weeks of fracture. Early axial micromovement of tibial fractures in humans led to earlier bending stiffness levels equivalent to clinical union within an average of 17.9 weeks compared to 23.2 weeks for the group treated with highly rigid fixation [46].

To stimulate progenitor cell activity, axial dynamization has been used in the treatment of fractures. It is defined as a fixation that allows unrestricted axial loading of the fracture by physiological weight bearing and muscle contraction while bending and rotational loading is controlled. Egger *et al.* [47] suggested that dynamization improved fracture healing by reducing fracture gap size and increasing weight bearing, without altering the pathway of fracture healing. Similar results are reported by Aro *et al.* [48] who compared the effect of physiologic dynamic compression on fracture healing of dogs with a rigid external fixation. Fracture gap size was reduced with dynamization leading to a contact-healing mechanism without differences in new bone formation, bone porosity, or maximum torque with or without dynamization. In a different study on sheep with a fracture of 0.6 mm, Claes *et al.* [49] found that early dynamization seemed to favour fracture healing by producing significantly more callus and with greater bone formation.

The effect of strain rate was investigated in an experimental study by Goodship *et al.* [18]. They showed that a short term interfragmentary cyclic micromovement applied at a high strain rate (400 mm/sec) induced a greater amount of periosteal callus than the same stimulus applied at a low (20

mm/sec) and moderate (40 mm/sec) strain rate.

2.2.2 Methods of fixation

Various methods of fixation, such as intramedullary fixation by nails, metal-plating, external fixation, and the use of cast and braces, are available for the treatment of fractures (Fig. 2.8). Each method has its advantages and disadvantages. Although plates reduce the fracture gap and provide stability, their use introduces the possibility of infection and overprotection from stress and causes reduced vascularisation of the cortex beneath the tight portion of the plate [40, 50].

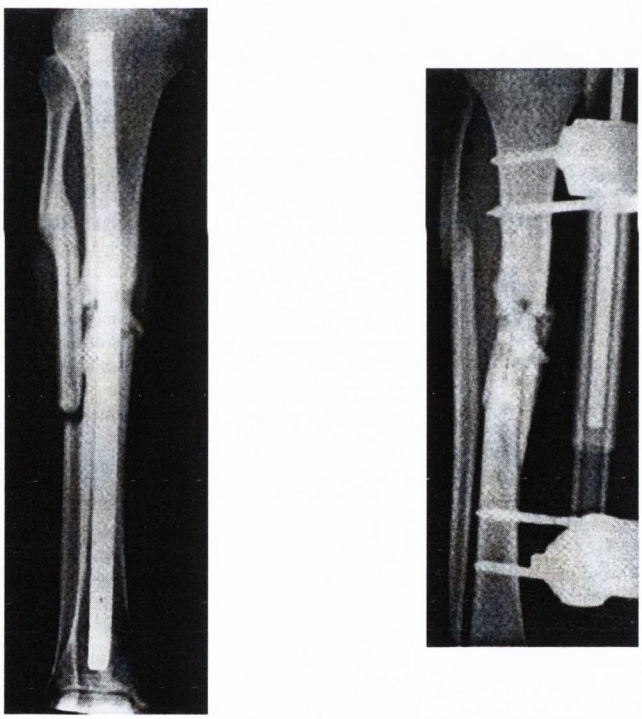

Figure 2.8. Radiographs of fractures treated with intramedullary pin fixation and external fixator. After Antich-Adrover *et al.* [51].

With intramedullary nailing, destruction of the blood supply is a serious consideration because medullary vessels furnish by far the greater proportion of arterial supply to the mature diaphysis. In tight-fitting nails, extensive pe-

riosteal callus is observed due to the obliteration of the medullary blood supply. Nevertheless intramedullary fixation of the tibia is a satisfactory method with early mobility for the patient.

External fixation is commonly used for tibial fractures. The rigidity achieved by external fixation depends on the number and size of the pins, the proximity of the fixation to the bone, and the stiffness of the fixator [52, 53]. Due to the advantage of controlled motion during fracture healing, several external fixators have been created to facilitate axial motion, and clinical results indicate higher rate of union [46, 54]. The differences in configuration of external fixators give different interfragmentary motion and result in different healing timing. Thus, a knowledge of the relationship between fixator geometry and interfragmentary movement would provide the means to control the rate of healing and adjustment of the micromotion displacement to the specific patient. An example of clinical monitoring was given by Richardson *et al.* [55] measuring the bending stiffness of the tibia as healing occurs. They concluded that a bending stiffness of 15 Nm/deg indicates successful healing. In a similar study, Marsh [56] defined delayed union as the failure to reach 7 Nm/deg after 20 weeks. Bending stiffness increases over the healing period but not as quickly for a delayed fracture (Fig. 2.9).

2.2.3 Fracture callus size

Oni *et al.* [57] found that callus volume does not correlate with severity of trauma, interval from fracture to weight bearing, fracture morphology, or fracture displacement. They did not find any correlation either with presence or absence of a fracture gap although the mean callus volume was higher with a fracture gap. On the other hand, Claes *et al.* [49] found that axial external fixator dynamization significantly showed greater callus formation; gap size was also found to have a significant influence on the amount of callus formation. A tendency towards increased callus formation was observed with larger interfragmentary movement for gaps as large as 2 mm, but opposite results

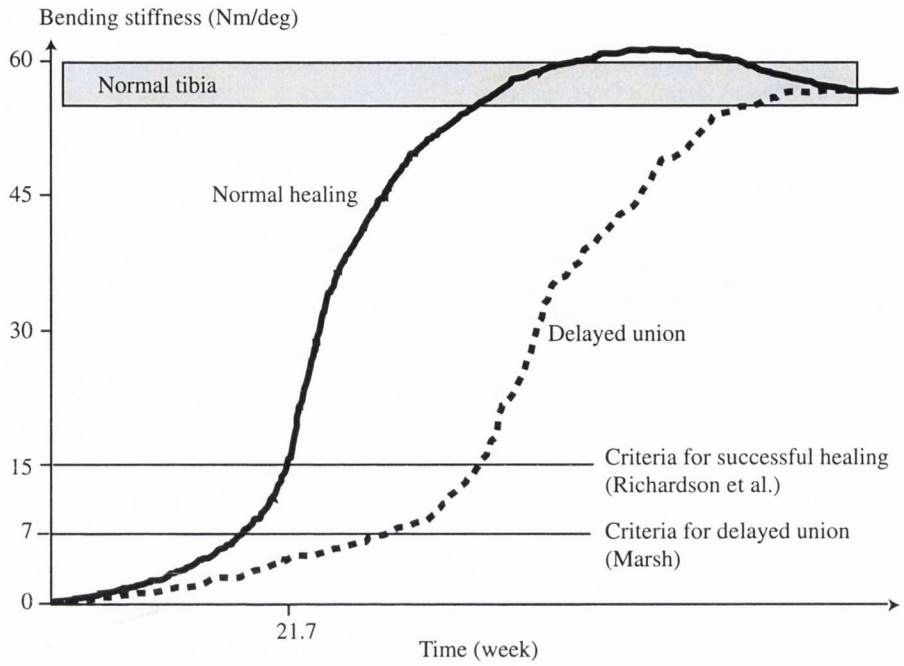

Figure 2.9. Diagram showing the increase of bending stiffness as healing occurs. Adapted from Richardson *et al.* [55] and Marsh [56].

were found for larger gaps (6 mm) [58].

2.2.4 Fracture gap size

Interfragmentary gap size was shown to be critical for the success of healing. In an experimental study on sheep by Claes *et al.* [58] and Augat *et al.* [15], three gap sizes (1, 2 and 6 mm) were created and axial movement of a rigid external fixator was controlled for two amounts of initial strain (7 or 31 %). They found that increasing the size of the osteotomy gaps resulted in poorer mechanical and histological qualities, and the repair process was less complete. Tensile strength measurements 9 weeks post-operatively (p.o.) showed a significant difference in strength between different fracture gap size (Fig. 2.10). Similar results were obtained for the bending stiffness [58].

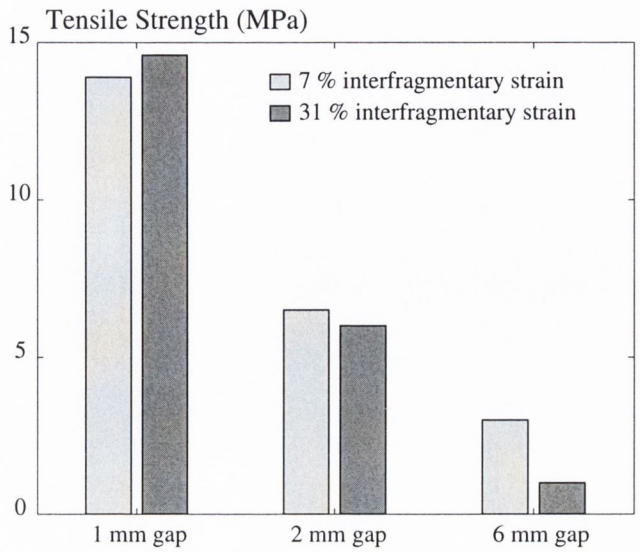

Figure 2.10. Tensile strength measurements at the interfragentary gap for a fracture gap size of 1, 2, and 6 mm. Two initial interfragmentary strains were considered: 7 % and 31 %. Adapted from Augat *et al.* [15].

2.3 Mechano-transduction during fracture healing

2.3.1 Mechanical stimuli on cells

In the 1940s, Pauwels performed work relating cell deformation to gross mechanical deformation [4]. Using solid mechanics theory and radiographs of fractures, Pauwels proposed that an external callus serves to improve the stability of the fracture but also to take up the damaging tensile stress and restore a functional compressive stressing in the marrow and the repair tissue (Fig. 2.11). He also suggested that the periosteal callus prevents excessive sliding in oblique fractures. The calcified tissue constitutes a more evolved material by resisting a combined stressing, *i.e.* a stressing combining tension, compression and shear.

Pauwels suggested that the important information for mechanical stimuli appeared to be contained in the stress and strain invariants (scalar quantities that are independent of the coordinate system). These scalars can be calculated from the full stress and strain tensors. Two stress invariants are

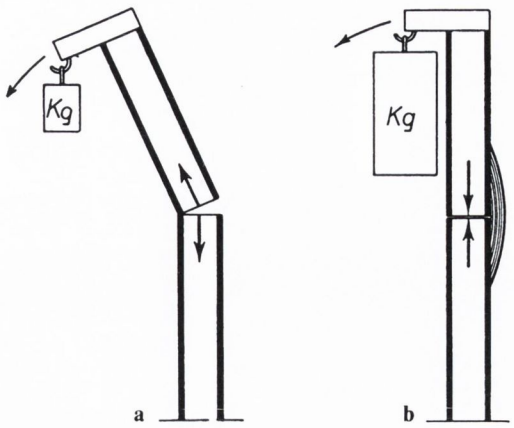

Figure 2.11. The mechanical effect of the external callus on the bending stress of a diaphyseal fracture. **a.** The fracture surfaces open up. **b.** The fracture surfaces are compressed one against each other. After Pauwels [4].

octahedral shear (or distortional) stress S, and hydrostatic (or dilatational) stress D which are defined as:

$$S = \frac{1}{3}\sqrt{(\sigma_1 - \sigma_2)^2 + (\sigma_2 - \sigma_3)^2 + (\sigma_3 - \sigma_1)^2} \tag{2.1}$$

$$D = \frac{1}{3}(\sigma_1 + \sigma_2 + \sigma_3) \tag{2.2}$$

where σ_1, σ_2, and σ_3 are the principal stresses. The corresponding strains are octahedral shear (or distortional) strain and volumetric strain. In a compressible, elastic, isotropic material, hydrostatic stress causes a change in material volume, or volumetric strain, but no distortion. Conversely, octahedral shear stress causes material deformation, or distortional strain, but no change in volume. The effect of this is illustrated in Fig. 2.12.

Pauwels suggested that cells and extracellular matrix elongation associated with distortional stress is a specific stimulus for the development of collagen fibers and that, hydrostatic compression is a specific stimulus for cartilage formation. However, Pauwels could not propose that one specific mechanical stimulus guided bone formation. A schematic representation of the concept

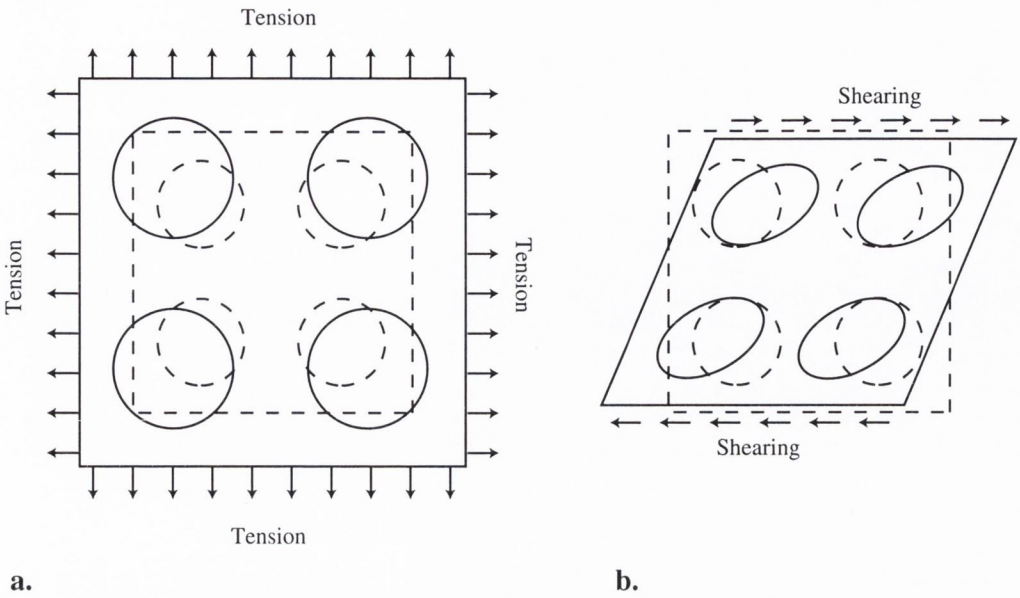

Figure 2.12. Deformation of the elementary particles of a cube of isotropic elastic material under **a.** biaxial tensile, and **b.** shearing forces. **a.** Under biaxial tensile forces, the elementary particles increase in volume but their shape remain the same. **b.** Under the effect of shearing forces, the volume of the elementary particles remain the same but the spherical shape becomes an ellipsoid. Adapted from Pauwels [4].

developed by Pauwels is presented in Fig. 2.13. Deformation of shape (*i.e.* shear) is on the horizontal axis and hydrostatic compression is on the vertical axis. A combination of these biophysical stimuli will act on the mesenchymal cell pool leading to either hyaline cartilage, fibrocartilage or fibrous tissue as represented on the perimeter of the quadrant. Depending on the mechanical stimuli, intramembranous or endochondral ossification will form leading to lamellar bone through remodelling.

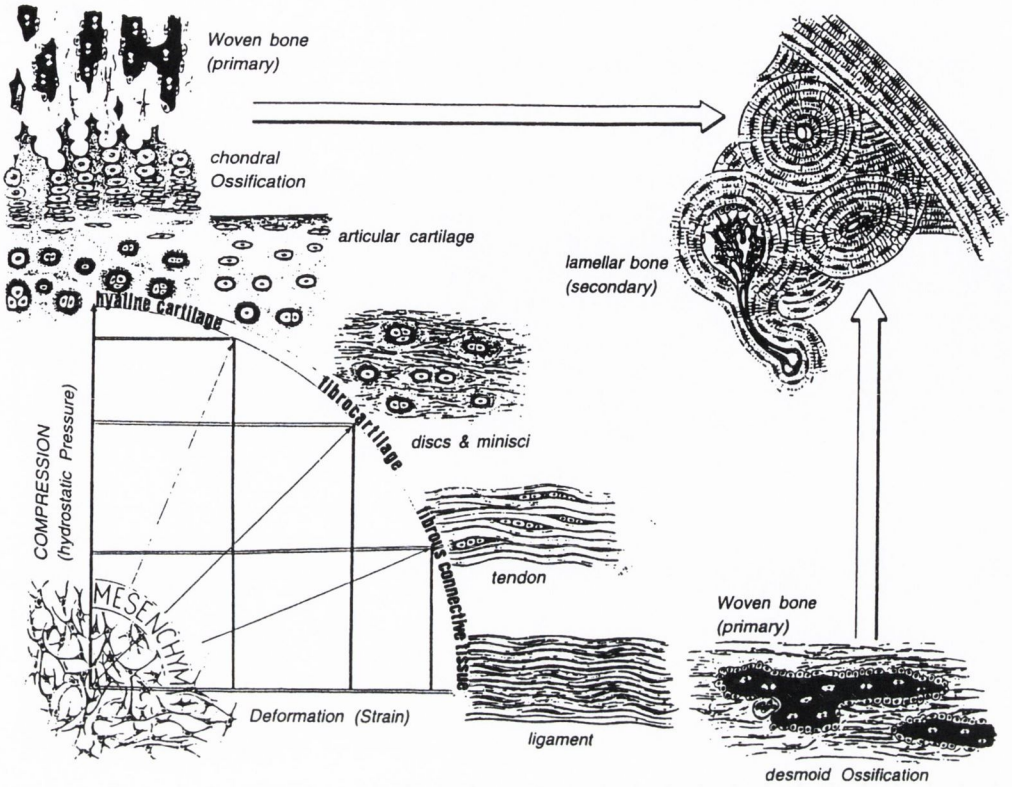

Figure 2.13. A schematic representation of the hypothesized influence of biophysical stimuli on tissue phenotypes proposed by Pauwels. After Weinans and Prendergast [59].

2.3.2 The interfragmentary strain theory

Based on a qualitative analysis of clinical results of fracture healing, Perren [60], and Perren and Cordey [61] proposed that tissue differentiation was controlled by the tolerance of various tissues to strain. In view of tissue reaction to mechanical input, a biomechanical theory of fracture healing based on the concept of strain, rigidity and strength was proposed. This concept is now refered to as the 'interfragmentary strain theory'. The basis of this theory is that a tissue that ruptures or fails at a certain strain level cannot be formed in a region experiencing strains greater than this level. The interfragmentary strain is defined as the interfragmentary motion divided by the fracture gap

size

$$\text{Interfragmentary strain} = \frac{\text{Interfragmentary motion}}{\text{Fracture gap size}} \tag{2.3}$$

Perren first showed that, due to a difference in strength and rigidity between tissues, the tolerance to elongation was very different. For example, lamellar bone would rupture under a strain of 2 %, cartilage would rupture for a strain of about 10 % whereas granulation tissue can widthstand strains up to 100 % (Fig. 2.14). Due to this different tolerance to rupture, healing occurs by a progressive tissue differentiation from the initial granulation tissue, to fibrous tissue, cartilaginous tissue and then bony tissue.

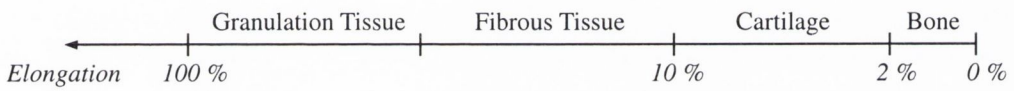

Figure 2.14. Strain tolerance of the repair tissues. Adapted from Perren [60].

The interfragmentary strain theory has the advantage of being simple and easy to use since interfragmentary movement can be monitored. However, it has many limitations. First, it models the fracture as a one dimensional entity thus ignoring the three dimensional complexity of the callus. Moreover, the theory was mainly conceptualised from primary healing fractures and therefore do not account for the different mechanical environments in the external callus during secondary healing which is a more common process. The interfragmentary strain theory predicts for a given interfragmentary movement better healing results with increasing gap size which contrasts with experimental results [15, 58]. Although interfragmentary strain theory has the merit of simplicity, it has not been established to date as a unified biomechanical theory for fracture healing.

2.3.3 Tissues modelled as a single solid phase

Carter and co-workers – Tensile strain/hydrostatic stress stimuli

Carter and co-workers [22, 23, 24] proposed a theory for the role of intermittently imposed stresses in the differentiation of mesenchymal tissue in fracture healing. They proposed that

- Intramembranous bone formation is permitted in areas of low magnitudes of tensile strain or shear stress, and hydrostatic stress.
- Hydrostatic compressive stress is a stimulus for chondrogenesis.
- High tensile strain or shear stress is a stimulus for fibrous tissue formation.
- Tensile strain or shear stress with a superimposed hydrostatic compressive stress stimulates the development of fibrocartilage.
- Low oxygen tension can promote chondrogenesis in an otherwise osteogenic environment.

These differentiation rules can be conceptualised graphically as shown in Fig. 2.15. They can be compared with the work of Pauwels who hypothesized that octahedral shear stress is a stimulus for the development of collagen fibers and that, hydrostatic compression is a specific stimulus for cartilage formation.

To represent the stimulus for bone formation Carter and co-workers calculated an osteogenic index I reflecting the tendency for ossification

$$I = \sum_{i=1}^{c} n_i(S_i + kD_i) \tag{2.4}$$

where n_i is the number of loading cycles for i discrete loading conditions ($i = 1, 2, 3, \cdots, c$), and k is an empirical constant to be determined. Contour plots of the osteogenic index were then used to predict areas of accelerated endochondral ossification (high I values) and areas of accelerated cartilage formation or maintenance (low I values).

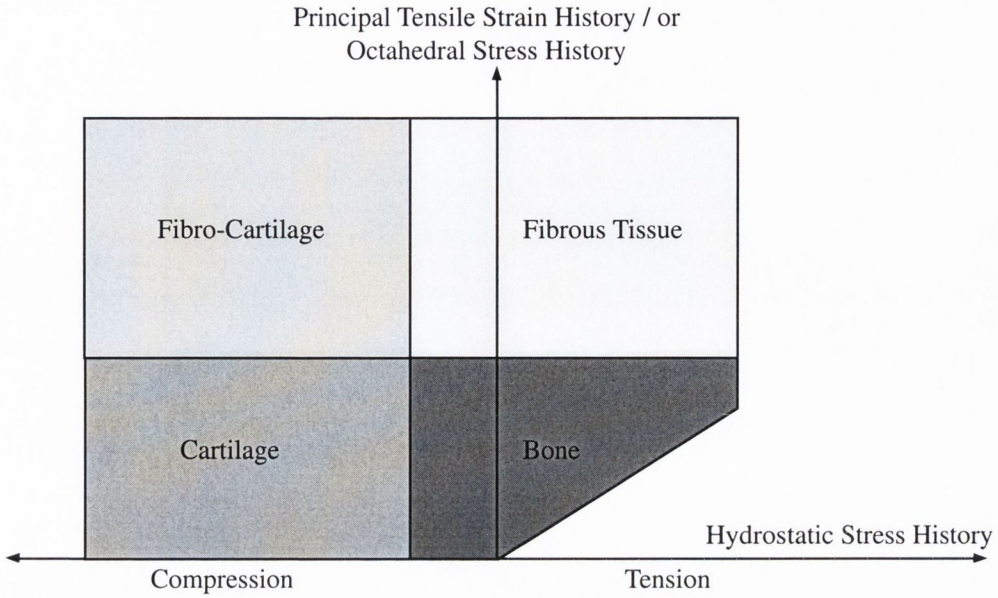

Figure 2.15. Concept of tissue mechanical loading history on skeletal tissue regeneration proposed by Carter and co-workers [24]. After Carter *et al.* [24].

In a first study, Carter *et al.* [23] used two-dimensional plane stress linear elastic FE models of initial fracture with varying axial and bending loads. They calculated the octahedral shear stress S and the hydrostatic stress D with k values of 0, 0.5, 1.0, and 2.0. Comparing their contour plots of osteogenic index with common histologies, they suggested a k value greater or equal to 2.0 giving best initial bone formation (Fig. 2.16). Thus, their results indicated that intermittent hydrostatic stresses may play an important role in influencing initial tissue differentiation. In a following study, they analysed three different stages of ossification with three different material representations of the external callus [22]. They predicted that an osteogenic index greater than 2.0 was more consistent with patterns of progressive callus ossification.

Carter and co-workers [24, 62] further tested their hypotheses using an axisymmetric model of a mouse femur fracture model and distraction model. Their results suggest that the stress/strain states as well as the tissue differentiation pattern in distraction osteogenesis are 'mirror images' of those in

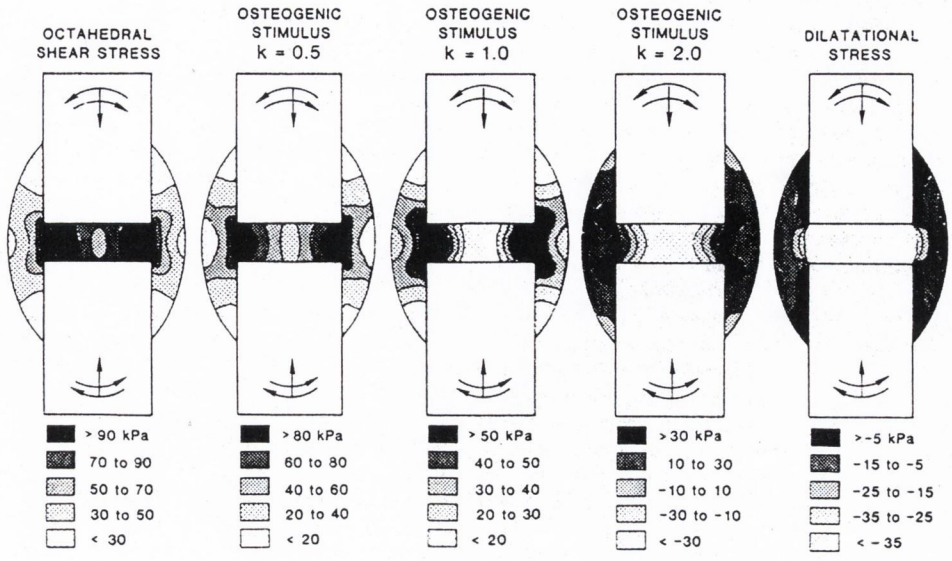

Figure 2.16. Total stress and osteogenic index contour plots in an early fracture callus with a loading history represented by an axial load and two oppositely directed bending loads. After Carter *et al.* [23].

fracture healing. Instead of using the octahedral shear stress as an ossification inhibitor, they used tensile principal strain. Thus no osteogenic index was calculated but they concluded that in areas of cartilage formation, subsequent endochondral ossification can be inhibited by intermittent hydrostatic compressive stress and accelerated by octahedral shear stress (or strain).

Using the same hypotheses, Loboa Polefka *et al.* [63] were able to correlate initial pseudoarthrosis formation locations in oblique fractures with high values of tensile strain and compressive hydrostatic stress.

Carter and co-workers have shown that computer models could be used to correlate mechanical stimuli with tissue differentiation patterns. However, they used linear elastic solid material to represent the soft and bony tissues, which may not be accurate due to the viscoelastic behaviour and the large strains that soft tissues undergo. Furthermore, tissues contain solid and fluid phases, the latter of which may have an important role in the mechano-biological regulation. An osteogenic index was calculated to indicate the tendency of

ossification. However, this index depends on an empirical constant k which was estimated as 2.0. Other biomechanical studies from the same group but applied to other tissue differentiation areas have found that k could vary from 0.3 to 1 [64]. Clearly, if the constants used to run the simulations are changed arbitrarily, it leads one to suspect the predictive power of the model.

Gardner and co-workers – A patient specific approach

In a two-dimensional FE study, Gardner *et al.* [19, 65, 66] calculated the maximum principal stresses at four different healing stages of one patient and related it to tissue damage. They deduced the material properties by comparing the predicted interfragmentary displacements with the measured interfragmentary displacements of one patient.

They found that initially, peak tissue strain during walking was greater than 70 % in the interfragmentary gap but decreased to 6 % by week 8. They related high values of maximum principal stress with tissue damage which would decrease callus stability and therefore delay the healing phase.

Gardner and co-workers advocated that their study represents the description of fracture healing in a specific patient and is thus more accurate than the generic model of Carter and co-workers for example. However, it may be argued that the use of only one patient may not validate their approach. Although it is useful to study the fracture pattern with exact geometries, it is necessary to do so for several patients before drawing general conclusions. Moreover, although the geometry was more realistic for this specific patient, the loading was only approximative and the fracture was represented in 2D.

Claes and co-workers – Strain/hydrostatic pressure stimuli

Claes and co-workers [16, 67] used an axisymmetric FE model to calculate strain and stresses in callus with tissues described as hyperelastic for connective tissue and linear elastic for other tissues. Three healing stages corresponding to 1 week p.o., 4 weeks p.o., and 8 weeks p.o. were modelled and the hydrostatic

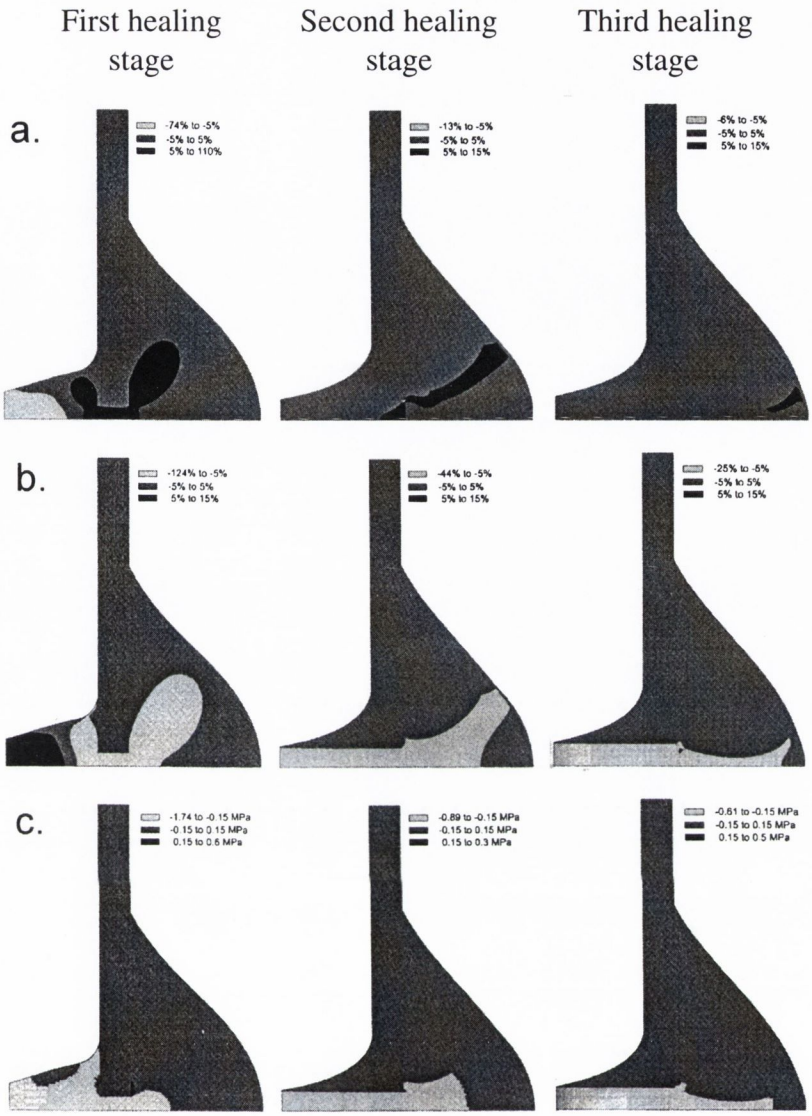

Figure 2.17. Mechanical stimuli distribution in three healing stages corresponding to week 1, 4, and 8 in sheep fractures. **a.** Strain in the radial direction. **b.** Strain in longitudinal direction. **c.** Hydrostatic pressure. Adapted from Claes and Heigele [67].

stress, longitudinal strains, and radial strains were calculated (Fig. 2.17).

In the model of Claes and Heigele [67], new bone formation occurs primarily on surfaces of existing bone or calcified cartilage, and the type of bone healing (intramembranous or endochondral) depends on local strain and stress magnitudes. Comparing their results with expected tissue type and cell culture

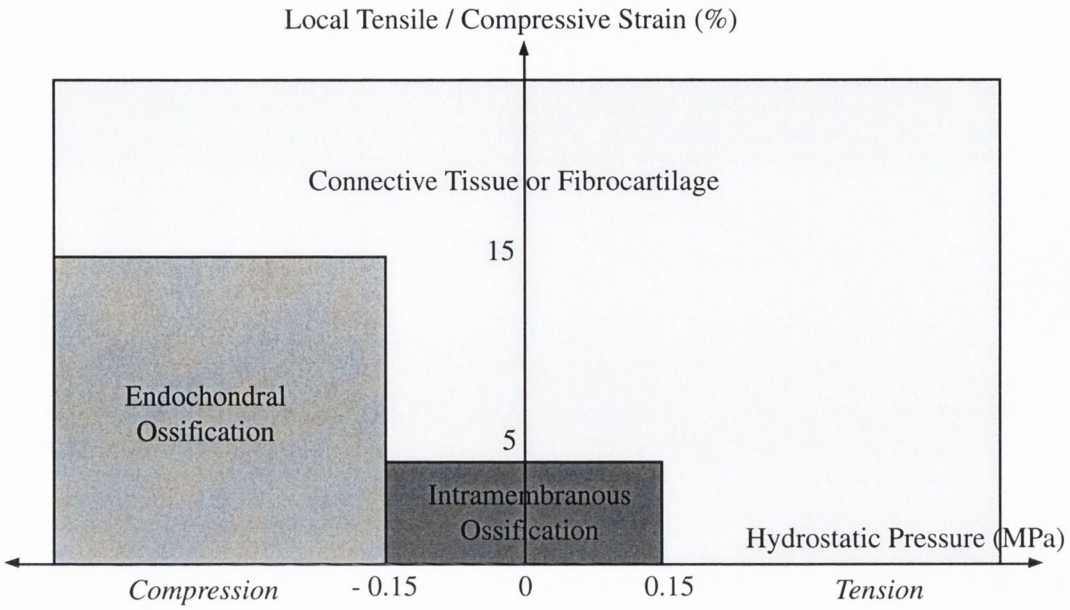

Figure 2.18. Tissue differentiation relating mechanical stimuli to tissue types hypothesized by Claes and Heigele [67]. Adapted from Claes and Heigele [67].

experiment [16], they suggested that intramembranous bone formation occurs with strain lower than 5 %. Compressive hydrostatic pressures greater than 0.15 MPa and strains smaller than 15 % appeared to stimulate endochondral ossification. All other conditions seemingly led to connective tissue or fibrous tissue (Fig. 2.18).

This tissue differentiation concept has some similarity with the concept proposed by Pauwels and Carter and co-workers. Bone cannot form in high compressive pressure or high strain and, connective tissue is predicted for high strain. However, the difference between endochondral and intramembranous ossification is accounted for due to the inability of osteoblasts to sustain high strain and high compressive pressure. Moreover, in contrast to Carter *et al.* [24], numeric values delineating the tissue types have been proposed. However, only fixed time healing stages were modelled.

Ament and Hofer – A fuzzy logic model

Recently, Ament and Hofer [20] proposed a tissue regulation model based on a set of fuzzy logic rules. Strain energy density was used as an indicator of the mechanical stimulus for tissue apposition or resorption. A set of rules was defined to predict bone, cartilage, or connective tissue formation. An osteogenic factor was also introduced to account for vascularisation and thus either intramembranous or endochondral ossification. Implementing this fuzzy logic model on a 2D plane stress transverse osteotomy, they were able to predict bridging of the bone ends with cartilage formation, followed by the growth of a callus cuff, and finally, the resorption of callus after ossification of the interfragmentary gap (Fig. 2.19).

Figure 2.19. Predicted modulus of elasticity at (a) day 3, (b) day 14, (c) day 21, (e) day 84, and (f) day 365. After Ament and Hofer [20].

The model of Ament and Hofer [20] is more advanced than any previous model by simulating a dynamic change in the tissue properties corresponding to a change in the mechanical stimuli. The model agrees well with histologic findings even though the geometry and loading are very simplified. The main limitations of this model are that tissues are represented as linear elastic materials and numerous rules are needed to predict tissue differentiation. It is questionable whether the use of so many different rules do not constrain excessively the model to a specific direction and therefore overgovern the fracture healing process.

2.3.4 The incorporation of the interstitial fluid phase in computational models

Since soft tissues consist mainly of collagen and water, they can be considered as a two-phase material. Both solid and fluid phases interact with each other to resist the mechanical loading applied daily. The fluid phase gives a viscoelastic property to the tissue due to the drag force that prevents the fluid flowing instantaneously as loading is applied.

The biphasic theory was proposed by Mow *et al.* [68] and applied to cartilage to represent more accurately the nature and behaviour of tissues. They present the biphasic theory as a development of the theory of mixtures. In the biphasic theory, the material is considered to be a continuum mixture of a deformable solid phase and a fluid phase. A poroelastic theory was developed by Biot [69] to model porous soil material. Using the poroelasticity theory, the material is considered as a porous elastic solid that is saturated by a pore fluid which flows relative to the deforming solid. Simon [70] reviewed applications of poroelastic and biphasic theories on biomechanic soft tissues and compared the two approaches. Simon showed that both were effectively equivalent. Prendergast *et al.* [10] and Wu *et al.* [11] showed that poroelastic problems solved using commercialised finite element codes gave similar results than the biphasic theory.

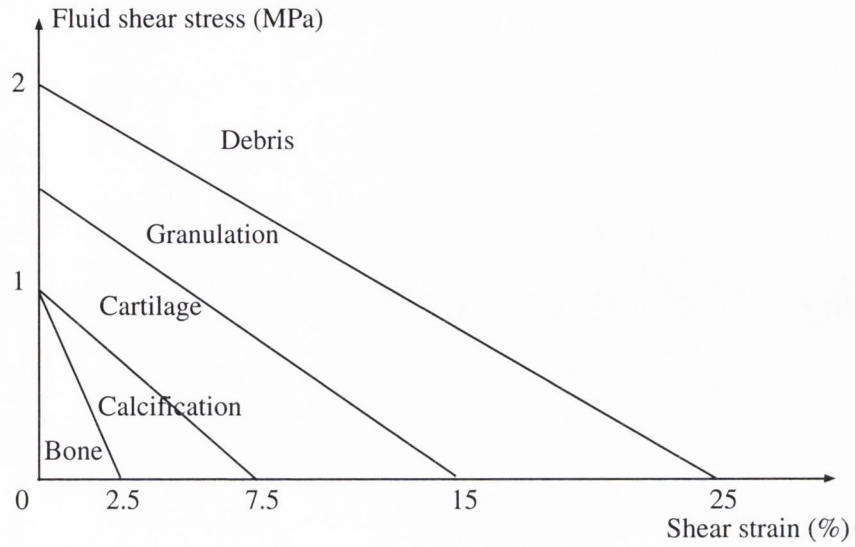

Figure 2.20. Tissue differentiation rule hypothesized, after Kuiper *et al.* [21].

Using an axisymmetric biphasic model of a fracture, Kuiper *et al.* [21, 71, 72] used tissue shear strain and fluid shear stress as mechanical stimuli regulating tissue differentiation (Fig. 2.20), and strain energy as the mechanical stimulus regulating bone resorption. Fluid shear stress τ is defined as a function of pressure gradient ∇p and specific matrix surface s

$$\tau = \frac{\nabla p}{s} \tag{2.5}$$

where the specific surface is related to tissue permeability k, porosity n, fluid viscosity ν, and constant G through the Carman-Kozeny equation [73]

$$k\nu G s^2 = n^3 \tag{2.6}$$

They found that strain provides the dominant cell differentiating stimulus in fracture callus and later simulated the regenerative and resorption phases. Typical healing patterns were predicted for a variation of applied movements on the cortical bone. By varying the amount of fracture bone movements, they found that larger movements increase callus size and delay bone healing.

Prendergast *et al.* [74] analysed tissue differentiation of cells at implant interfaces using a biphasic FE model. To assess the feasibility of biophysi-

cal stimuli as mediators of tissue differentiation, they analysed interfacial tissue formation adjacent to a micromotion device implanted in the condyles of dogs. They found that a variation over time of biophysical stimuli (octahedral shear strain and relative fluid flow) within the tissue can be plotted as a mechano-regulatory pathway (Fig. 2.21), which would predict the differentiation of granulation tissue (mesenchymal cells) into bone, (fibro-)cartilage or fibrous connective tissue. A linear model of the same analysis could not predict ossification patterns at interfaces [75]. Since biomechanical stress acting on the cells is due both to the stress acting in the extracellular matrix and fluid flow, they concluded that both deformation *and* fluid flow must be taken together to define the mechanical milieu in the cell [76]. Using this concept, a regulatory feedback model was developed in which the eventual phenotype depends on the combined value of tissue strain (maximum distortional strain) γ, and interstitial fluid flow v [26, 77]. It was proposed that depending on the

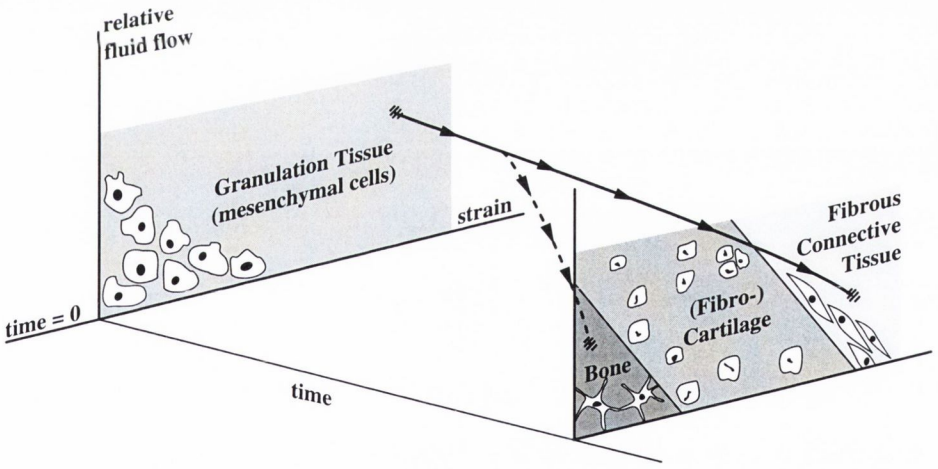

Figure 2.21. Mechano-regulatory pathway hypothesized to regulate tissue differentiation. If the initial motion is maintained (motion-control given by the full line), then the shear strain and fluid flow stay high and no bone will form. On the other hand, if the motion is reduced (load control given by the dashed line), then the shear strain and fluid flow reduce and ossification occurs. After Prendergast *et al.* [74].

stimuli values, three types of tissue would emerge if

- for bone,

$$\gamma/a + v/b < 1 \tag{2.7}$$

- for cartilage,

$$\gamma/a + v/b > 1 \qquad \text{and} \qquad \gamma/a + v/b < 3 \tag{2.8}$$

- for fibrous connective tissue,

$$\gamma/a + v/b > 3 \tag{2.9}$$

where $a = 3.75\,\%$ and $b = 3.0\,\mu m/s$. They showed that the regulatory model combined with an iterative FE model predicting the mechanical stimuli can eventually develop into a powerful tool for predicting tissue differentiation processes around implants. The concept can also be applied to fracture healing and could become very useful in predicting the phases of fracture healing.

2.4 Summary

In this chapter, it was shown that fracture healing is a complex biological process that is influenced mainly by the mechanical environment. Many different clinical factors have been used in experimental and clinical studies. Results indicate that there is a mechanical environment for which healing occurs most rapidly. However, the combination of mechanical stimuli have not yet been determined. Several researchers have tried to relate mechanical environment to tissue formation and cell differentiation using computer models. However, some do not describe accurately the physical behaviour of tissues or the geometry of fractures; while others do not simulate the healing process continuously. A model predicting the regenerative and resorptive phases of fracture healing using a more accurate description of tissues has not yet been developed.

It is the contention of this thesis that tissue differentiation during fracture healing can be simulated based on a mechano-regulation model, if the model

describes tissues as biphasic and incorporates the influence of the interstitial fluid phase. To see if this is true, the mechano-regulation concept proposed by Prendergast *et al.* [74] will be further developed and applied to the problem of fracture healing. The model will simulate the healing process continuously by relating mechanical stimuli to tissue differentiation using the mechano-regulation diagram proposed by Huiskes *et al.* [26]. It will iteratively update the fracture healing state from the formation of granulation tissue to the end of the bone resorption phase. The model will be tested on various 2D and 3D representations of a fracture callus.

Chapter 3

Methods

Contents

3.1 Introduction

Due to the difficulty in measuring mechanical stimuli other than interfragmentary movement during fracture healing, FE studies have become increasingly useful. So far, most studies have considered axisymmetric or plane stress models due mainly to the complexity of biological processes during fracture healing. In this study, an axisymmetric model was first used to investigate the feasibility of the concept to simulate fracture healing. The effect of the origin of cells was first investigated. The loading magnitude and fracture gap size were changed to investigate its influence on the healing period. A plane strain model was generated to investigate the effect of a bending load in transverse and oblique fractures. Finally, a 3D model of a human tibia was reconstructed to investigate the mechanical stimuli in three dimensions and see whether fracture healing could be simulated in 3D.

In the first section, the numerical approach used in this study to model tissue differentiation is described. In the following section, the geometry and loading conditions of investigated fracture healing cases are presented.

3.2 Computational approach

3.2.1 Poroelasticity theory

Given a geometry, applied boundary conditions, and known stress-strain law, mechanical stimuli can be calculated. In this study, the FE calculations were performed using DIANA (TNO, Delft, The Netherlands). The principal equations for the poroelasticity theory implemented in DIANA will be recalled and the necessary material properties will be identified. The reader is referred to Biot [69], Mow *et al.* [68], and Simon [70] for detailed descriptions.

According to the poroelasticity theory, tissues can be modelled as a mixture of solid and fluid constituents present at each material point. Because of this continuity, the sum of the volume fractions has to equal one and the apparent

total density of the mixture, ρ, can be formulated as follows

$$\rho = (1 - n)\rho^s + n\rho^f \tag{3.1}$$

where n is the porosity (equal to the fluid volume fraction), and ρ^s and ρ^f are the apparent density of the solid and fluid phases respectively. The porosity, n, can be expressed in terms of n_R, the porosity in the reference configuration as follows

$$n = 1 - \frac{1 - n_R}{J} \tag{3.2}$$

where J is the ratio of the current volume, dV, to the reference volume, dV_R, or also the determinant of the deformation gradient with respect to the reference configuration

$$J = \frac{dV}{dV_R} = \det \nabla \mathbf{x} \tag{3.3}$$

where ∇ is the gradient operator and $\mathbf{x}$ the deformation vector. The total stress $\boldsymbol{\sigma}$, (positive in tension) acting on the total area of the solid and the pores is separated into inter-granular stress (solid phase stress) $\boldsymbol{\sigma}'$, and pore pressure p, (positive in compression) corresponding to the fluid stress when the fluid is inviscid

$$\boldsymbol{\sigma} = \boldsymbol{\sigma}' - p\mathbf{I} \tag{3.4}$$

where $\mathbf{I}$ is the identity matrix. Assuming that the gravity field, the convective terms and the relative acceleration between solid and fluid phases are neglected, the momentum conservation leads to

$$div(\boldsymbol{\sigma}) = \rho \ddot{\mathbf{u}}_\mathbf{s} \tag{3.5}$$

where $\ddot{\mathbf{u}}_\mathbf{s}$ is the acceleration of the solid. Using Equ. 3.4, this equation reads

$$div(\boldsymbol{\sigma}') - \nabla \mathbf{I} p = \rho \ddot{\mathbf{u}}_\mathbf{s} \tag{3.6}$$

If we assume the material to be isotropic, and if the infinitesimal strain-displacement relationship is assumed, we can write a constitutive law as follows

$$\boldsymbol{\sigma}' = \lambda e \mathbf{I} + 2\mu\boldsymbol{\varepsilon} \tag{3.7}$$

where $\boldsymbol{\varepsilon}$ denotes strain tensor, e denotes the dilatational strain, λ and μ are the Lamé constants related to the Young's modulus and Poisson's ratio. Finite strain can be accounted for by using a total or updated Lagrange formulation.

There are two possible ways in which the volume of the tissue can change. The first is expelled fluid from the tissue. This produces a relative fluid velocity according to Darcy's law

$$\dot{\mathbf{u}}_\mathbf{f} = -\frac{\mathbf{k}}{\nu} \nabla p \tag{3.8}$$

where $\dot{\mathbf{u}}_\mathbf{f}$ is the relative fluid velocity vector with respect to the solid velocity, $\mathbf{k}$ is the permeability vector and ν is the kinematic viscosity. The second way in which the volume of the tissue can change is by compression of the solid and fluid phases themselves. If we assume that the compression modulus of the porous solid is much smaller than the intrinsic compression modulus of the non-porous solid, the general mass conservation law leads to

$$div(\dot{\mathbf{u}}_\mathbf{s}) + div(\dot{\mathbf{u}}_\mathbf{f}) + \frac{\dot{p}}{Q} = 0 \tag{3.9}$$

where $\dot{\mathbf{u}}_\mathbf{s}$ is the velocity vector of the solid and $\dot{\mathbf{u}}_\mathbf{f}$ is the relative fluid velocity vector with respect to the solid velocity, and Q is the Biot material parameter related to the compressibility of the fluid and solid by

$$\frac{1}{Q} = \frac{n}{K_f} + \frac{1-n}{K_s} \tag{3.10}$$

where K_f and K_s are the intrinsic compression modulus of the fluid and solid phases respectively.

Thus, six parameters (Young's modulus, permeability, Poisson's ratio, porosity, and solid and fluid compression moduli) need to be known to completely define a poroelastic compressible isotropic model.

The basic FE assumption is the interpolation of coordinates, displacements and pore pressure potentials for each element from the values in nodes. Based on the previous equations, a FE space discretisation is derived via the standard Galerkin procedure. The space discretisation is evaluated at several time steps using an Euler backward time integration.

3.2.2 A time predictive mechano-regulation concept

Mechanical stimuli used

In the previous chapter, several mechanical stimuli have been explored by different research teams. In this study, following on the work of Prendergast and colleagues [26, 74, 77] studying tissue differentiation at implant-bone interfaces using a mechano-regulation concept described in Section 2.3.4, interstitial fluid flow and collagenous octahedral shear strain were used as regulators of tissue differentiation. These two stimuli are invariants and represent a measure of the cell deformation from each solid and fluid phase.

The concept was refined by separating the bone forming field into an immature woven bone and a mature woven bone field to account for the different mineralisation process of woven bone during the remodelling phase (Fig. 3.1). Initially, all tissues in the fracture gap and in the external callus are made of granulation tissue that is filled with progenitor cells. As loading is applied,

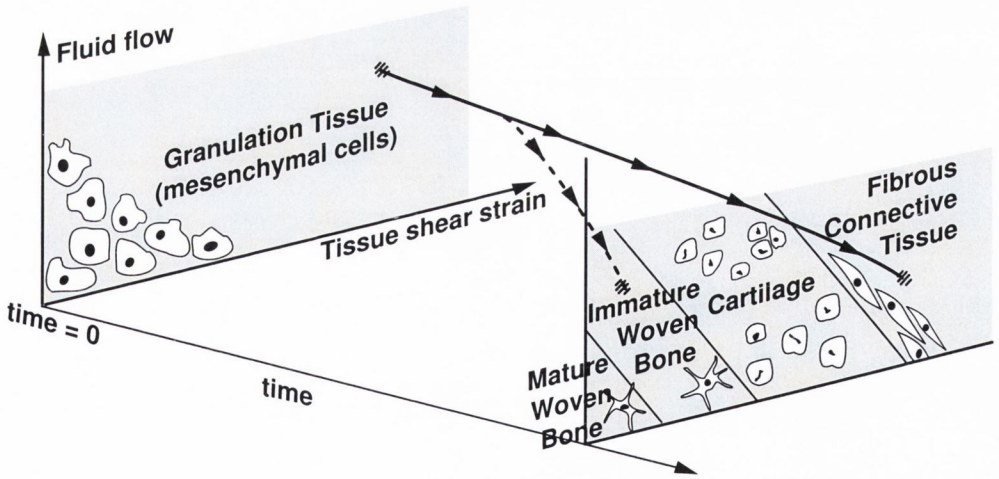

Figure 3.1. The mechano-regulation concept adapted from Prendergast *et al.* [74]. The bone field region was divided into an immature and mature woven bone to represent two mineralisation stages of bone formation.

two options are possible. Firstly, if the mechanical stimuli are too high, there is no stabilisation and only fibrous tissue can form over time (straight line in Fig. 3.1). Secondly, if stabilisation occurs at some time during the differentiation process, the mechanical stimuli will decrease leading to formation of cartilaginous tissue or bone tissue (dotted line in Fig. 3.1).

An iterative procedure

The mechano-regulation concept predicts the type of tissue that should be formed at some location depending on the predicted mechanical stimuli. This concept can be included in an iterative process that (1) calculates the biophysical stimuli for a specific loading, geometry and material properties, (2) predicts the tissue type formation, and (3) updates the new tissue phenotype. The process can be looped from (1) to (3) until there are no more changes of mechanical stimuli (Fig. 3.2).

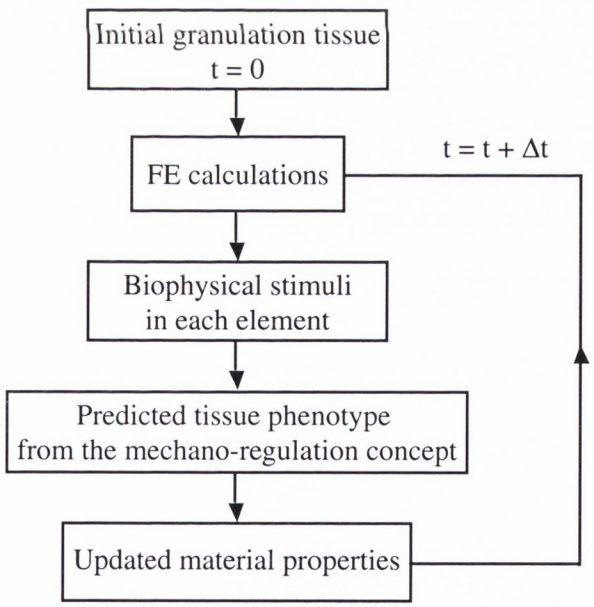

Figure 3.2. The iterative process regulating tissue differentiation.

3.2.3 Temporal smoothing procedure

Four tissue phenotypes can be predicted: fibrous tissue, cartilage, immature, and mature woven bone. Each of these tissue phenotypes has different material properties (defined by the Young's modulus, permeability, Poisson's ratio, porosity, and compression bulk moduli). Therefore, as the mechanical stimuli of each element of the FE mesh representing the fracture change, the tissue phenotype may change. Thus, the material properties would also vary. However, a sudden change of material properties might occur from one iteration to another and creates instabilities due to the highly non-linear coupled equations [78].

To solve this problem, a temporal smoothing procedure was introduced whereby the material properties were only increased or decreased by a small amount every iteration. Initially, an array of n values was defined with the material properties of the granulation tissue. For example, before the first iteration, the Young's modulus array of dimension n is

$$\mathbf{E} = [E_{granu}\ E_{granu}\ \ldots\ E_{granu}\ E_{granu}]^T \tag{3.11}$$

where E_{granu} is the Young's modulus of the granulation tissue. After predicting the new tissue phenotype at the first iteration ($i = 1$), the n^{th} value in the array is given the value of the new phenotype and all the others are moved one row higher (the first row being deleted). Thus after one iteration, the Young's modulus array is

$$\mathbf{E} = [E_{granu}\ E_{granu}\ \ldots\ E_{granu}\ E_{i=1}]^T \tag{3.12}$$

where $E_{i=1}$ is the Young's modulus of the predicted tissue at iteration 1. For the second iteration, a new tissue phenotype is predicted, giving the following array

$$\mathbf{E} = [E_{granu}\ E_{granu}\ \ldots\ E_{i=1}\ E_{i=2}]^T \tag{3.13}$$

This goes into a loop until $i = n$, where

$$\mathbf{E} = [E_{i=1}\ E_{i=2}\ \ldots\ E_{i=n-1}\ E_{i=n}]^T \tag{3.14}$$

Note that the dimension of $\mathbf{E}$ is always n. The material properties after each iteration were calculated using the following equation

$$E_{updated} = \frac{1}{n}\sum_{j=1}^{n} E_j \tag{3.15}$$

where $E_{updated}$ is the updated Young's modulus for iteration i, and E_j is the j^{th} row of the Young's modulus array. Similar equations were used for the permeability, Poisson's ratio, porosity, and compression moduli. The tissue type was determined as the most dominant tissue among the n previous iterations with each iteration having the same weight. A value of 10 was given to n, therefore it would take at least five iterations for the cells to be under similar mechanical environment until a new tissue phenotype is predicted.

3.2.4 Simulation of cell proliferation/migration

Proliferation/migration concept

As discussed in the previous chapter, there is some uncertainty in the literature about the origin of the progenitor cells during fracture healing. However, it seems clear that in some way, cells are recruited from either one or a combination of these origins: the external soft tissues, the inner cambial layer of periosteum, or the bone marrow. It is also rather unclear how cells move, migrate, or proliferate within the tissues. No study so far has investigated cell motion during fracture healing. Random, nondirected cell movement is analogous to diffusion of particles in a gas or a liquid. To mathematically model cell movement, the diffusion equation has been suggested as a first approximation to describe cell motion [79]. This approach was used in this study and the standard equation is of the form

$$c\,\nabla^2 \rho_{cell} = \frac{d\rho_{cell}}{dt} \tag{3.16}$$

where ρ_{cell} is the cell density as a function of time t, c is the proliferation rate of the cells, and ∇ is the gradient operator.

To illustrate this approach, cells moving through a channel of width equal to unity were simulated using the FE method. A channel was meshed and a fixed cell concentration was imposed on one end of the channel (Fig. 3.3). No cells were initially present in the rest of the channel. Using the equation above, cell density was calculated over time. Cell concentration increased over time to simulate the creation of new cell types (Fig. 3.4). The proliferation can be represented by plotting the formation of new cells between times t and $t + \Delta t$, Δt being a fixed period during which cell differentiation occurs. It is shown that initially, the proliferation is highest (cell front) close to the origin of the cells and the cell front moves over time down the channel.

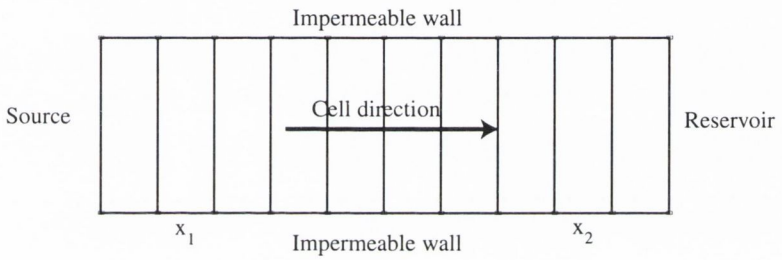

Figure 3.3. Mesh of a channel simulating cell proliferation.

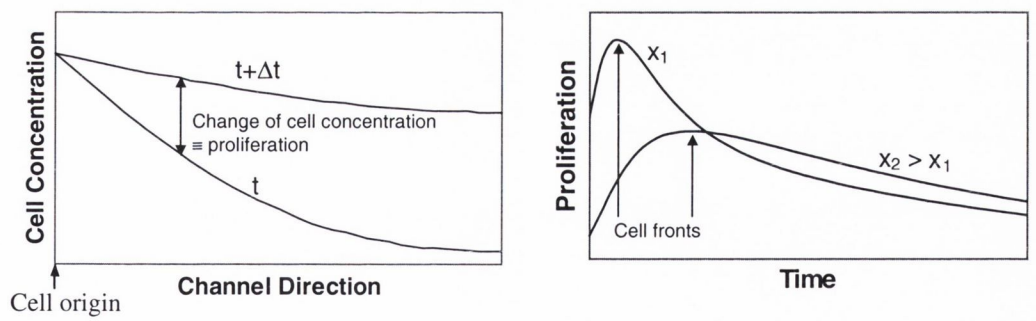

Figure 3.4. Simulation of cells flowing through a channel. The cell density over the length of the channel is shown on the left figure. The change of cell concentration over time for two different positions x_1 and x_2 is shown on the figure on the right.

The rule of mixtures

Cell concentration can be calculated in each element of the fracture healing mesh. However, part of the element considered may still be filled with granulation tissue. Thus, the element is partly composed of differentiated tissue and uncommited granulation tissue. To account for this dual state, the rule of mixtures was used in the following form for the determination of the homogeneised material properties of each element

$$E_{final} = \frac{\rho_{max} - \rho_{cell}}{\rho_{max}} E_{granu} + \frac{\rho_{cell}}{\rho_{max}} E_{updated} \tag{3.17}$$

where E_{final} is the final Young's modulus, ρ_{max} is the maximum cell density, ρ_{cell} is the cell density calculated using Equ. 3.16, and $E_{updated}$ is the Young's modulus determined from Equ. 3.15. Similar equations were used for the permeability, Poisson's ratio, porosity, and compression moduli.

3.2.5 Bone resorption

Bone resorption is a constant process throughout life with removal of osteons by osteoclast cells. During fracture healing resorption occurs once healing has been successful, to restore the initial anatomy of the bone and therefore to restore the 'maximum-minimum design' principle from Roux [3].

It has been shown by Frost [28] that bone resorption is linked with the activity that the patient undergoes. Bone resorption is therefore related to the mechanical loading and more precisely to the strain applied on the tissues. An overloading activity increases bone formation to reduce the local stress while an underactivity increases bone resorption due to stress shielding. In this study, it was hypothesized that once healing has occured the biophysical stimuli in the external and internal calluses are low and resorption progresses due to this low mechanical stimulation.

To test this hypothesis, a resorption field was added in the mechanoregulation concept (Fig. 3.5). It was included in the algorithm and bone resorption was simulated by deleting the corresponding element for the subsequent

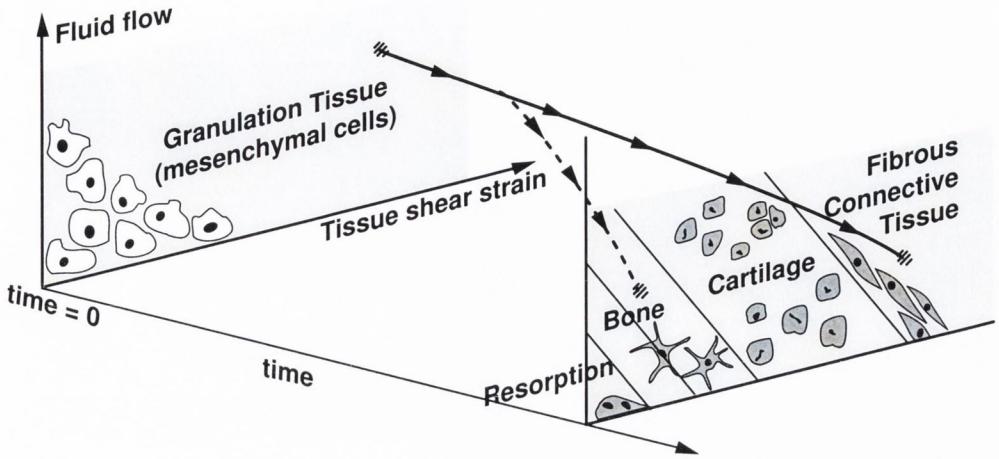

Figure 3.5. Mechano-regulation concept including bone resorption. When the mechanical stimuli become low, the cells are understrained and the osteoclasts start resorbing bone. A resorption field was added for low mechanical stimuli.

FE analyses.

3.2.6 Summary – Algorithm

In summary, a computational approach has been described to predict dynamically tissue differentiation during fracture healing based on a mechano-regulation concept and using a poroelastic FE model. The approach incorporates (i) cell proliferation/migration to account for the origin of the cells during fracture healing and for the gradual proliferation/migration of the cells over the whole healing period, (ii) tissue resorption under low mechanical stimuli. This approach can be summarised in a flow chart shown in Fig. 3.6 that describes the algorithm implemented in this thesis.

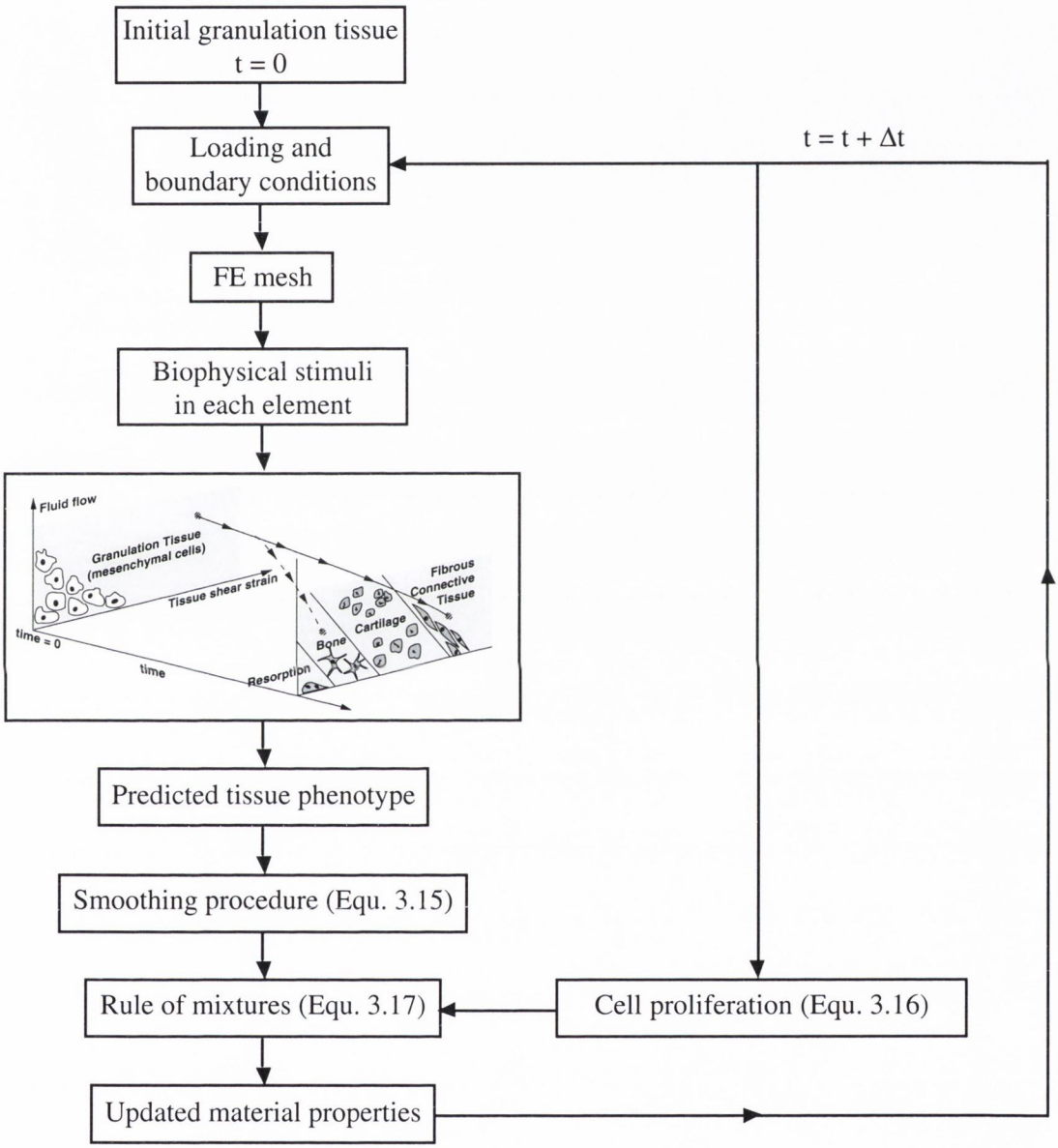

Figure 3.6. Flow chart describing the algorithm implemented to predict tissue differentiation during fracture healing.

3.3 Fracture healing cases

3.3.1 An investigation on the origin of progenitor cells

The effect of cell origin on fracture healing patterns was first investigated since it is unclear from the literature where the cells originate.

Model of a bone fracture

An idealised transverse fracture was modelled using an axisymmetric FE model. The bone diaphysis was cylindrical with a 20 mm outer diameter and a 14 mm inner diameter (dimensions were taken from a mid-diaphysis cross-section composite tibia, SAWBONES Europe Ltd. and are given in Appendix A). A 3 mm fracture gap was modelled and the external callus had a maximum diameter of 28 mm, giving a callus index of 1.4 [56], see Fig. 3.7.

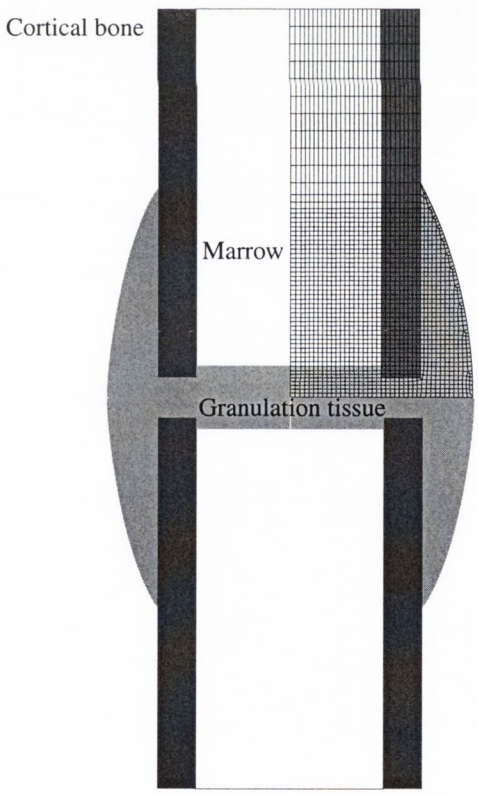

Figure 3.7. Axisymmetric finite element model of a fractured bone.

Following Claes and Heigele [67], an axial ramp loading of 500 N was applied on the cortical bone in 0.5 sec. Nodes in the transverse plane through the centre of the fracture were constrained on the longitudinal direction, while nodes on the centre line of the medullary canal were constrained radially (Fig. 3.8). The mesh had 2048 four-noded isoparametric elements and 2144 nodes.

Cell origin

From the literature, it appears that cells originate from the periosteum and/or the bone marrow. However, the effect of each separate origin has not been studied during fracture healing. In this study, the origin of the progenitor cells

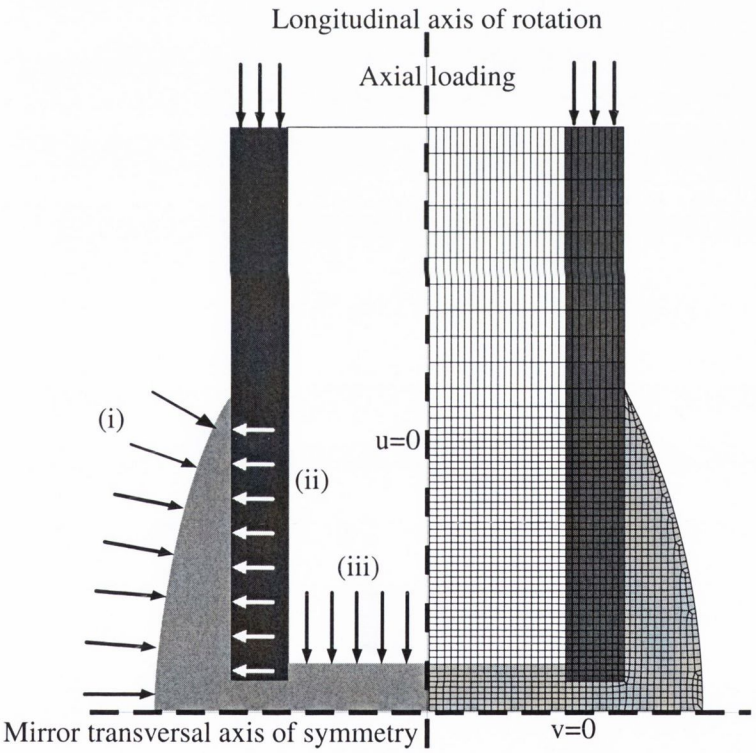

Figure 3.8. Axisymmetric quarter model of a fractured long bone. Due to axis symmetry, only a quarter model of a long bone was modelled. The origin of the cells was modelled by defining a fixed cell concentration on either (i) the periosteum layer, (ii) the periosteum cortical interface, or (iii) the bone marrow interface.

was modelled by defining a fixed cell concentration on either (i) the periosteum layer, (ii) the periosteum bone interface, or (iii) the bone marrow interface, as shown in Fig. 3.8. An equal combination of the three sources was also investigated. The proliferation coefficient was estimated by assuming that a steady-state cell concentration would be reached in the granulation tissue at the end of a 16 week healing period when cells originate from the three origins. This gave a proliferation coefficient of 1.2 mm^2/day when cells originate from one site and a coefficient of 0.06 mm^2/day when cells originate from all three sites. Cell concentration was calculated and the differentiation scheme was implemented to predict tissue phenotype forming every day of the healing period.

Material properties

A value of 20000 MPa was taken for cortical Young's modulus [67]. The permeability of cortical bone is very low (1×10^{-17} m^4/Ns [80]), due to a low porosity of 0.04 [81, 82]. A Poisson's ratio of 0.3 was taken [80].

Two types of woven bone were modelled representing different stages of maturation. A value of 6000 MPa for the Young's modulus of the mature bone was taken according to Claes and Heigele [67]. For the immature woven bone, a value of 1000 MPa was taken corresponding to a lower mineralisation rate. The trabecular bone permeability is rather high [83] due to its high porosity of 0.8 [84]. The value of Ochoa and Hilberry [85] was taken as the permeability of mature woven bone (3.7×10^{-13} m^4/Ns), while a lower value was taken for an immature woven bone (1×10^{-13} m^4/Ns). A Poisson's ratio of 0.3 was taken for both types of woven bone.

The Young's modulus of cartilage was taken as 10 MPa (large variation of values available from the literature) and a permeability of 5×10^{-15} m^4/Ns was taken [86]. The Poisson's ratio of cartilage varies between 0.1 and 0.3 [87]. Thus, a Poisson's ratio of 0.1667 was taken. A porosity of 0.8 was taken for cartilage [68]. For all other soft tissues, the same porosity and Poisson's ratio

	Granulation tissue	Fibrous tissue	Cartilage	Marrow	Immature bone	Mature bone	Cortical bone
Young's modulus (MPa)	0.2	2	10	2	1000	6000	20000
Permeability (m^4/Ns)	1E-14	1E-14	5E-15	1E-14	1E-13	3.7E-13	1E-17
Poisson's ratio	0.1667	0.1667	0.1667	0.1667	0.3	0.3	0.3
Solid compression modulus (MPa)	2300	2300	3400	2300	13920	13920	13920
Fluid compression modulus (MPa)	2300	2300	2300	2300	2300	2300	2300
Porosity	0.8	0.8	0.8	0.8	0.8	0.8	0.04

Table 3.1. Material properties of tissues.

as cartilage were chosen [26, 75, 88]. The Young's modulus of fibrous tissue was taken as 2 MPa [89] for a permeability of 1×10^{-14} m^4/Ns. The material properties for the bone marrow were estimated to be 2 MPa for the Young's modulus (soft tissue), and 1×10^{-14} m^4/Ns for the permeability (same as fibrous tissue). The Young's modulus of the granulation tissue was determined so that an initial interfragmentary displacement of 1 mm was obtained for a loading of 500 N, as used for example by Goodship and Kenwright [17]. This gave a value of 0.2 MPa. The permeability of the granulation tissue had the same value as that of fibrous tissue.

The fluid compression modulus of the interstitial fluid is assumed to be the same as salt water and a value of 2300 MPa was taken for each tissue [90]. The solid compression modulus of soft tissues is about the same value as the fluid compression modulus [80], and thus a value of 2300 MPa was used for the granulation tissue, the fibrous tissue, and the bone marrow. The solid compression modulus of cartilage was taken as 3400 MPa [91]. The material properties are given in Table 3.1.

Mechano-regulation diagram

The mechano-regulation diagram used to regulate tissue differentiation is shown in Fig. 3.9. The boundary values were taken directly from Huiskes *et al.* [26],

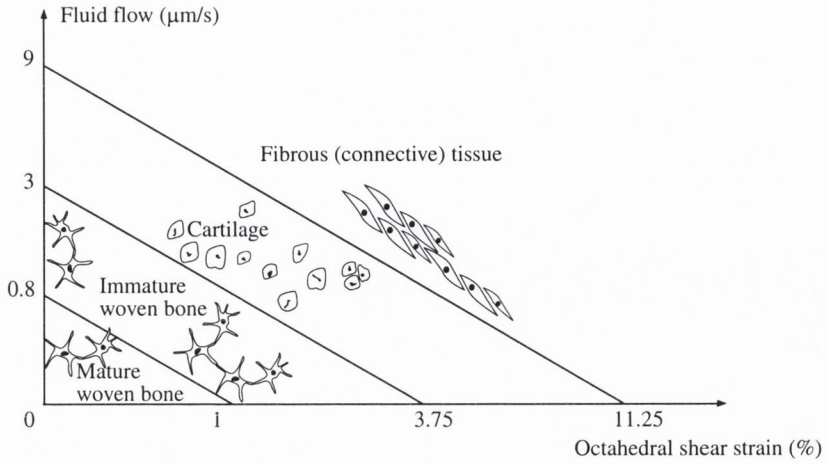

Figure 3.9. Mechano-regulation diagram regulating tissue differentiation (not drawn to scale).

except that the woven bone field was divided into two fields: an immature woven bone and a mature woven bone.

Parametric study

Some of the material properties used in this study are not well defined from experimental results, therefore a parametric study on the material properties was performed. A parametric study on Young's modulus (Table 3.2), Poisson's ratio (Table 3.3), permeability (Table 3.4), solid compression modulus (Table 3.5), fluid compression modulus (Table 3.6), and porosity (Table 3.7) was performed. For most cases only one material property for only one tissue type was changed. A low and high bound were studied and the values stayed within reasonable limits.

To investigate the influence of the boundaries of the mechano-regulation diagram, the boundaries separating the formation of one tissue type to another were varied, as illustrated in Fig. 3.10.

Tissue type	Cortical bone	Marrow	Granulation tissue	Fibrous tissue	Cartilage	Immature bone	Mature bone
#	1	2	3	4	5	6	7
'Normal'	20000	2	0.2	2	10	1000	6000
Low 1	15000	–	–	–	–	–	–
High 1	25000	–	–	–	–	–	–
Low 2	–	0.1	–	–	–	–	–
High 2	–	10	–	–	–	–	–
Low 3	–	–	0.01	–	–	–	–
High 3	–	–	1	–	–	–	–
Low 4	–	–	–	0.1	–	–	–
High 4	–	–	–	10	–	–	–
Low 5	–	–	–	–	1	–	–
High 5	–	–	–	–	100	–	–
Low 6	–	–	–	–	–	300	–
High 6	–	–	–	–	–	6000	–
Low 7	–	–	–	–	–	–	1000
High 7	–	–	–	–	–	–	10000

Table 3.2. Young's modulus parametric study (in MPa). – indicates that the material properties were identical to Table 3.1.

Tissue type	Cortical bone	Marrow	Granulation tissue	Fibrous tissue	Cartilage	Immature bone	Mature bone
#	1	2	3	4	5	6	7
'Normal'	0.3	0.1667	0.1667	0.1667	0.1667	0.3	0.3
Low 1	0.25	–	–	–	–	–	–
High 1	0.35	–	–	–	–	–	–
Low 2	–	0.1	–	–	–	–	–
High 2	–	0.3	–	–	–	–	–
Low 3	–	–	0.1	–	–	–	–
High 3	–	–	0.3	–	–	–	–
Low 4	–	–	–	0.1	–	–	–
High 4	–	–	–	0.3	–	–	–
Low 5	–	–	–	–	0.1	–	–
High 5	–	–	–	–	0.3	–	–
Low 6	–	–	–	–	–	0.2	0.2
High 6	–	–	–	–	–	0.35	0.35

Table 3.3. Poisson's ratio parametric study. – indicates that the material properties were identical to Table 3.1.

Tissue type	Cortical bone	Marrow	Granulation tissue	Fibrous tissue	Cartilage	Immature bone	Mature bone
#	1	2	3	4	5	6	7
'Normal'	1E-17	1E-14	1E-14	1E-14	5E-15	1E-13	3.7E-13
Low 1	1E-19	–	–	–	–	–	–
High 1	1E-15	–	–	–	–	–	–
Low 2	–	1E-16	–	–	–	–	–
High 2	–	5E-13	–	–	–	–	–
Low 3	–	–	1E-16	–	–	–	–
High 3	–	–	5E-13	–	–	–	–
Low 4	–	–	–	1E-16	–	–	–
High 4	–	–	–	5E-13	–	–	–
Low 5	–	–	–	–	1E-16	–	–
High 5	–	–	–	–	5E-13	–	–
Low 6	–	–	–	–	–	1E-14	–
High 6	–	–	–	–	–	3.7E-13	–
Low 7	–	–	–	–	–	–	1E-14
High 7	–	–	–	–	–	–	5E-13

Table 3.4. Permeability parametric study (in m^4/Ns). – indicates that the material properties were identical to Table 3.1.

Tissue type	Cortical bone	Marrow	Granulation tissue	Fibrous tissue	Cartilage	Immature bone	Mature bone
#	1	2	3	4	5	6	7
'Normal'	13920	2300	2300	2300	3400	13920	13920
Low 1,6,7	10000	–	–	–	–	10000	10000
High 1,6,7	15000	–	–	–	–	15000	15000
Low 2,3,4,5	–	1000	1000	1000	1000	–	–
High 2,3,4,5	–	5000	5000	5000	5000	–	–
High 5	–	–	–	–	7000	–	–

Table 3.5. Solid compression modulus parametric study (in MPa). – indicates that the material properties were identical to Table 3.1.

Tissue type	Cortical bone	Marrow	Granulation tissue	Fibrous tissue	Cartilage	Immature bone	Mature bone
#	1	2	3	4	5	6	7
'Normal'	2300	2300	2300	2300	2300	2300	2300
Low	1000	1000	1000	1000	1000	1000	1000
High	5000	5000	5000	5000	5000	5000	5000

Table 3.6. Fluid compression modulus parametric study (in MPa). – indicates that the material properties were identical to Table 3.1.

Tissue type	Cortical bone	Marrow	Granulation tissue	Fibrous tissue	Cartilage	Immature bone	Mature bone
#	1	2	3	4	5	6	7
'Normal'	0.04	0.8	0.8	0.8	0.8	0.8	0.8
Low 1	0.01	–	–	–	–	–	–
High 1	0.1	–	–	–	–	–	–
Low 2	–	0.4	–	–	–	–	–
High 2	–	0.9	–	–	–	–	–
Low 3	–	–	0.4	–	–	–	–
High 3	–	–	0.9	–	–	–	–
Low 4	–	–	–	0.4	–	–	–
High 4	–	–	–	0.9	–	–	–
Low 5	–	–	–	–	0.4	–	–
High 5	–	–	–	–	0.9	–	–
Low 6	–	–	–	–	–	0.4	–
High 6	–	–	–	–	–	0.9	–
Low 7	–	–	–	–	–	–	0.7
High 7	–	–	–	–	–	–	0.9

Table 3.7. Porosity parametric study. – indicates that the material properties were identical to Table 3.1.

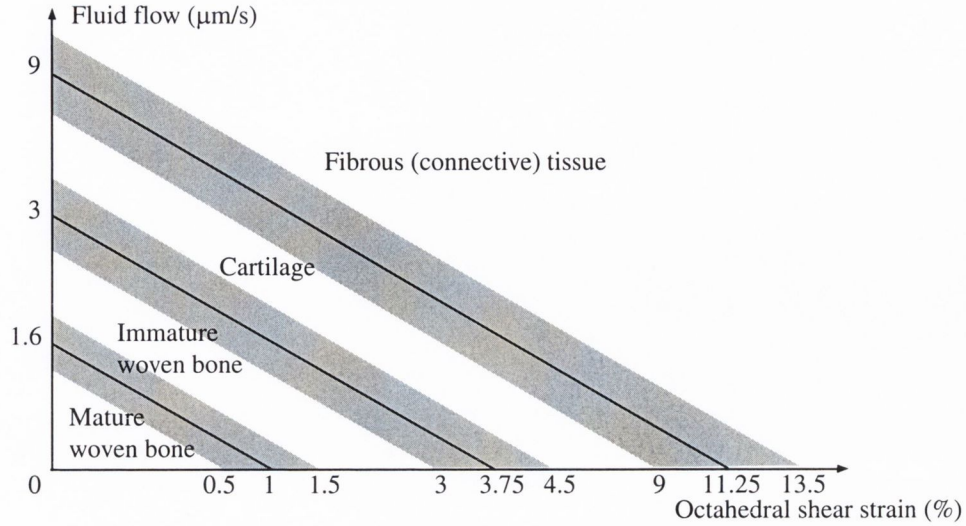

Figure 3.10. Parametric study of the boundaries of the mechano-regulation diagram (not to scale).

3.3.2 Influence of fracture gap

To investigate the influence of fracture gap and to test the stability of the algorithm, two other fracture gap sizes were investigated: 1 and 6 mm (Fig. 3.11). The 1 mm fracture gap mesh had 1926 four-noded isoparametric elements and

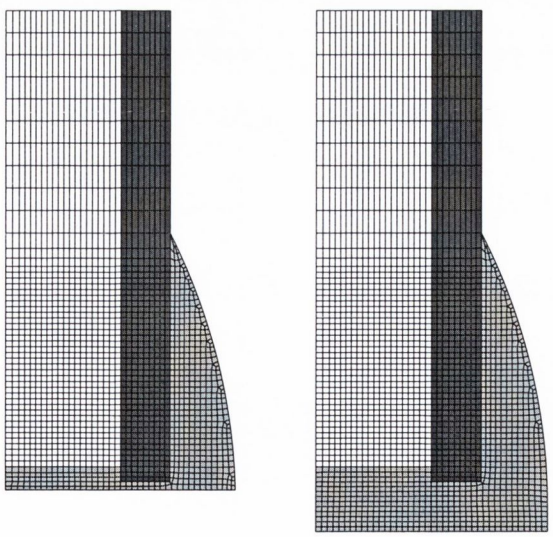

a.) 1mm. b.) 6 mm.

Figure 3.11. 1 mm and 6 mm fracture gap size models.

2020 nodes. The 6 mm fracture gap mesh had 2242 four-noded isoparametric elements and 2343 nodes. Both meshes were based on the same geometry as the 3 mm gap size described in Section 3.3.1. The dimensions are shown in Appendix A.

To investigate the influence of loading depending on the fracture gap size, an axial loading of 300 N and 500 N were investigated. The loading and boundary conditions were the same as described in Section 3.3.1. The material properties were the same as described in Table 3.1. Cells originated equally from three sources: periosteum layer, periosteum cortical interface, and bone marrow interface. The same proliferation coefficient of 0.06 mm^2/day was used. Bone resorption was simulated for the three different fracture gap sizes and the two loading magnitudes (Fig 3.12).

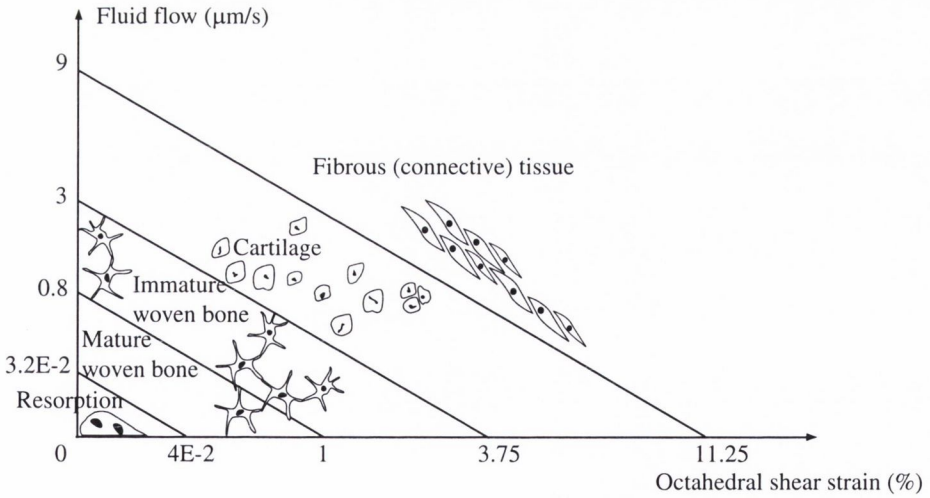

Figure 3.12. Mechano-regulation diagram including bone resorption (not drawn to scale).

3.3.3 Influence of bending loading

Bending loading generates higher stresses and strains than axial loading. However, no bending load could be simulated using the axisymmetric model solved in DIANA. Thus, a plane strain study was undertaken.

A plane strain fracture model

A plane strain mesh was created from the same dimension as the axisymmetric model (Fig. 3.13). A fracture gap of 3 mm was simulated. The mesh had 4096 four-noded isoparametric elements and 4231 nodes.

The cells originated from three sources: (i) the periosteum layer, (ii) the periosteum cortical interface, and (iii) the bone marrow interface as shown in Fig. 3.13. The same proliferation coefficient of 0.06 mm^2/day was used.

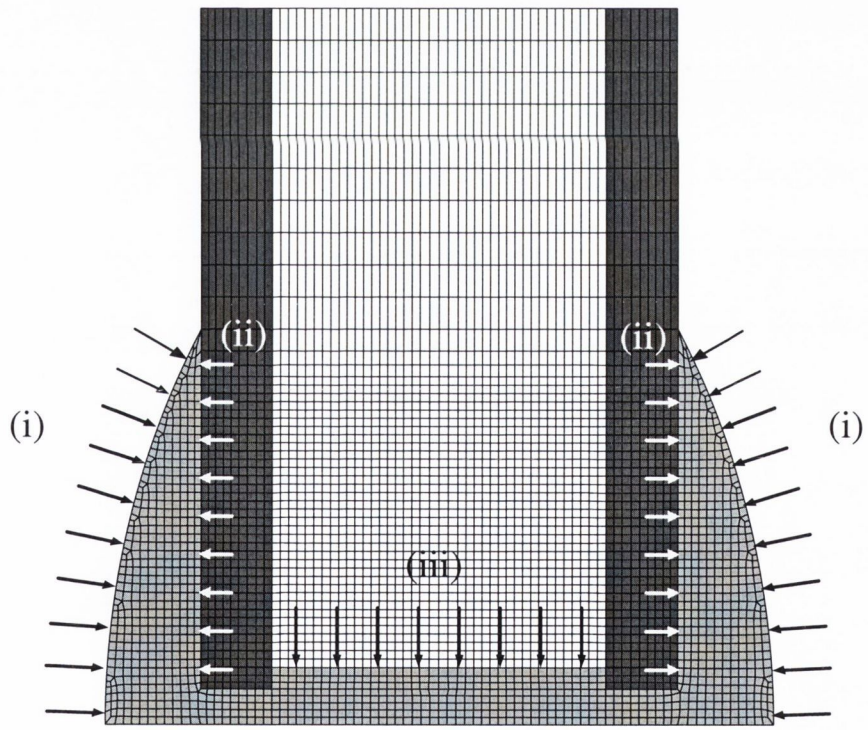

Figure 3.13. Transverse plane strain model. The origin of the cells are (i) the periosteum layer, (ii) the periosteum cortical interface, and (iii) the bone marrow interface.

All tissues were modelled as poroelastic materials with properties defined in Table 3.1.

Loading and boundary conditions

A ramp axial loading was investigated with different loading conditions. An axial load of identical magnitude on both sides was applied to simulate loading in compression only. Both lower and higher loading conditions (± 12.5 %) were simulated. The magnitude of the loading was applied so that the same deformation between the bone ends would occur in an axial loading with the plane strain model as with the 3 mm axisymmetric model with a loading of 500 N. The model was constrained to move longitudinally in the medial section and radially at the proximal part of the cortical bone (Fig. 3.14). The mechano-regulation diagram used to regulate tissue differentiation was the same as in Fig. 3.12.

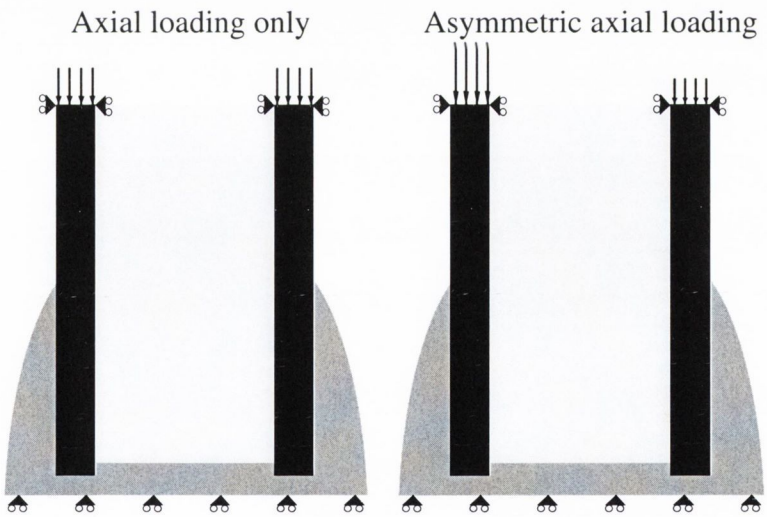

Figure 3.14. Boundary conditions and loading for the transverse plane strain model.

3.3.4 The influence of fracture type

An oblique fracture with a gap size of 3 mm and a callus index of 1.4 was modelled to investigate the influence of fracture type. The mesh had 8732 four-noded isoparametric elements and 8931 nodes (Fig. 3.15). The cells were simulated to originate from (i) the periosteum layer, (ii) the periosteum cortical interface, and (iii) the bone marrow interface (Fig. 3.15). The material

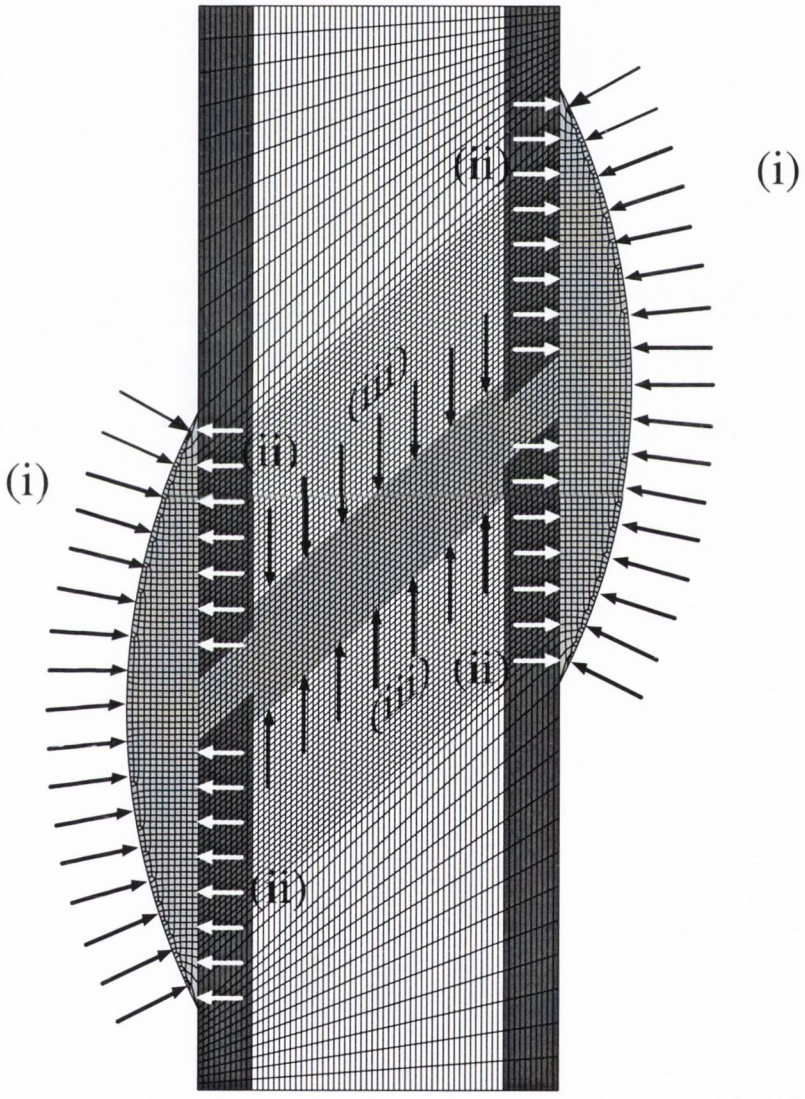

Figure 3.15. Oblique plane strain model. The origin of the cells are (i) the periosteum layer, (ii) the periosteum cortical interface, and (iii) the bone marrow interface.

properties were the same as defined in Table 3.1. The same mechano-regulation diagram described in Fig. 3.12 was used. As investigated in the case of a transverse fracture, an axial loading combined with bending load was perfomed as shown in Fig. 3.16.

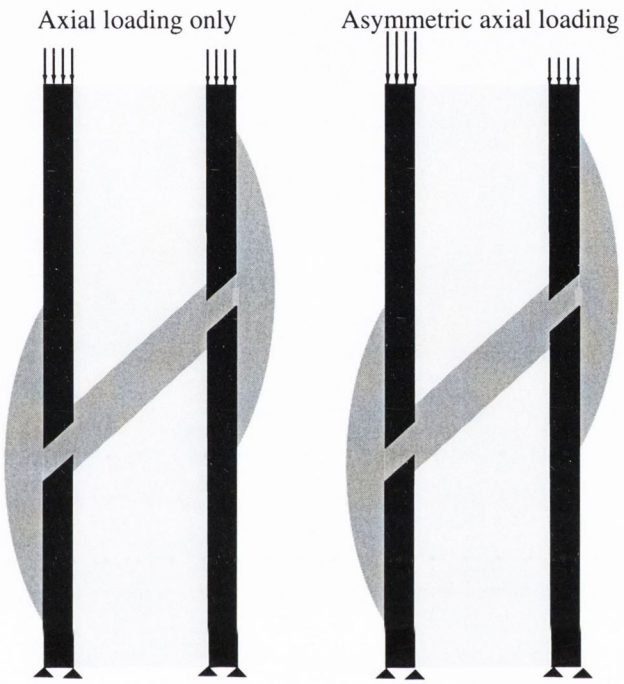

Figure 3.16. Boundary conditions and loading for the oblique model.

3.3.5 A 3D model of a human tibia

Axisymmetric or plane strain models have many limitations and can never fully describe the exact geometry and/or loading of the bone. Therefore, a 3D model was developed and solved for one fracture type and loading conditions.

Model

The replica of a human left tibia was obtained from SAWBONES EUROPE AB, Sweden (Part # 1101). The composite tibia was sectioned every 3 mm and each slice was scanned. The contours of the cortical bone on the outer and inner diameter were digitised for each slice. The interface between the

medullary cavity and the cancellous bone were also digitised when available. Each boundary was imported as an IGES file in ANSYS (Swanson Analysis Systems Inc., Houston, PA). The tibia was reconstructed and meshed in ANSYS. A fracture of 3 mm was simulated with a homogeneous external callus of callus index of 1.4.

A unilateral external fixator was modelled and inserted in the anterior-medial side of the tibia. The fixator has a relatively low stiffness due to the modelling of two pins only. The dimensions of the fixator are given in Appendix B. The mesh has 12411 eight-noded hexahedral elements and 15225 nodes (Fig. 3.17). A cross-section of the partial mesh is shown in Fig. 3.18 in the antero-posterior and medio-lateral directions. To reduce computing time, cortical bone was modelled as a linear elastic material. The external fixator was also modelled as linear elastic with a Young's modulus of 200 GPa and a Poisson's ratio of 0.3. All other tissues were modelled as poroelastic materials as given in Table 3.1. However, to further reduce computing time, the model was first solved using linear elastic properties and the calculated deformations at the proximal and distal parts of the partial mesh were applied in a subsequent analysis. The partial mesh was solved as a poroelastic analysis. To the author's knowledge, the physiological muscle loading acting during a daily activity of a normal or fractured tibia is not known from the literature. Thus, an axial load was applied on the proximal part of the tibia while the distal part was restrained from any movement. Two loading magnitudes were investigated: 300 N and 500 N. Cell proliferation was also modelled from the periosteum layer, the periosteum cortical interface, and the bone marrow interface. A total healing period of 16 weeks was simulated, giving a proliferation coefficient of 0.1 mm^3/day. To reduce computing time, cell concentration was calculated every week, time for wich tissue differentiation was simulated. Healing was defined as successful when all the callus was ossified. In that case, the external fixator was removed and the analysis continued until no more mechanical stimuli changes occured. The flow chart given in Fig. 3.6 was thus

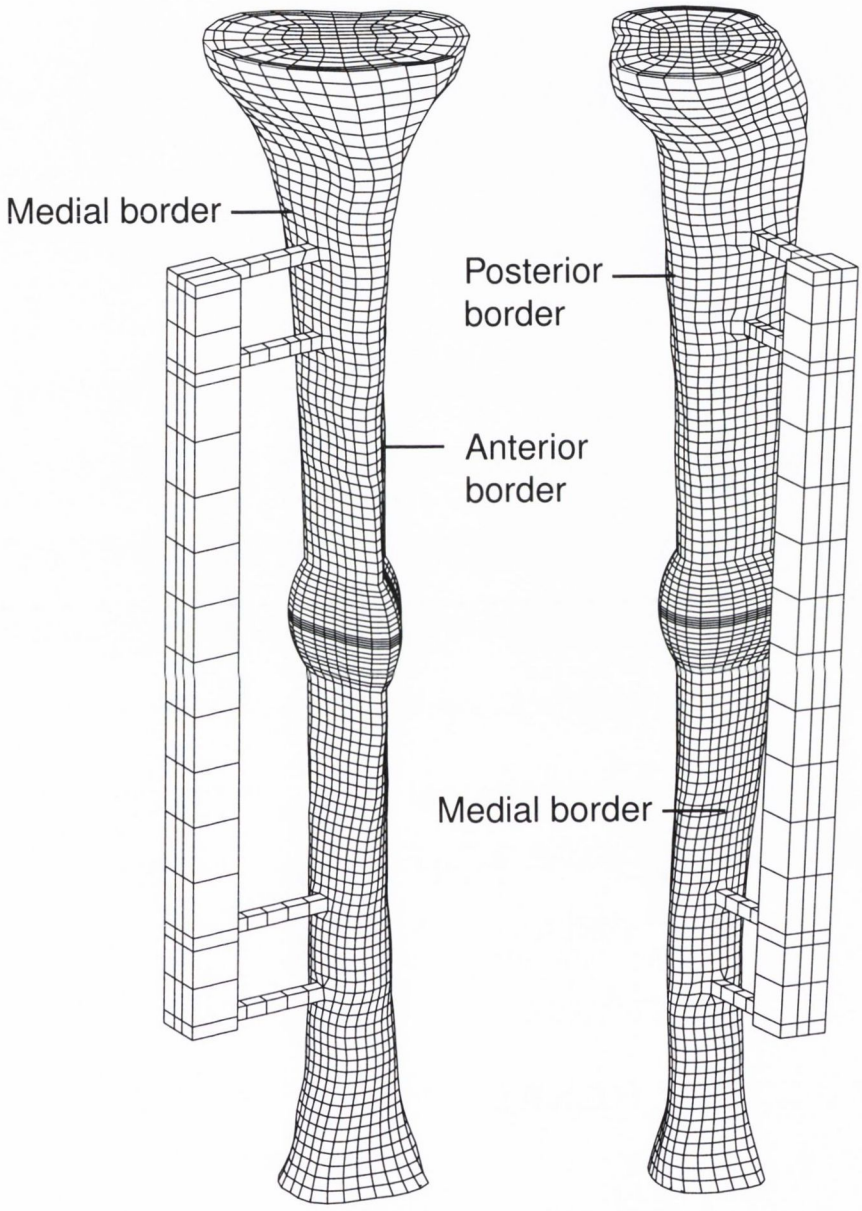

Figure 3.17. Anterior and medial views of the 3D mesh.

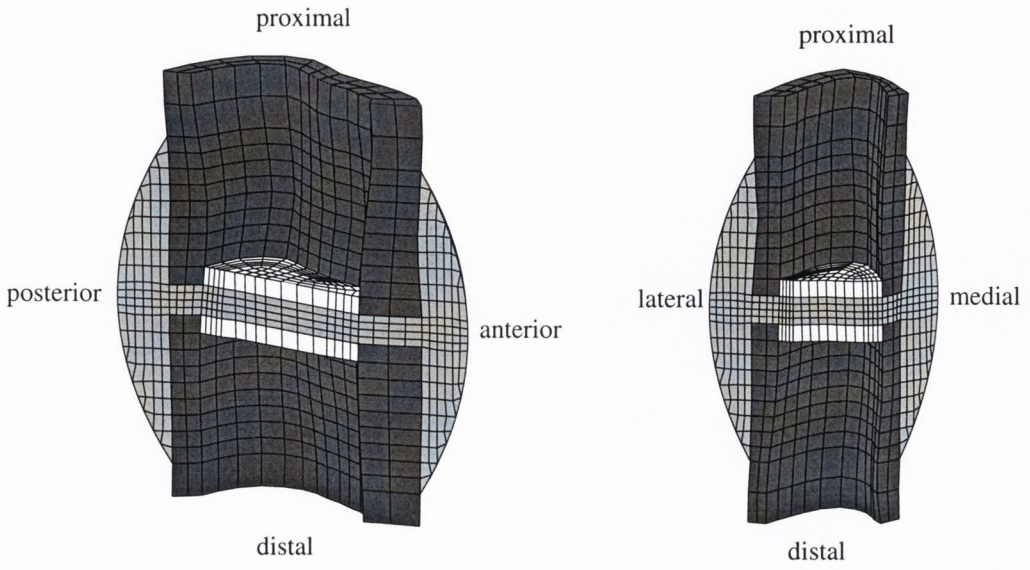

Figure 3.18. Cross sections of the partial mesh.

modified and the flow chart given in Fig. 3.19 was implemented for the 3D analysis.

3.3.6 Clinical applications for monitoring of fracture healing

External fixators in the tibia have remained very popular due to the ease of controlling the amount of motion transferred to the fracture. In this section, two methods used clinically to monitor fracture healing are described.

Bending test

A simulated four-point bending test was performed at every stage of tissue differentiation to predict the bending stiffness of the fracture as healing occurs (Fig. 3.20). A force, F, was applied on both ends of the bone. Constraints, R, were applied close to the fracture callus and the deflection of the bone was calculated. In black is shown the undeformed tibia, and in grey a magnified view of the deformed tibia.

The fracture stiffness is defined as the bending moment of the healing tibia over the angle of deformation [55]. Thus, following Fig. 3.20 and assuming

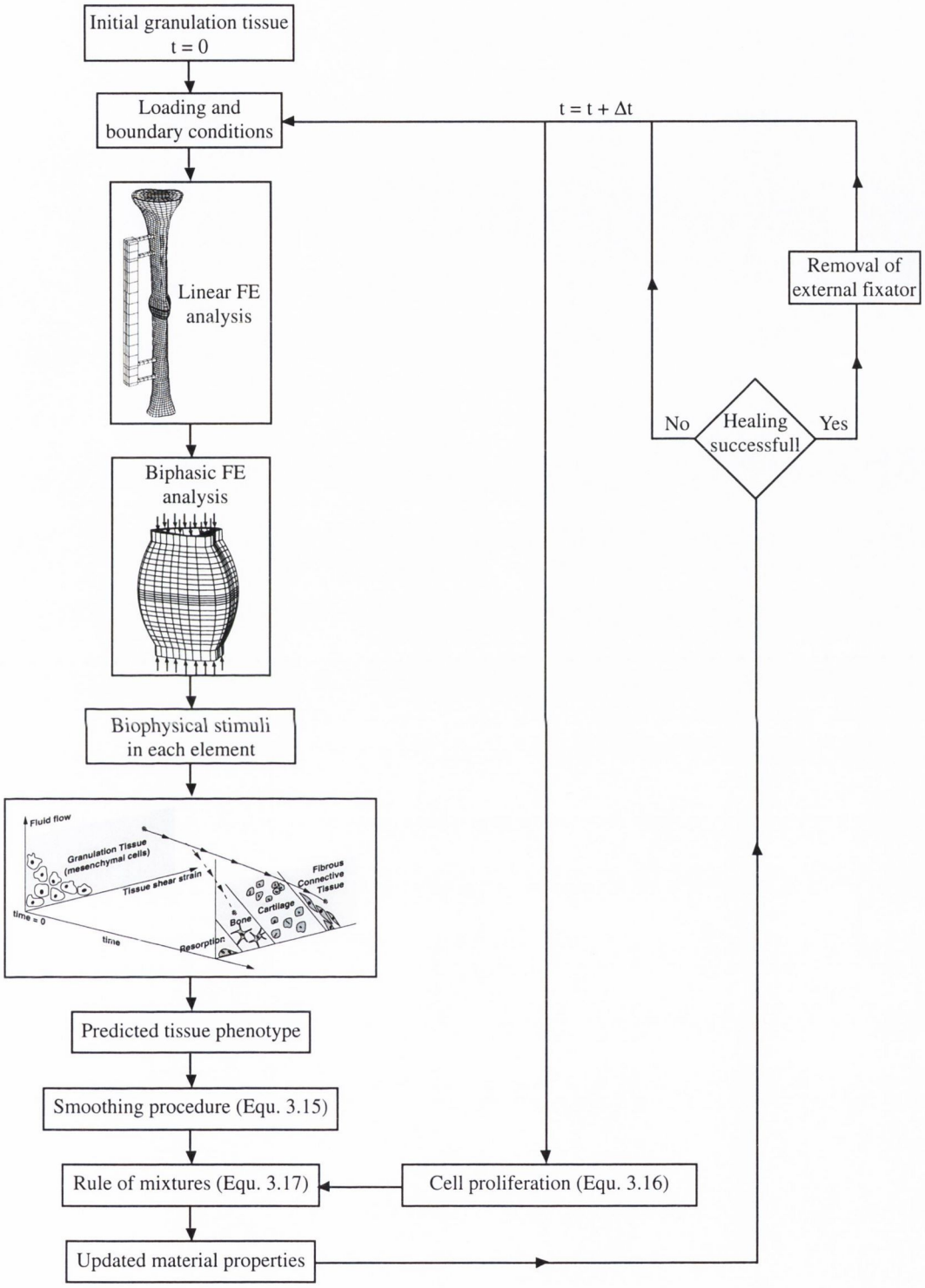

Figure 3.19. Flow chart describing the fracture healing simulation for the 3D model.

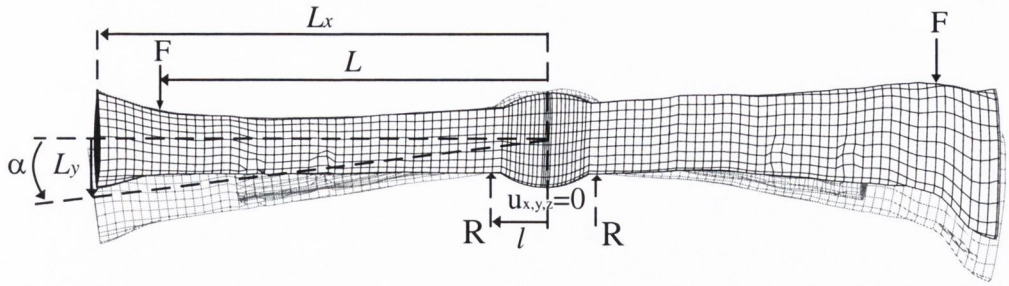

Figure 3.20. Simulation of bending test to predict bending fracture stiffness of the fractured bone.

small deflection

$$\text{Fracture stiffness} = \frac{FL - Rl}{\alpha} \tag{3.18}$$

where F is the force acting at one end of the tibia, L is the distance between the fracture and the force F, R is the reaction force at the restrained point of the tibia, l is the distance between the fracture and the restrained point, and α is the angle between the undeformed tibia (in black) and the deformed tibia (in grey). To calculate the angle of deformation α, the following equation was used

$$\tan \alpha = \frac{L_y}{L_x} \tag{3.19}$$

For each iteration, the material properties of the predicted callus were used and a linear analysis was performed to save computational time. The reaction forces and the deformation were calculated and plotted over time.

Interfragmentary strain as an indicator of healing

It was suggested by Perren [60] that interfragmentary strain could be an indicator of fracture healing. This was followed by experimental and clinical studies where the interfragmentary strain (or the movement of the external fixator) was controlled or monitored. To investigate whether the interfragmentary strain could be used as an indicator of success of healing, the loading applied in the axisymmetric model was applied depending on the value of the predicted interfragmentary strain. It has been shown that as healing oc-

curs, the body weight applied on the cortical bone increases over time [92]. Thus, it is hypothesized that initially a constant low load is applied on the fracture reflecting the unability of the tissues to support a compressive load. As healing occurs, cartilage is the first tissue able to withstand compressive loading (corresponding to an interfragmentary strain of about 10 %). Thus, it is hypothesized that loading increases until full weight bearing is achieved (Fig. 3.21). This hypothesis was implemented in the algorithm for the axisymmetric model with a fracture gap size of 3 mm when cells originate from the periosteum layer, the periosteum cortical interface, and the bone marrow. To obtain a similar initial interfragmentary displacement as in the constant load model, the stiffness of the granulation tissue was reduced to 0.02 MPa.

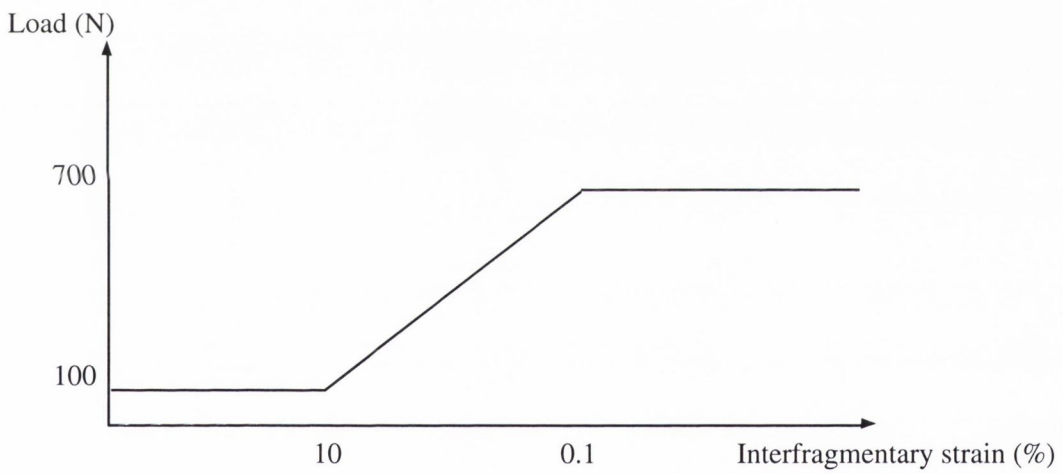

Figure 3.21. Loading variation as a function of interfragmentary strain.

3.4 Conclusion

A numerical approach has been described in this chapter to simulate tissue differentiation and modelling during fracture healing. It is based on the mechano-regulation concept developed by Prendergast *et al.* [74] and accounts for the proliferation/migration of progenitor cells. It is intended to simulate the regenerative and resorptive phases of fracture healing.

For the model to have any predictive value, it must give different results in different circumstances, and the results must, at the very least, show the same trends as those observed by experiment or in clinical practice. To do this, (i) an axisymmetric model is investigated for which cell origin, loading and fracture gap size are varied, (ii) the effect of bending and oblique fracture are investigated using a plane strain model, and (iii) the approach is applied to a more realistic 3D model of a tibia and to clinical applications for monitoring fracture healing.

Chapter 4

Results

Contents

All the predicted healing patterns are shown dynamically in a video format on the web: www.mme.tcd.ie/Groups/Bioengineering/Fracture-Healing/DLacroix/

4.1 Origin of the progenitor cells

Using the method described in Section 3.2.4, the effect of cell origin on tissue differentiation in the fracture callus was investigated. Cells were simulated to originate from the periosteum layer, the periosteum cortical interface, and the bone marrow interface. The effect of cell origin on the mechanical stimuli and therefore on the predicted tissue phenotype was investigated. Finally, the difference of results obtained by simulating cell proliferation/migration as opposed to simulating the cells immediately distributed within the callus was analysed.

4.1.1 Healing patterns

When progenitor cells originate from the periosteum layer, it is predicted that intramembranous bone formation occurs along the periosteum at some distance from the fracture site, see the green region in Fig. 4.1 (note the lighter colours indicates a lower amount of differentiated tissue). Cartilaginous tissue is predicted in the remaining external callus and in the medullary cavity. Fibrous tissue is predicted close to the fracture ends. Ossification of the external callus follows, giving rise to a bridging of the fracture gap through endochondral ossification. Bridging causes the strain to reduce in the remaining soft tissues – the result is that the fibrous tissue in the interfragmentary gap is replaced by cartilage, and then bone, as stabilisation occurs.

When cells originate from the periosteum cortical interface, similar healing patterns occur except that the region of intramembranous bone formation is somewhat larger. As in the case of cells originating from the periosteum layer, endochondral ossification of the external callus proceeds to complete ossification and bridging of the external callus. Final bony bridging occurs

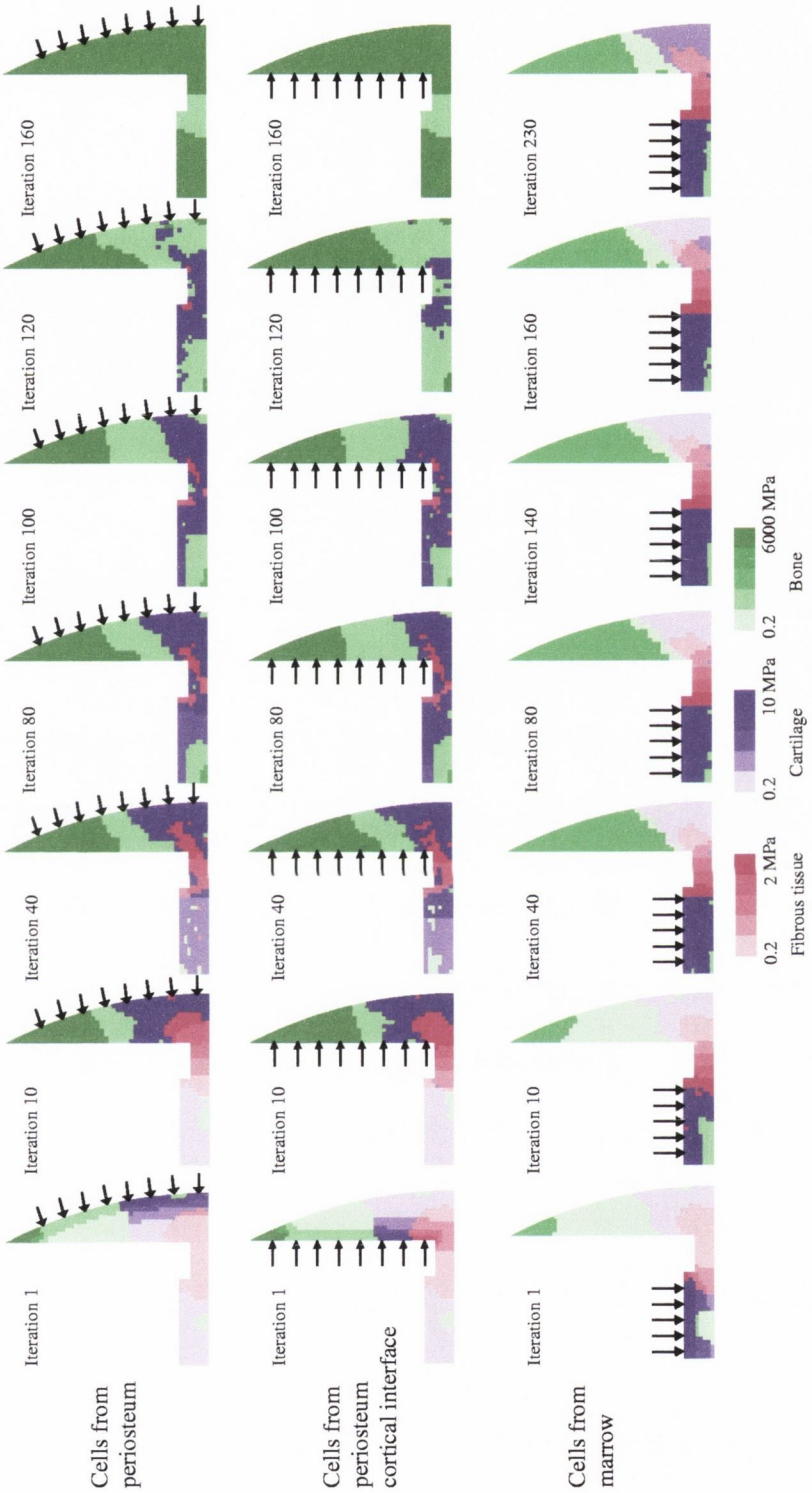

Figure 4.1. Predicted healing patterns when cells originate from the periosteum layer, the periosteum cortical interface, or the bone marrow interface. The tissue phenotype is given and its stiffness that depends on the amount of differentiated cells is also shown. The arrows indicate the origin of the cells.

close to the bone ends and is followed by differentiation of the interfragmentary soft tissue into bone.

When cells originate from the bone marrow only, cartilage is first predicted in the medullary cavity. Bone ossification is predicted in the exernal callus. However, due to the cell distribution, there is a small cell density in the external callus and therefore no stiff external callus forms. For this reason, ossification does not proceed because of a lack of stabilisation at the fracture ends. When the interfragmentary strain is reduced, ossification proceed but through ossification in the medullary canal leading to the very different situation of bridging in the internal callus [93].

Considering the results described previously and the hypotheses of cell origin described in the literature, it may be expected that cells originate from several origins and therefore that in some way, each of the three origins contributes to the cell distribution within the fracture. When cells originate from the three sources, it is predicted that, healing occurs through formation of both an external callus and an internal callus (Fig. 4.2). Stabilisation is mainly achieved by bone formation in the external callus since the contribution from the bone marrow is much slower than from the periosteum sources (Fig. 4.1).

For comparison, the prediction when cells are instantaneously distributed in the callus was analysed. It is found that intramembranous bone is predicted further from the fracture site and cartilaginous tissue is predicted in the remaining callus and medullary cavity (Fig. 4.2). There is a very rapid ossification of the callus leading to bridging of the fracture gap.

4.1.2 Mechanical stimuli

The predicted healing patterns change over time due to a change of mechanical stimuli leading to a different tissue formation field in the mechano-regulation diagram (Fig. 4.3). It is predicted that at the first iteration, the fluid flow and the octahedral shear strain are generally high but the elements cross over the different fields of fibrous tissue, cartilaginous tissue and immature bone. At

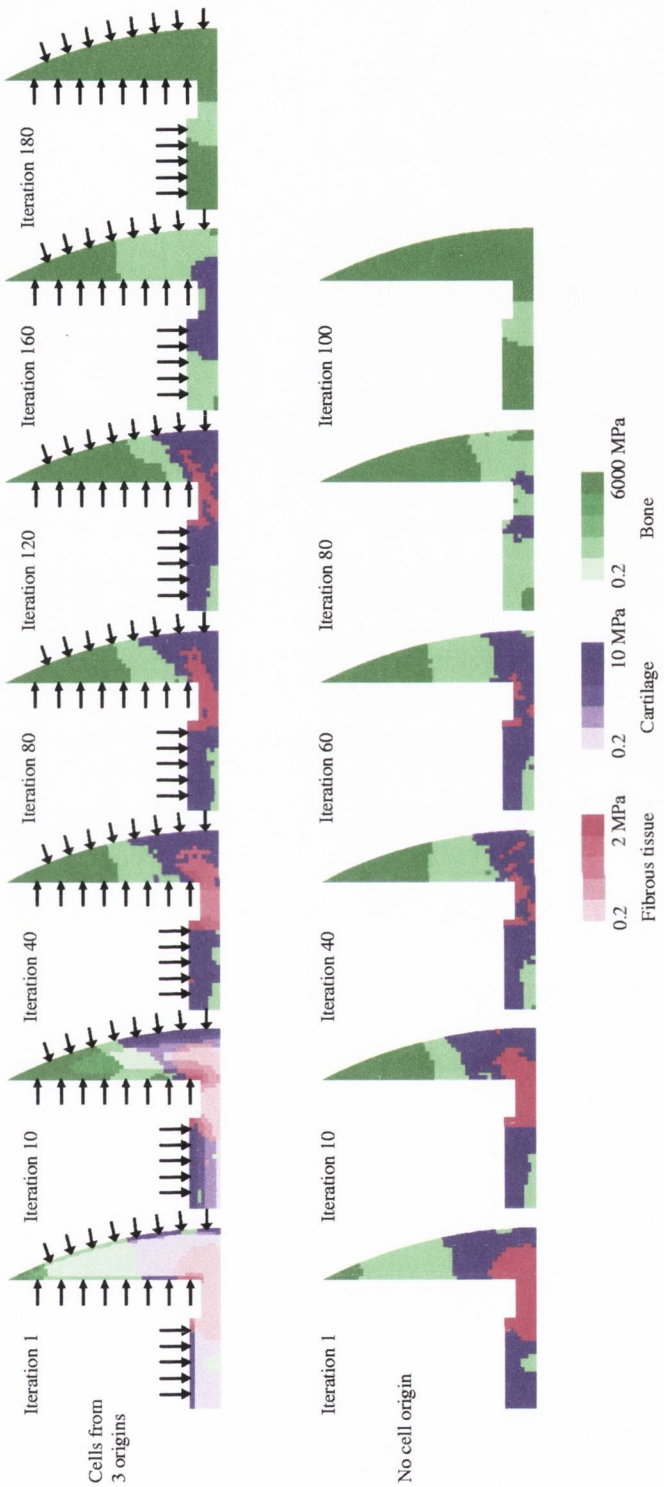

Figure 4.2. Predicted healing patterns when cells originate from the three origins and when cells are immediately distributed within the fracture. The tissue phenotype is given and its stiffness that depends on the amount of differentiated cells is also shown. The arrows indicate cell origin.

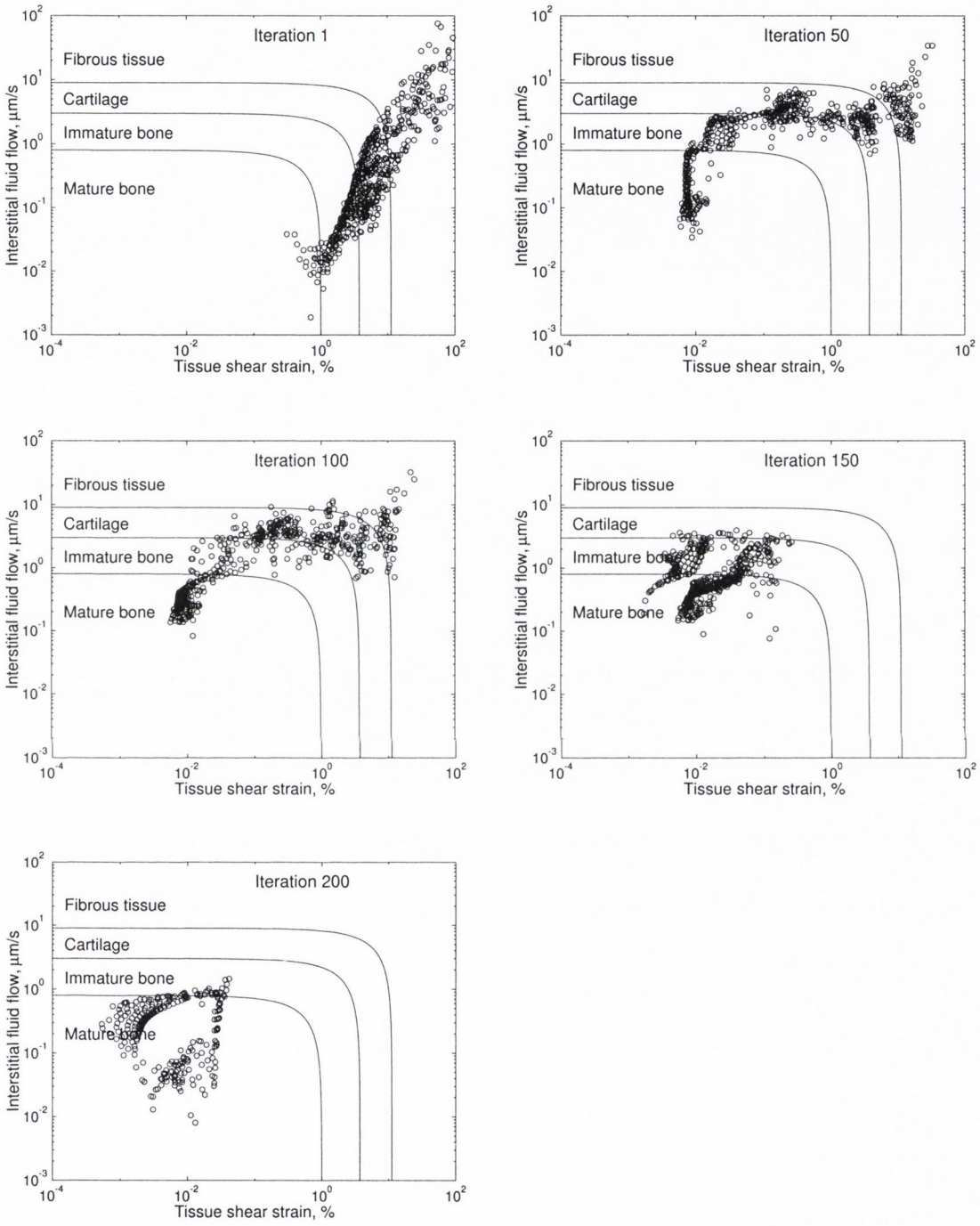

Figure 4.3. Mechano-regulation diagrams at iteration 1, 50, 100, 150, and 200 when cells originate from the three sources. The interstitial fluid flow is plotted against the tissue shear strain for each element represented as a circle dot. Note the log-log scale.

iteration 50, the fluid flow is significantly increased although the strain reduces. The mechanical stimuli do not change much over the next 50 iterations. Fluid flow and octahedral shear strain decrease little by little to predict mainly cartilage and immature woven bone at iteration 150. Once stabilisation is sufficient, both mechanical stimuli decrease to form bone in the entire fracture.

There are differences of mechanical stimuli within the fracture callus (Fig. 4.4). Initially, the mechanical stimuli are highest between the fracture ends. As tissue differentiates, the shear strain is reduced in the medullary cavity and in the external callus. Once bridging starts, the shear strain in the fracture ends reduces and finally fluid flow and shear strain reduce further. There is a clear difference in mechanical stimuli between the external callus and the internal callus, suggesting that two different differentiation processes operate.

Large differences in mechanical stimuli are predicted from one origin to another (Fig. 4.5). It is predicted that when cells originate from the marrow, strain and fluid flow reduce gradually but not enough to allow final stability. A delayed healing may be the final result if cells were to originate only from the marrow. For other cell origins, the shear strain decreases gradually. It finally reaches a very low value at a time that depends on the cell origin. The fluid flow is rather inhomogeneous and remains at a constant value of about 0.5 μm/s.

Due to an initial displacement of 1 mm, an initial interfragmentary strain of 33 % was calculated (Fig. 4.6). It is predicted that the interfragmentary strain decreases over time as healing occurs. Four decrease stages are predicted. A first sharp decrease is predicted by the differentiation of granulation tissue far from the fracture site into bone. A maturation stage is then predicted where strain decreases, but at a much slower rate. A third phase corresponds to tissue differentiation in the fracture gap from fibrous tissue to cartilaginous tissue formation. Finally, once bony bridging starts, the strain decreases at a much higher rate until ossification is complete.

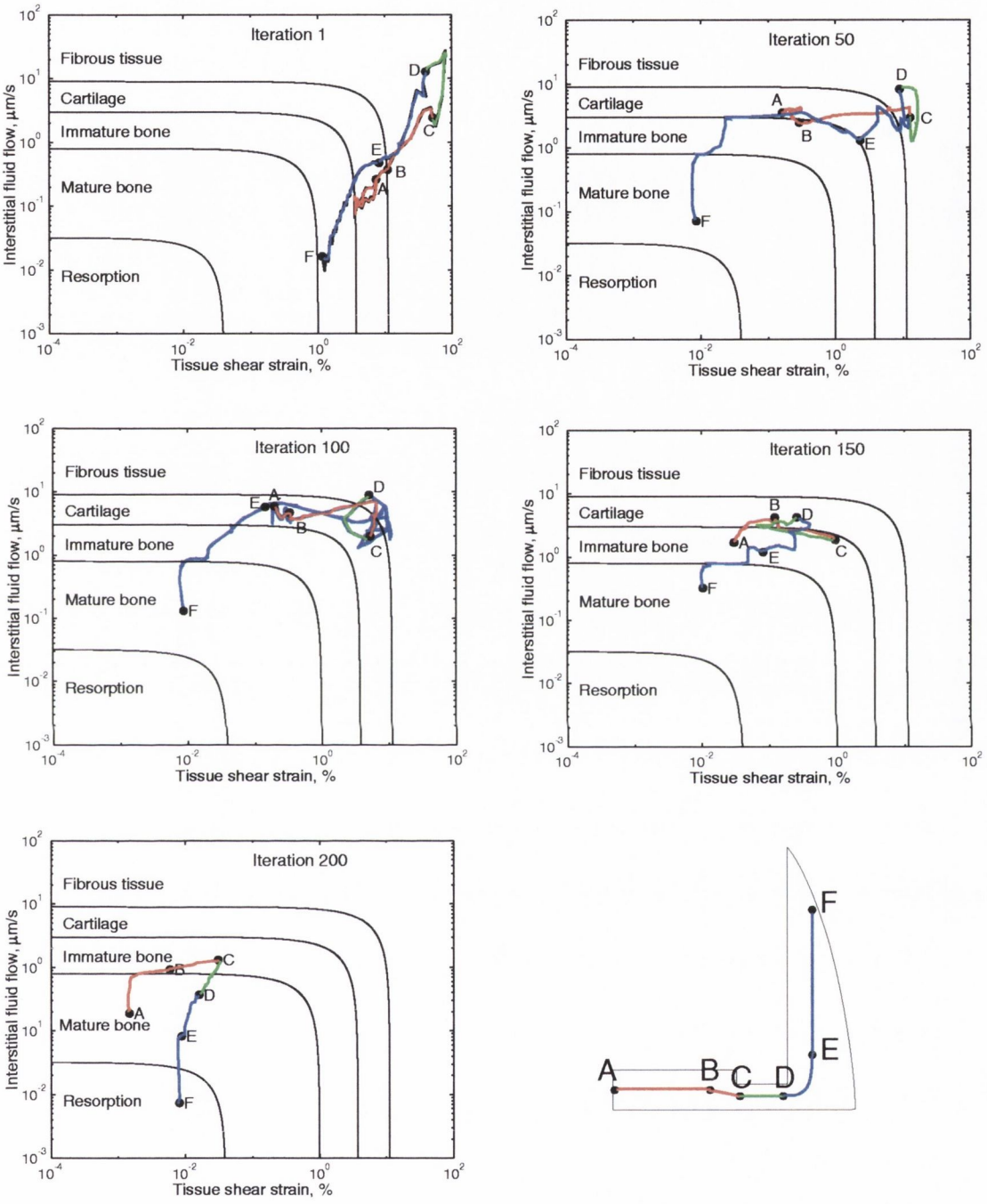

Figure 4.4. Mechano-regulation diagrams at iteration 1, 50, 100, 150, and 200 when cells originate from the three sources. The mechanical stimuli are shown along a pathway from medullary cavity (A) to external callus (F).

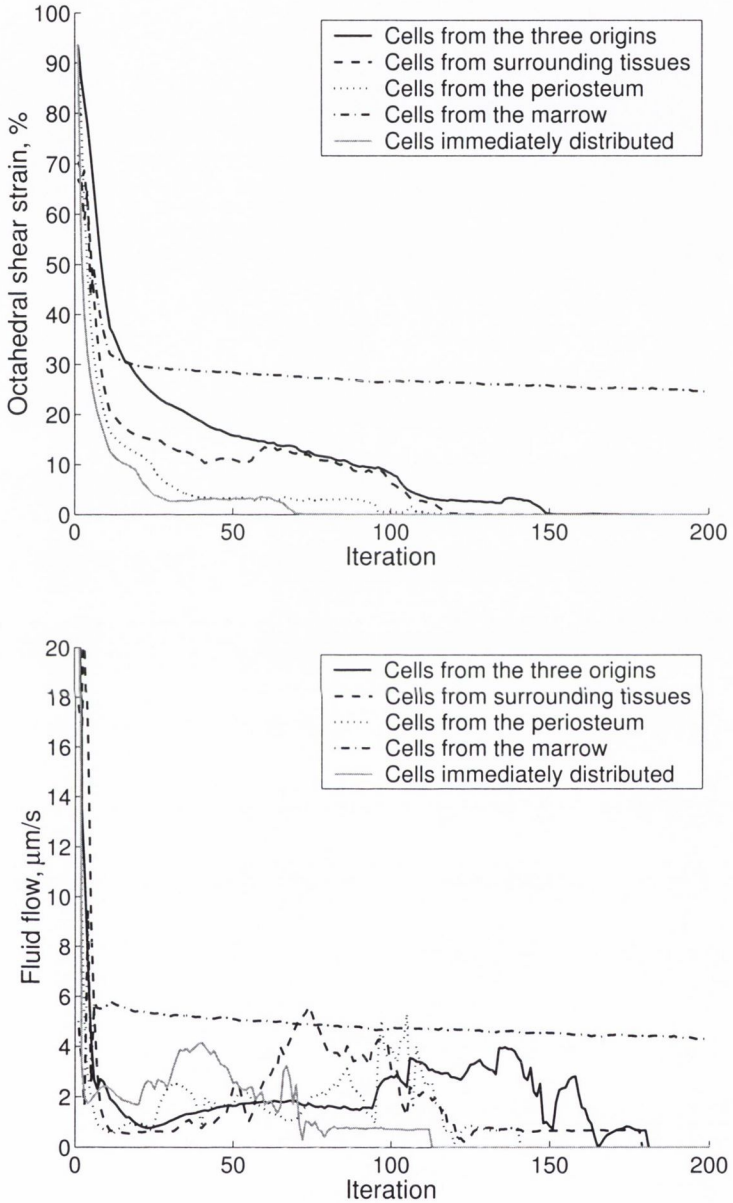

Figure 4.5. Octahedral shear strain and fluid flow in the interfragmentary gap over time for each origin.

The octahedral shear strain distribution shows that it is highest between the bone fragments but remains quite high in the external callus forming a V shape in the external callus close to the fracture gap (Fig. 4.7a). This V shape may be associated with the characteristic V shape seen in fracture histologies during endochondral ossification. The fluid flow distribution is rather spatially irregular due to the different permeability properties used for each element (Fig. 4.7b). The highest fluid flow is predicted just below the fracture close to the external callus. It is predicted that the fluid pressure is highest in the bone fragments and in the medullary cavity, and very low in the external callus (Fig. 4.7c). The fluid pressure distribution varies from 0 to 1.5 MPa and decreases over time between the fragment ends. However, the pressure decreases considerably in the medullary cavity and increases in the external callus.

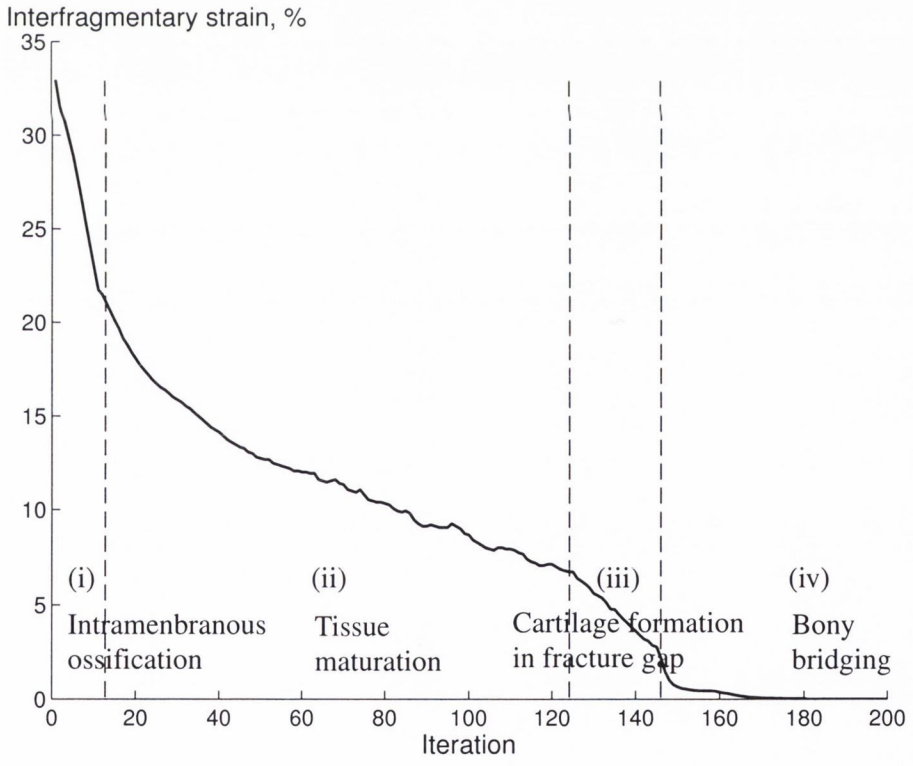

Figure 4.6. Interfragmentary strain as a function of time when cells originate from the three sources.

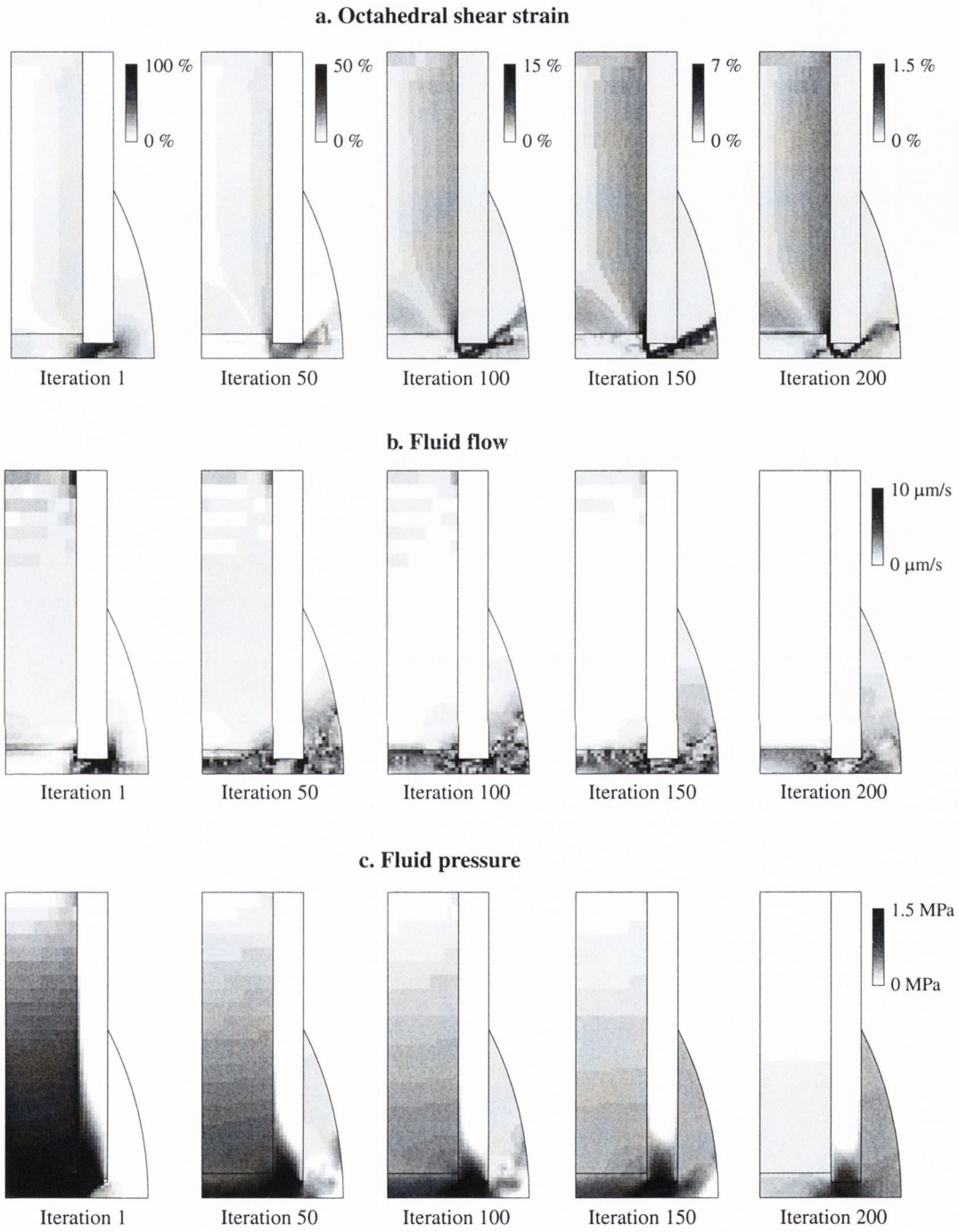

Figure 4.7. a. Octahedral shear strain, **b**. Fluid flow, **c**. Pressure distributions at iteration 1, 50, 100, 150, and 200 when cells originate from the three origins.

4.2 Parametric study

To investigate the sensitivity of the model to input parameters, a parametric study on material properties and mechano-regulation diagram boundaries was conducted.

4.2.1 Material properties

The interfragmentary mechanical stimuli in the fracture gap (octahedral shear strain and relative fluid flow) were plotted over time and compared with the material properties used in Table 3.1. To keep this chapter as concise as possible, the results are given in an Appendix. In this section, a summary of the results is given.

Young's modulus parametric study (results given in Appendix C)

- The stiffness of the granulation tissue has an important influence on the mechanical stimuli. No results could be obtained for the low stiffness (0.01 MPa) due to a too high distortion of the elements. When the stiffness is increased to 1 MPa, the initial strain is reduced greatly to 27 % (Fig. C.1). However, as differentiation is simulated, the effect of granulation tissue stiffness reduces.

- For a low value of fibrous tissue Young's modulus (0.1 MPa), no convergence is obtained after iteration 17 due to too high a strain and fluid flow (Fig. C.2). For a high stiffness (10 MPa), strain and fluid flow reduce very rapidly.

- A low stiffness for cartilage (1 MPa) induces a gradual decrease of the shear strain until iteration 100 but it remains stable thereafter (Fig. C.3). When a higher stiffness is used (100 MPa), the strain reduces considerably and tissue differentiation occurs earlier.

- A reduction of stiffness of the immature woven bone to 300 MPa affects the mechanical stimuli after iteration 90 due to insufficient stability achieved (Fig. C.4). For a higher stiffness (6000 MPa), the mechanical stimuli reduce earlier.

- The stiffness of the mature woven bone has more effect on mechanical stimuli for higher stiffness (Fig. C.5).

- The change in cortical bone Young's modulus has some effect after iteration 90 where the soft tissues in the interfragmentary gap are able to bear loading (Fig. C.6).

- The value of the marrow Young's modulus has a large influence on the mechanical stimuli and the healing period (Fig. C.7). A low value (0.1 MPa) gives a solution that could not converge. On the other hand, a high value (10 MPa) significantly reduces the shear strain. With a high stiffness, the shear strain increases in the medullary cavity but decreases in the external callus.

Permeability parametric study (results given in Appendix D)

- No convergence is obtained for a high granulation tissue permeability (5×10^{-13} m^4/Ns). This is due to a high fluid flow. For a lower permeability (1×10^{-16} m^4/Ns), little difference was predicted (Fig. D.1).

- A high fibrous tissue permeability (5×10^{-13} m^4/Ns), did not converge after 23 iterations due to too high a fluid flow in the fracture gap (Fig. D.2). A low permeability value (1×10^{-16} m^4/Ns) accelerates the reduction of mechanical stimuli.

- Cartilage permeability has a large influence on the mechanical stimuli. No healing is predicted for a high permeability (5×10^{-13} m^4/Ns), Fig. D.3. However, earlier healing is predicted for a low permeability (1×10^{-16} m^4/Ns).

- The permeability for the immature woven bone has some effect on the fluid flow (Fig. D.4).
- Permeability of the mature woven bone does not have much influence on the mechanical stimuli (Fig. D.5).
- The change of permeability of cortical bone has little influence on the mechanical stimuli (Fig. D.6).
- Similar results are obtained for the permeability of the bone marrow (Fig. D.7).

Poisson's ratio parametric study (results given in Appendix E)

- Poisson's ratio variation had little influence on the mechanical stimuli; especially for the Poisson's ratio of granulation tissue, cartilage, cortical bone, and bone marrow (Fig. E.3, E.5, & E.6).
- A high Poisson's ratio (0.3) for the fibrous tissue generated higher fluid flow and shear strain in the fracture gap (Fig. E.2).
- A low woven bone Poisson's ratio (0.2) increased the fluid flow and thus fracture healing was delayed (Fig. E.4).

Parametric variation of porosity (results given in Appendix F)

The porosity was varied for each tissue type. It was found that the porosity value had little or no influence on the mechanical stimuli. The most important influence was for the porosity of the cortical bone, the granulation tissue, and the woven bone (Fig. F.1, F.2, F.3, F.4, F.5, & F.6).

Solid compression modulus parametric study (results given in Appendix G)

The solid compression modulus of bone had a small influence on the mechanical stimuli (Fig. G.1). When the solid compression modulus of soft tissues were

varied, it was found that it only had a major influence for a high compression modulus of cartilage (7000 MPa), Fig. G.2.

Fluid compression modulus parametric study (results given in Appendix H)

The value of the fluid compression modulus has little influence on the mechanical stimuli within the fracture (Fig. H.1).

4.2.2 Mechano-regulation boundaries parametric study

When the boundary varies between fibrous tissue and cartilage, it does not initially affect the mechanical stimuli. However, as healing progressed, there is a clear difference in biophysical stimuli in the callus between the three boundaries (Fig. 4.8a). For the lower boundary, strain in the fracture gap decreases slowly and there is an insufficient decrease of the mechanical stimuli to allow ossification. When the boundary is higher, cells differentiate more easily into cartilage giving more stability and an accelerated healing period.

At the cartilage - immature woven bone boundary, similar results are obtained. A low value for cells to diffentiate into immature woven bone predicts very slow healing compared to normal, or non-healing (Fig. 4.8b). On the other hand, a higher value for cells to differentiate into immature woven bone predicts an earlier reduction of mechanical stimuli.

When the boundary between immature woven and mature woven bone is changed, there is little influence on the mechanical stimuli (Fig. 4.8c). Once tissues have differentiated into immature woven bone, it does not make much difference on the mechanical stimuli as tissues mineralise into a more advanced stage.

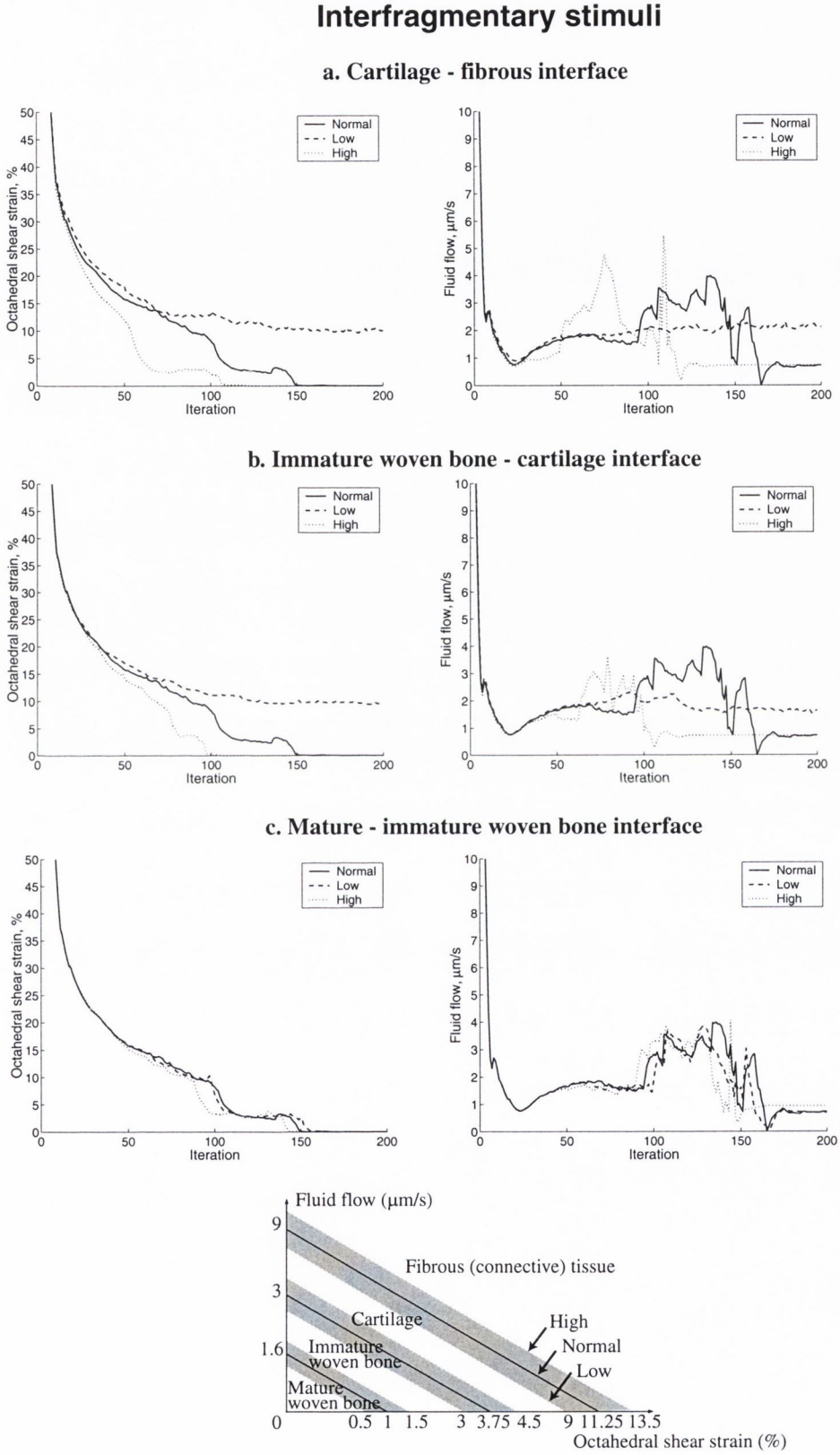

Figure 4.8. Octahedral shear strain and fluid flow in the interfragmentary gap when the boundaries of the mechano-regulation diagram are varied.

4.3 Influence of fracture gap size and loading

For a 3 mm gap size with an axial loading of 500 N, it is predicted that bone forms further from the fracture site while cartilage is predicted in the external and internal callus (Fig. 4.9). Fibrous tissue is predicted between the bone fragments. Cartilage is predicted to remain until stabilisation is sufficient to allow osseous bridging of the fracture at the external side of the callus. Next, cartilage is resorbed and bone forms, leading to a complete ossification of the bone after iteration 160. Once this has occured, the load transfer between the fracture ends leads to a reduction of the strain in the external callus – this causes the external callus to be resorbed until the initial geometry of the bone is restored. However, no resorption in the medullary cavity is predicted due

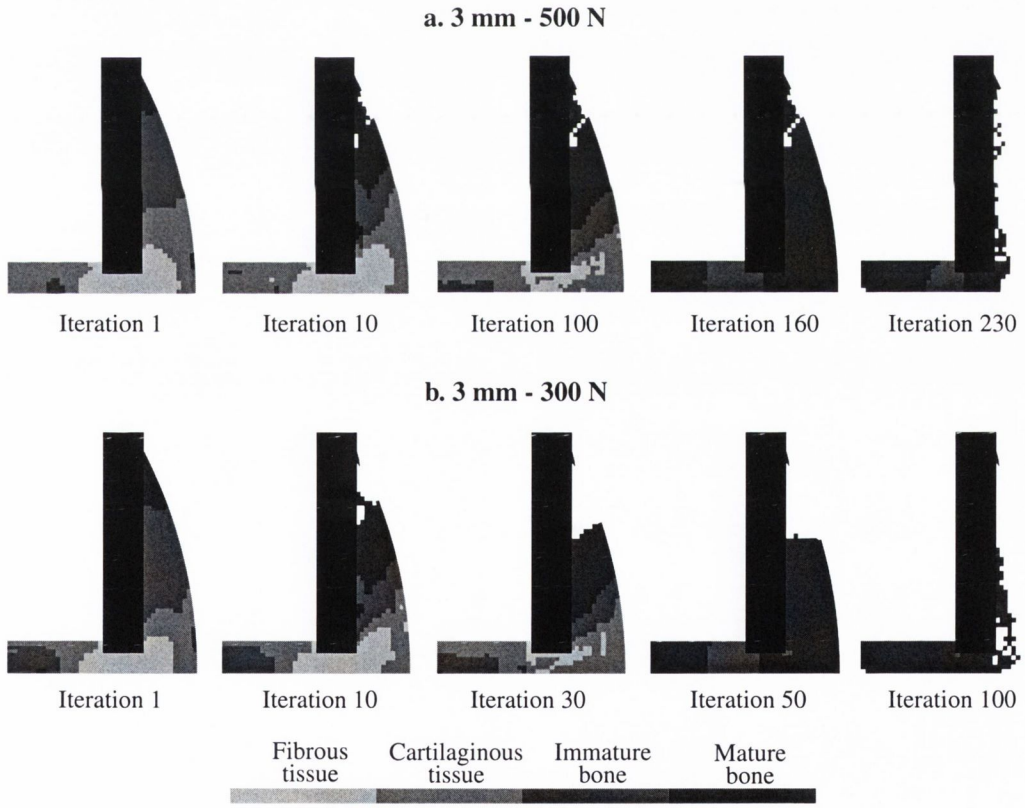

Figure 4.9. Predicted healing patterns for the 3 mm fracture gap with **a.** 500 N loading and **b.** 300 N loading.

to too high a fluid flow.

A reduction in loading accelerates the rate of healing (Fig. 4.9). For a 300 N loading, bone is predicted to form further from the fracture site and in the centre of the medullary cavity, while fibrous tissue is predicted between the bone fragments. Cartilage forms between the fibrous tissue and bone. Due to a lower loading, resorption is predicted very early (iteration 10), indicating that less external callus is necessary for lower loading. With a lower loading, full ossification occurs earlier (iteration 50) and the resorption process is also quicker.

When the fracture gap size is reduced to 1 mm, it is predicted that the amount of fibrous tissue formed between the bone ends is less than with a 3 mm gap size (Fig. 4.10). The amount of bony tissue in the external callus

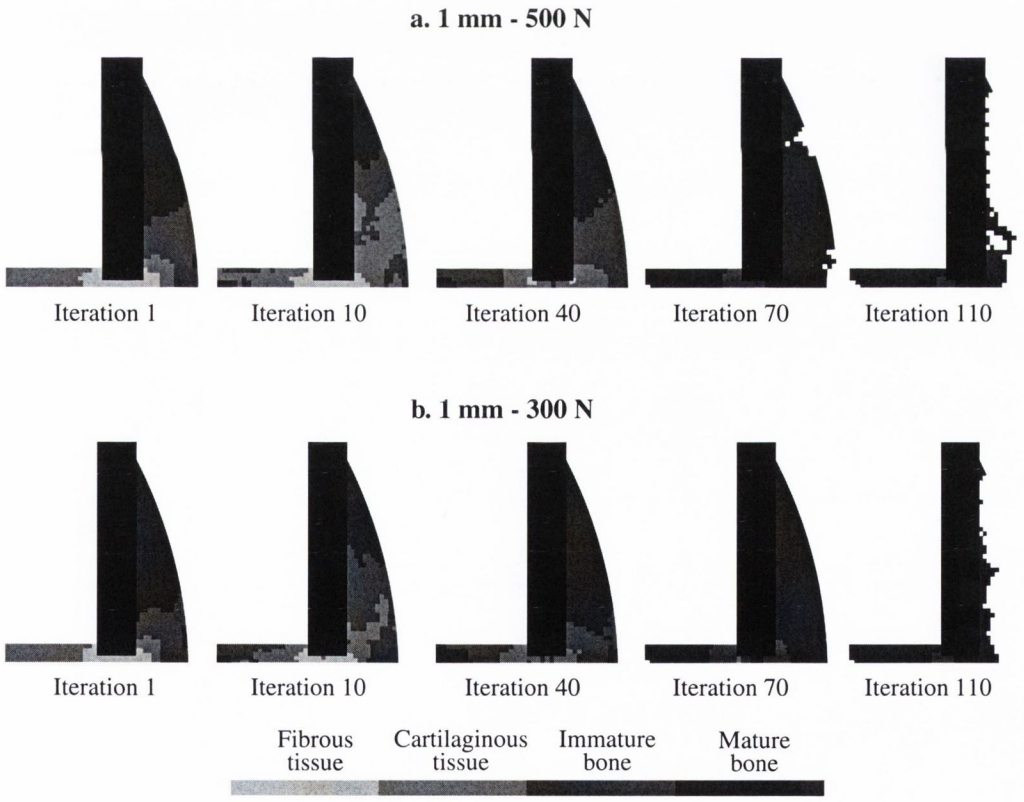

Figure 4.10. Predicted healing patterns for the 1 mm fracture gap with **a.** 500 N loading and **b.** 300 N loading.

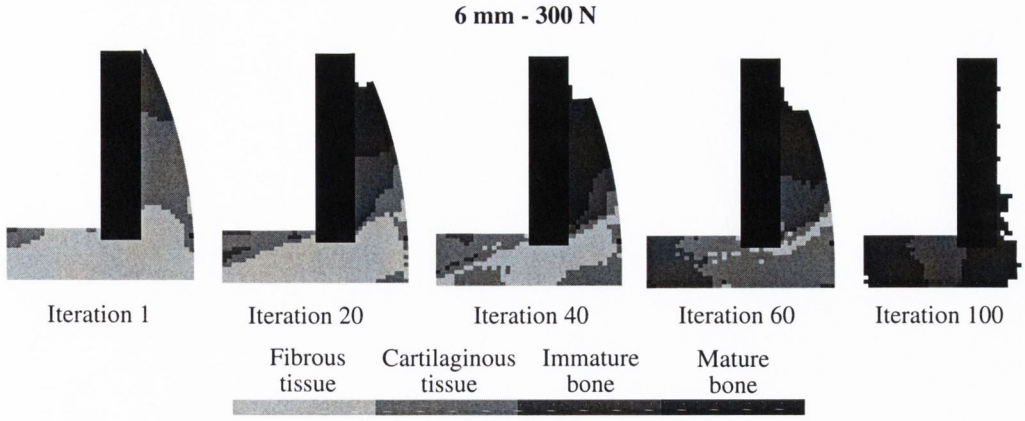

Figure 4.11. Predicted healing patterns for the 6 mm fracture gap with 300 N loading.

is more important. With a small fracture gap, bony bridging in the external callus occurs at a much earlier stage. This leads to a quicker bone formation in the external callus and a quicker resorption of the external callus.

When the load is reduced to 300 N, similar healing patterns are obtained compared to the 500 N loading case (Fig. 4.10). From these healing patterns, it can be seen that the effect of loading plays a different role than the effect of fracture gap size, the latter being more determinant in the healing patterns.

A large amount of fibrous tissue is predicted between the fracture ends for a 6 mm fracture gap (Fig. 4.11). Bone is predicted further from the fracture site and cartilage is predicted in the remaining external callus. Fibrous tissue slowly resorbs into cartilaginous tissue until cartilage forms between the bone ends and in the external callus (iteration 60). Then, bone ossification progresses due to the low loading and once bridging occurs, complete ossification is obtained and resorption of the external callus is predicted.

The healing patterns for the 6 mm fracture gap size with an axial loading of 500 N could not be predicted. The amount of deformation for this loading was too high, resulting in too great distortion of some elements. Clinically, this may indicate that the amount of movement is too high and therefore no

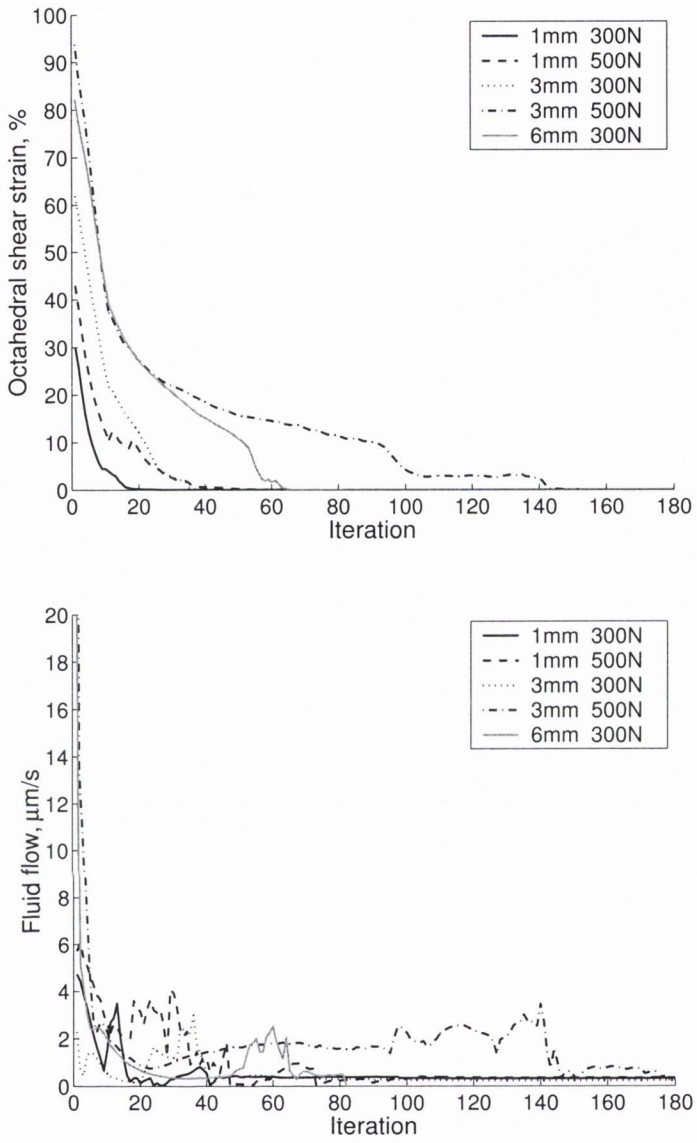

Figure 4.12. Octahedral shear strain and fluid flow in the interfragmentary gap as a function of gap size and loading magnitude.

such load would be put onto the fracture by the patient.

The octahedral shear strain in the fracture gap is very high initially but decreases over time (Fig. 4.12). Highest strain is predicted for the 3 mm – 500 N and 6 mm – 300 N cases. The strain decreases more quickly for the 6 mm – 300 N case due to a lower loading. The strain is lowest for the 1 mm fracture gap size and decreases the quickest. Until complete bone healing has

occured, the fluid flow remains rather high in the order of 2 to 4 μm/s. When bone formation occurs though, the high stiffness of the bone reduces the fluid flow considerably.

To investigate the influence of fracture gap size on the interfragmentary strain, the interfragmentary strain was calculated as healing progressed. It is predicted that the interfragmentary strain is high for the 6 mm fracture gap but reduces quickly due to low loading (Fig. 4.13). It can be seen that gap size has a critical influence on interfragmentary strain. The interfragmentary strain is greatly reduced for a 1 mm gap size compared to a 3 mm fracture gap size. The loading magnitude is also predicted to have a large influence on the healing rate.

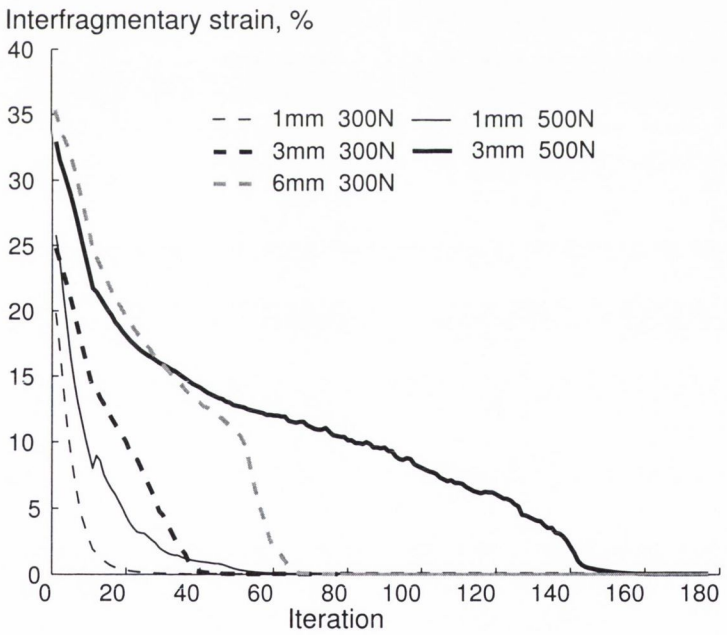

Figure 4.13. Interfragmentary shear strain over time as a function of fracture gap size for a 1, 3, and 6 mm fracture gap size with a loading of 300 N and 500 N.

4.4 Influence of bending load

To investigate the effect of bending on the healing patterns, a model with an asymmetric load was compared with an axial loading model. The load was 12.5 % higher on the left cortical bone and 12.5 % lower on the right cortical bone compared to the axial loading model, therefore keeping the total load magnitude identical. The main phases of fracture healing are also predicted with the plane strain model in axial loading (Fig. 4.14a). Bone formation is predicted further from the fracture site, fibrous tissue is predicted between the bone ends, and cartilage is predicted in the remaining callus and medullary cavity. There is a progressive resorption of the fibrous tissue to leave place to cartilage which is also resorbed during endochondral ossification. Once healing has occured, the bone resorption phase begins and the external callus is resorbed. The healing patterns shown in Fig. 4.14a can be compared to Fig. 4.9 since the geometry and the cell proliferation are the same. It can be seen that the healing patterns are very similar. However, the healing rate for the plane strain model is somewhat quicker indicating that the biophysical stimuli have reduced earlier. As in the axisymmetric model, no resorption in the medullary cavity is predicted due to a too high fluid flow.

The asymmetric loading changes the mechanical environment by creating more deformation on one side of the fracture than on the other. This has a considerable effect on the healing patterns (Fig. 4.14b). Initially, more fibrous tissue is predicted on the left side due to a higher loading. The fibrous tissue is gradually resorbed on the right side but remains longer in the left side. The healing phases in the left side are delayed while healing in the right side operates at the same speed as under the axial loading. Resorption is predicted on the right side when healing is not complete on the left side (iteration 120). Finally, complete bone formation reduces considerably the strain in both sides and thus accelerates the resorption phase. Until complete resorption of the external callus, it is predicted that the amount of woven bone is greater in the

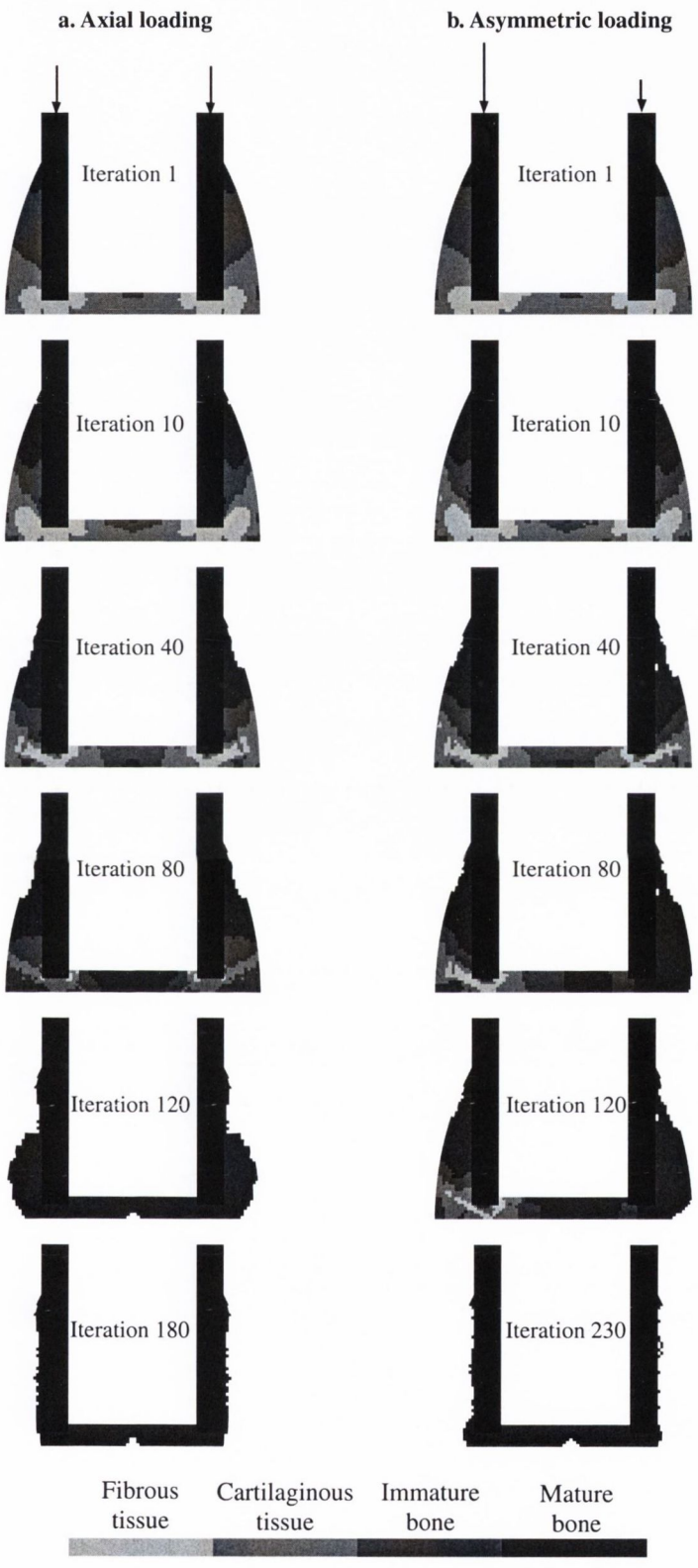

Figure 4.14. Predicted healing patterns for **a.** an axial loading, and **b.** an asymmetric loading in a transverse fracture.

left side than in the right side.

The calculation of interfragmentary strain shows the influence of bending (Fig. 4.15). It is predicted that the initial strain is slightly higher for the more loaded side. As healing occurs, the difference becomes more important due to a lack of support from the more loaded callus side.

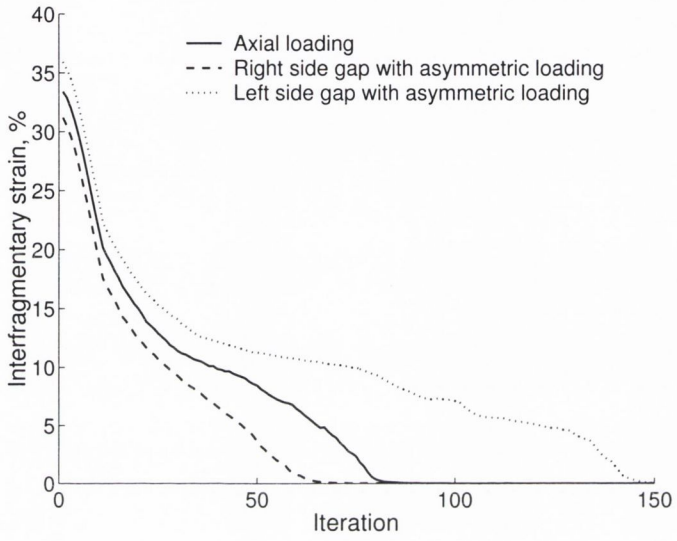

Figure 4.15. Interfragmentary strain for the transverse fracture with an axial loading or a bending loading.

It is interesting to investigate which of the two mechanical stimuli delay fracture healing under bending load. Higher strain and fluid flow are predicted for the more loaded side (Fig. 4.16). As differentiation proceeds the strain reduces everywhere except in the more loaded gap, whereas fluid flow increases or remain stable. Once sufficient bone has formed, fluid flow reduces and resorption is predicted. As in the axisymmetric model, two different regions of mechanical stimuli are predicted for the medullary cavity and the external callus. Fluid flow in the marrow is predicted to remain at a value of about 0.3 μm/s, which is too high to allow resorption. Bending has more influence on the fluid flow and shear strain in the external callus.

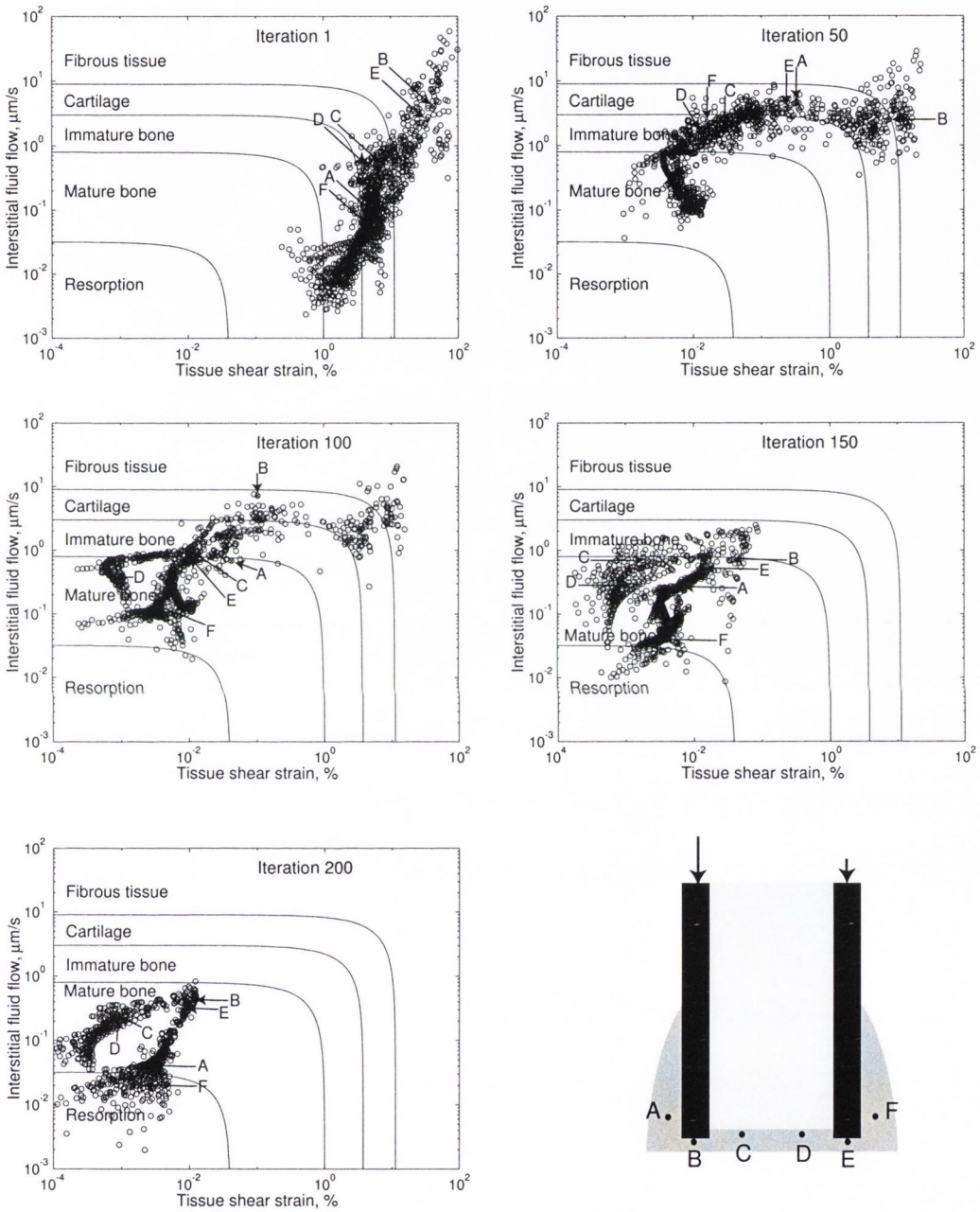

Figure 4.16. Mechano-regulation diagrams of the asymmetric transverse model.

4.5 Influence of fracture type

4.5.1 Oblique versus transverse fracture

A fracture healing simulation was done for an oblique fracture to compare with a transverse fracture. Due to an initial large displacement predicted by the oblique model, the loading was reduced by a factor of 3.2 compared to the plane strain transverse fracture to avoid large distortions of the elements (Fig. 4.17). Fibrous tissue is first predicted between the fracture ends and

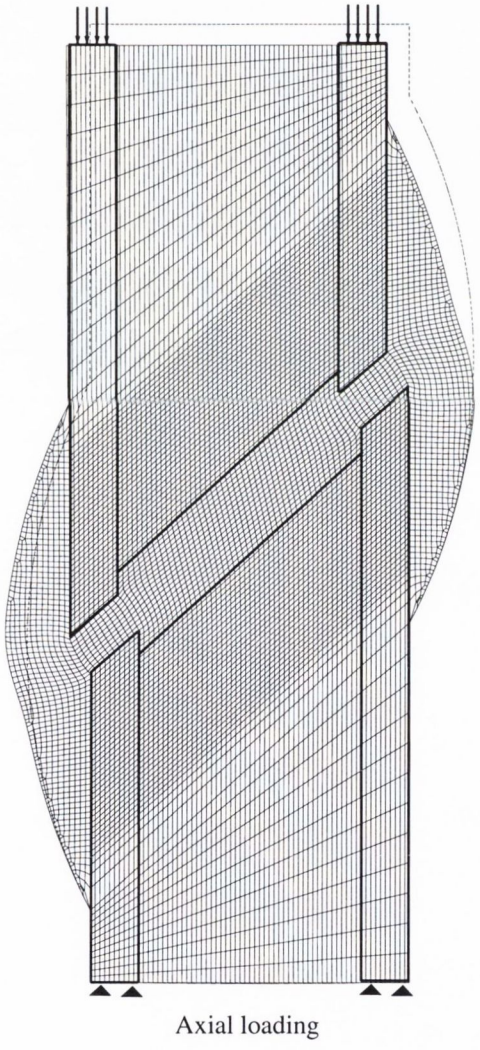

Figure 4.17. Deformation of the oblique fracture with the axial loading. The deformed mesh and the undeformed position (dotted line) are shown.

the marrow cavity (Fig. 4.18). Bone is predicted on both sides of the fracture further from the fracture site while a large amount of cartilage is predicted in the rest of the external callus. As healing occurs, it is predicted that the bone, formed in the external callus, progresses near the fracture ends through endochondral ossification. As more stability is achieved, fibrous tissue starts to resorb in the medullary cavity and cartilage is resorbed in the external callus until complete ossification is predicted (iteration 25). Due to the symmetric loading, similar tissue patterns are predicted on both sides. However, due to the oblique fracture, octahedral shear strain is predicted to be higher in the proximal part of the left external callus and in the distal part of the right external callus. A gradual resorption of the external and internal calluses are predicted. At iteration 150, all the external callus and part of the internal callus are resorbed. A small amount of bone resorption is predicted at the bone ends due to the low loading applied on the bone.

The results can be compared with Fig. 4.14a where an axial loading was applied on a transverse fracture. Fibrous tissue is predicted in the medullary cavity in the oblique fracture but very little in the transverse case. Similar healing patterns are predicted for both cases in the external callus. However, more callus seems to be needed in the oblique fracture when total ossification is predicted. Resorption in the medullary cavity is predicted while it was not the case for the transverse fracture. This is due to a reduced loading in the oblique model, thereby reducing fluid flow. Finally, the timing is very different for both predictions. Complete resorption of the external callus occurs at iteration 180 for the transverse fracture while it occurs at iteration 50 for the oblique fracture. This is explained by the smaller loading that reduces the strain considerably once stability is achieved.

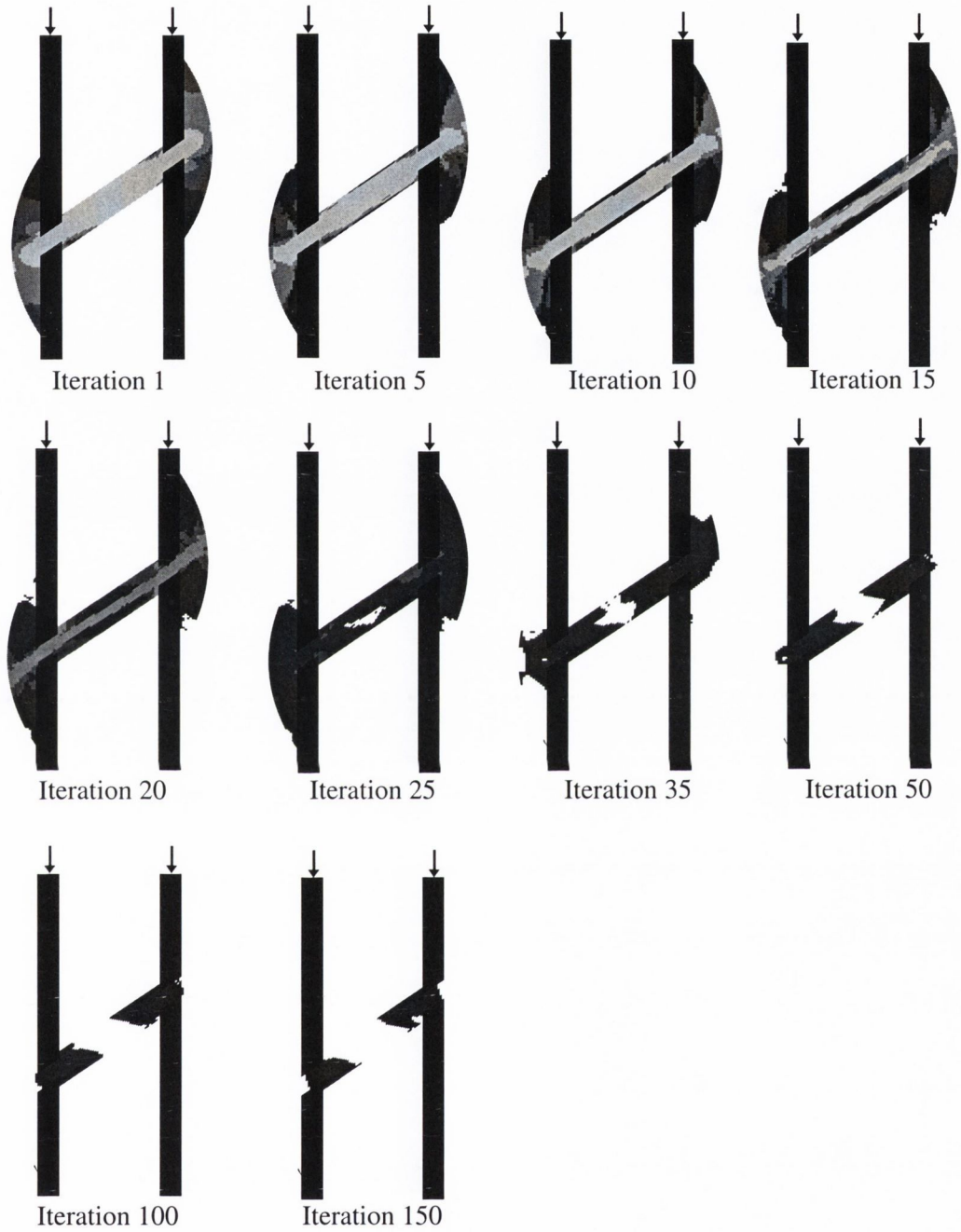

Figure 4.18. Predicted healing patterns for the axial loading in an oblique fracture.

4.5.2 Asymmetric loading of an oblique fracture

The effect of an asymmetric loading on an oblique fracture was investigated. As in the asymmetric transverse fracture, the same total loading was applied on the bone and a higher load was applied on the left cortical side than on the right side. The initial healing patterns are very similar to the axial loading (Fig. 4.19). However, the ossification progression is much slower on the left side than on the right side. At iteration 25, complete ossification of the right external callus is predicted while cartilage remains in the fracture gap and in the external callus on the left side. Resorption of the right external callus is complete at iteration 35 while this process has not started on the left side. As in the axial loading case, resorption of the medullary cavity is then predicted. It can be seen that due to the very low loading on the right side of the cortical bone, the woven bone is predicted to be resorbed on that side between the bone ends. However, due to the higher loading on the left side, all the load is taken by the cortical ends on the left side.

The asymmetric loading changes the mechanical stimuli quite considerably. In the asymmetric loading, the strain in the fracture gap is 5 % higher on the left side and 5 % lower on the right side. The effect of an oblique fracture is seen in the external callus where very different strains in the distal and proximal external callus are predicted (Fig. 4.20). The fluid flow is also predicted to be much smaller than in the transverse fracture. Differences between the proximal and distal part of the external callus are also predicted. The fluid flow is about twice as high in the proximal part compared to the distal part of the right side.

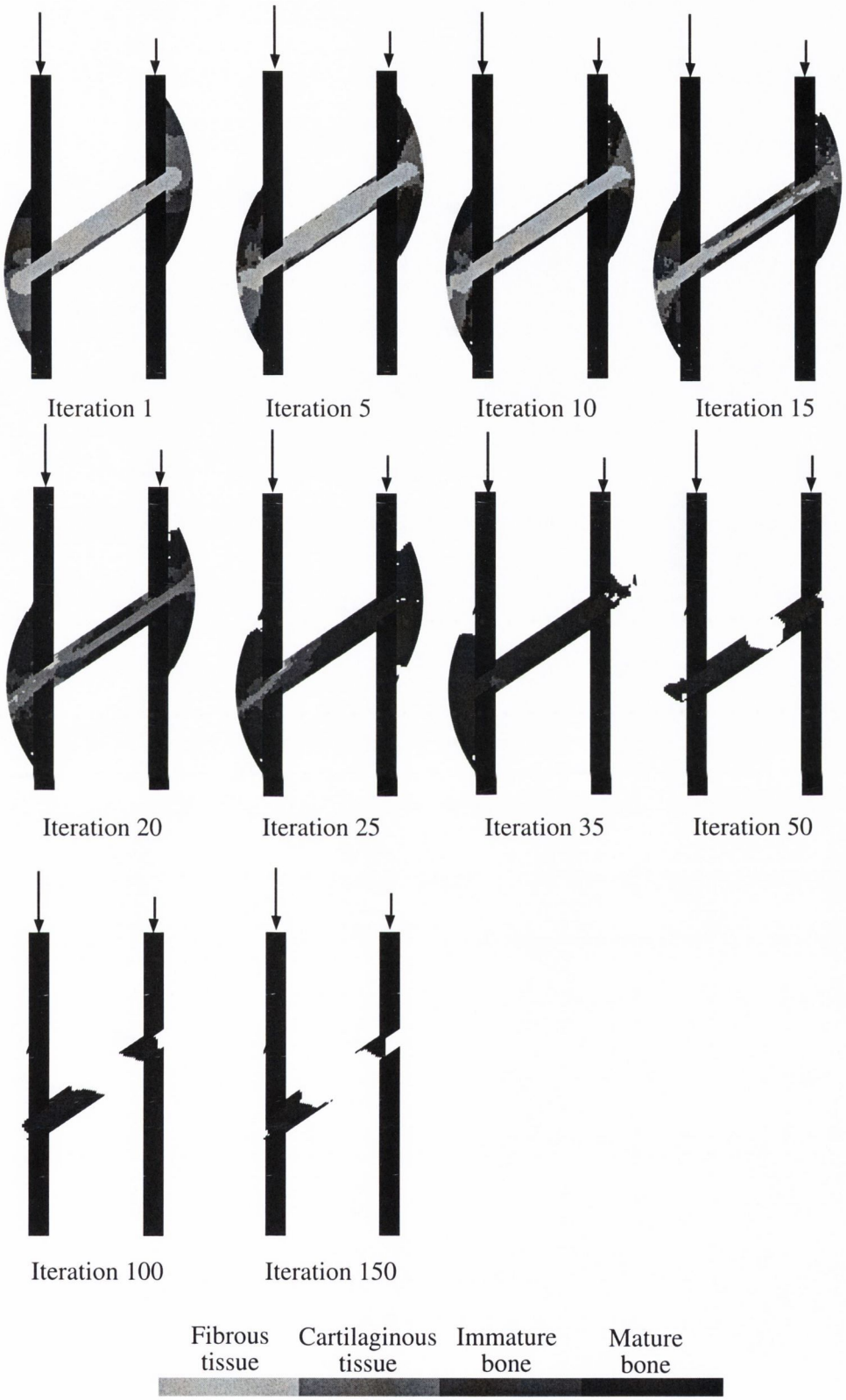

Figure 4.19. Predicted healing patterns for the asymmetric loading in an oblique fracture.

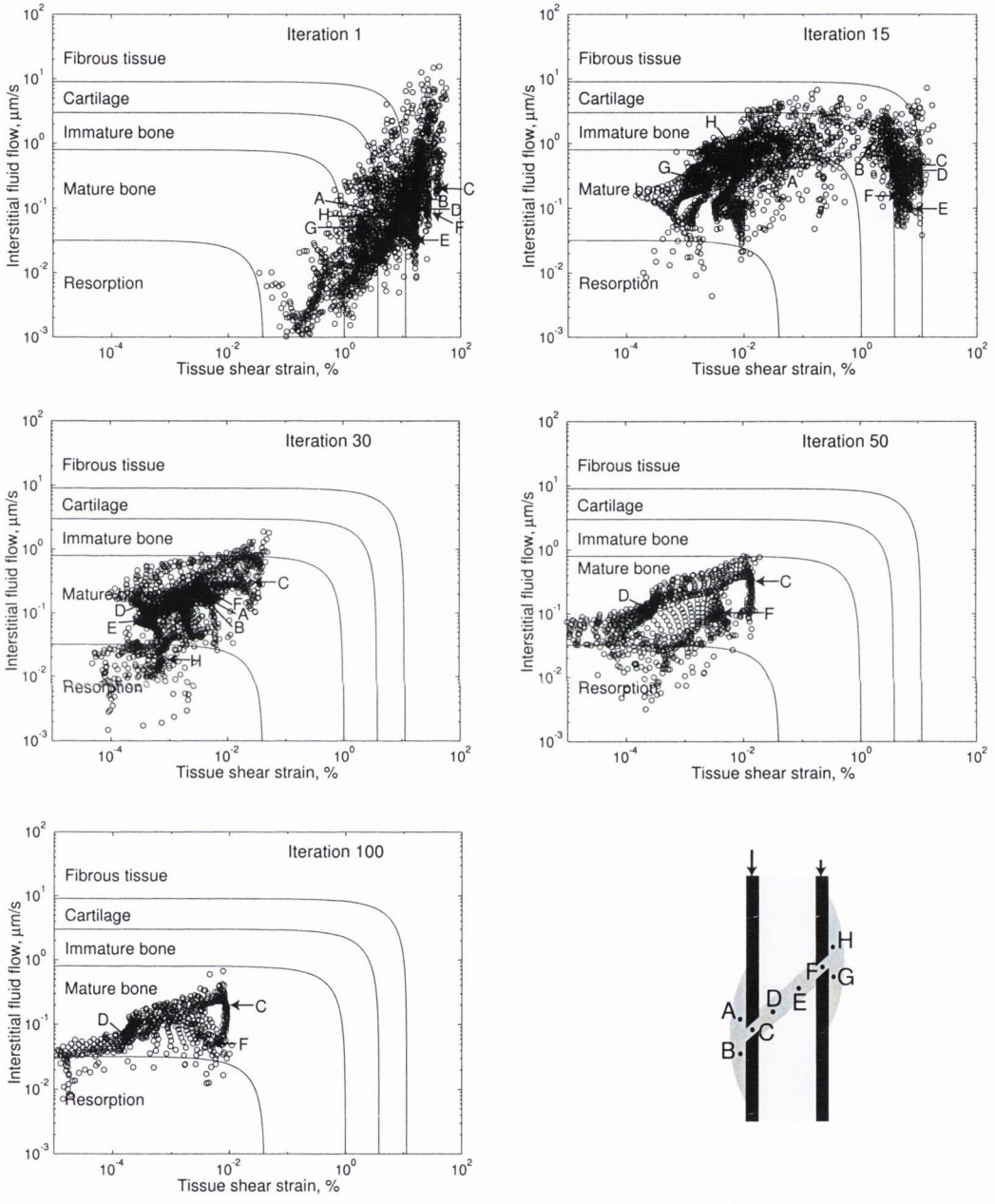

Figure 4.20. Mechano-regulation diagrams for the oblique fracture with an asymmetric loading.

4.6 3D model

Using a 3D model of a human tibia with an axial load of 300 N, fibrous tissue is predicted between the bone ends; cartilage is predicted in the medullary cavity and in the external callus near the fracture gap; bone is predicted in the remaining external callus (Fig. 4.21). However, as the external callus is mostly populated with progenitor cells, the tissue phenotype in the external callus is driving towards bone formation. At iteration 5, fibrous tissue is resorbed and cartilage tissue takes place in the posterior part of the external callus while bone forms in the anterior part. Endochondral ossification is predicted in the posterior external callus and gradually, cartilage is only predicted between the bone ends. Finally, complete healing is predicted after iteration 21.

When the loading is increased to 500 N, a much higher strain was computed therefore predicting initially a higher amount of fibrous tissue (Fig. 4.22). Fibrous tissue is mostly predicted in the medullary cavity and the bone gaps; cartilage is predicted in the external callus near the fracture; and bone is predicted further from the fracture site. At iteration 5, more cartilage is predicted in the external callus while fibrous tissue is replaced by cartilage in the medullary cavity, except in the posterior side. However, as differentiation occurs, no stabilisation is predicted and cartilage forms in the anterior side, and fibrous tissue remains in the posterior side after iteration 30.

Comparison of the mechanical stimuli for the 300 N and 500 N loading case indicates that the strain and fluid flow are higher for 500 N loading than 300 N loading (Fig. 4.23). Strain and fluid flow are higher in the posterior than in the anterior side. For both loadings, the shear strain reduces over time in the anterior and posterior sides. However, in the 500 N loading case, this decrease is not sufficient to allow stabilisation of at least one side. Similar results are obtained for the fluid flow. In the 300 N case, the fluid flow decreases over time to reach a value near nil. However, for the 500 N loading case, the fluid flow in the posterior side remains at a value of 6 μm/s. The mechanical stimuli

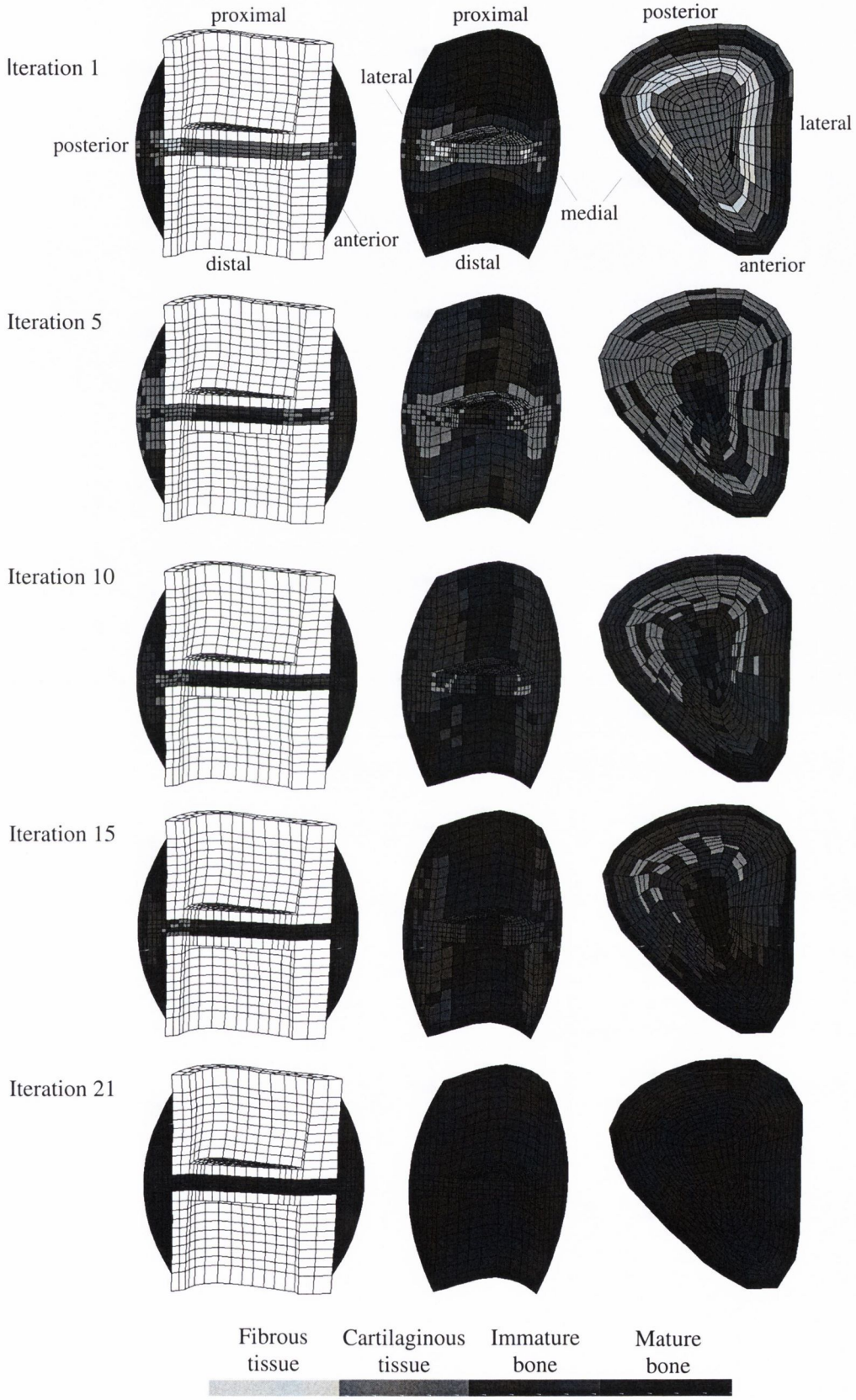

Figure 4.21. Predicted healing patterns for the 300 N load.

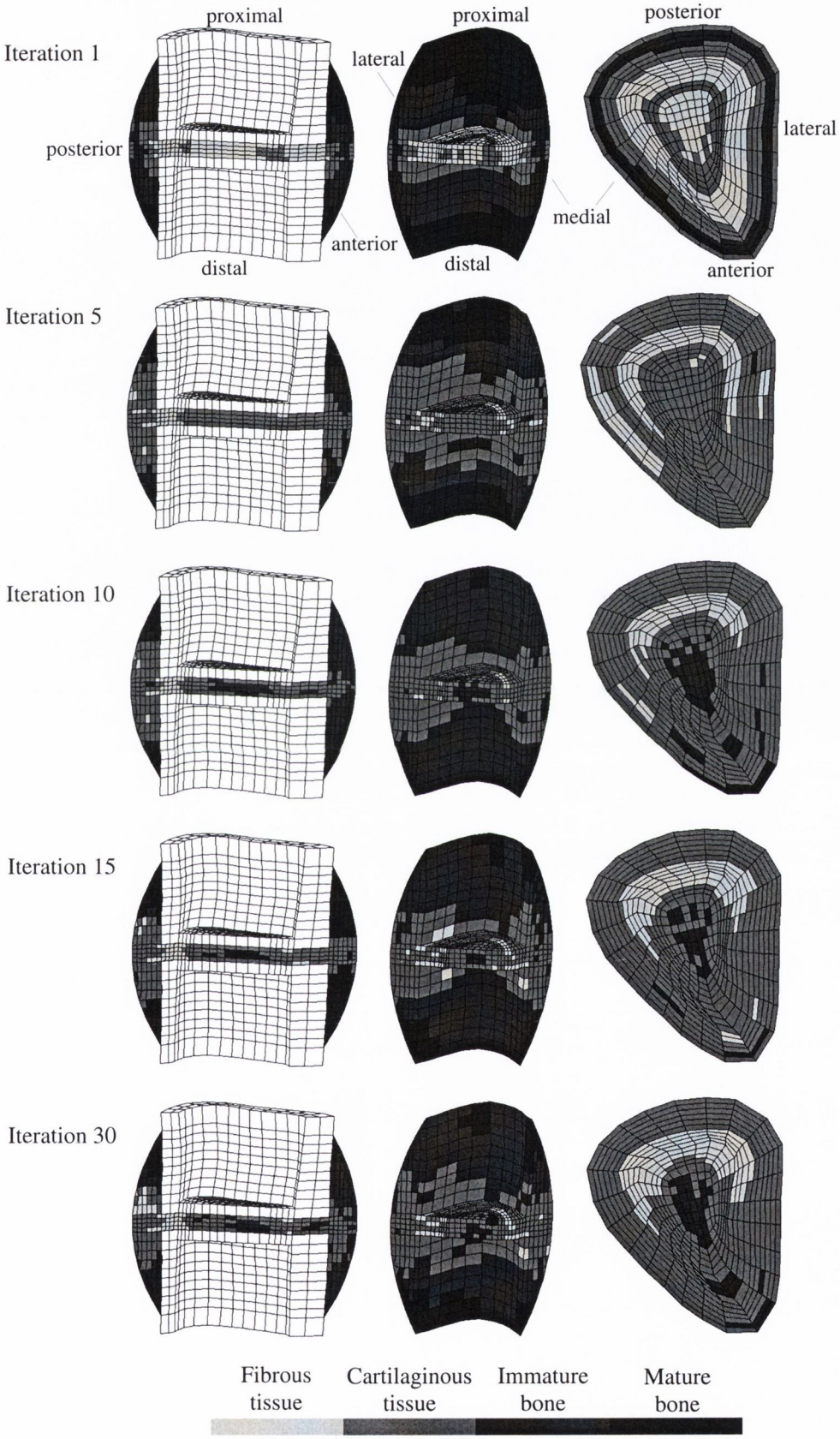

Figure 4.22. Predicted healing patterns for the 500 N load.

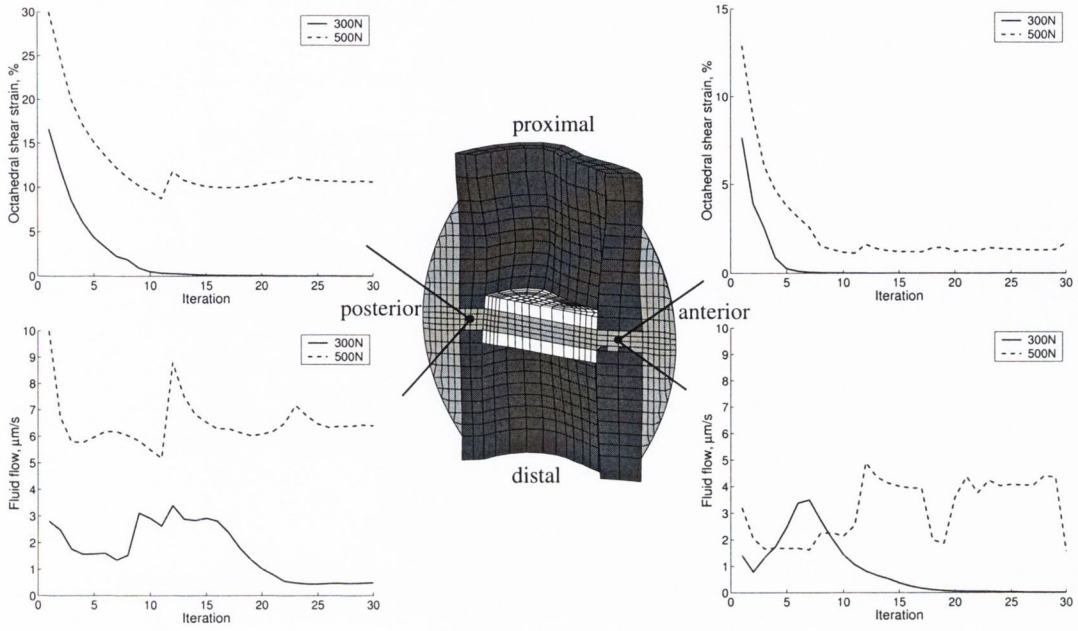

Figure 4.23. Predicted mechanical stimuli in the fracture gap in the posterior-anterior direction at 300 N and 500 N loading.

are not very much higher for the 500 N loading case than in the axisymmetric study (Fig 4.24).

To describe the mechanical stimuli predicted in this 3D model of human tibia, tissue shear strain, fluid pressure, and fluid flow distributions were plotted for the 300 N loading case since healing was predicted for that load. Initially, the strain is relatively high (17 %), but not as high as in the 2D models (Fig. 4.25). Bending occured in the sagittal plane (anterior-posterior plane) since high strain is obtained in the posterior gap and low ones in the anterior gap. On the other hand, a very similar strain distribution is obtained in the medio-lateral direction. Highest strains occur in the fracture gap cross section. As differentiation occurs, the strain decreases. However, the distribution remains more or less constant.

Initially, the fluid flow is predicted to be highest in the fracture gap (maximum of 4 μm/s), see Fig. 4.26. However, after few iterations, fluid flow is predicted to be highest in the posterior side of the external callus and near the

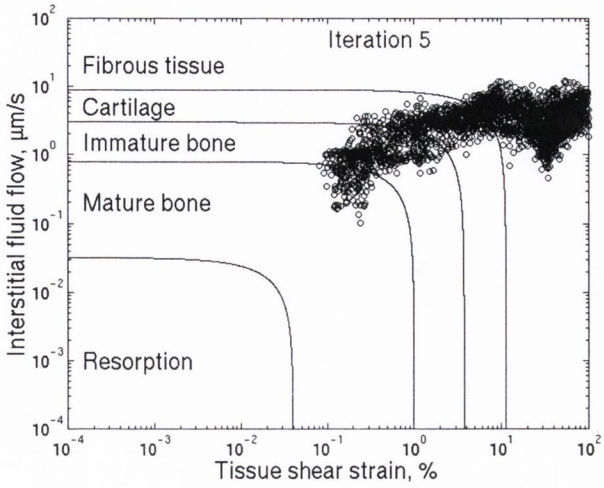

Figure 4.24. Mechanical stimuli in the 500 N loading 3D model.

fracture site in the external callus. During differentiation, different permeability values are assigned to each element and the fluid flow distribution becomes very heterogenous. As stabilisation occurs, fluid flow decreases gradually to reach a maximum of 2 μm/s when fracture healing is predicted.

The fluid pressure is initially concentrated in the fracture gap with a maximum in the posterior side (Fig. 4.27). However, as differentiation occurs, the fluid pressure extends to the external callus and is highest in the medio-lateral direction. Further differentiation reduces the fluid pressure but it becomes maximal in the postero-lateral side. Once healing has occured, the fluid pressure is relatively low and is mainly located in the posterior side of the external callus. As opposed to the findings in the 2D models, it is predicted that the fluid pressure distribution is not symmetric in the external callus due to the bending moment. Moreover, fluid pressure is very small in the medullary cavity.

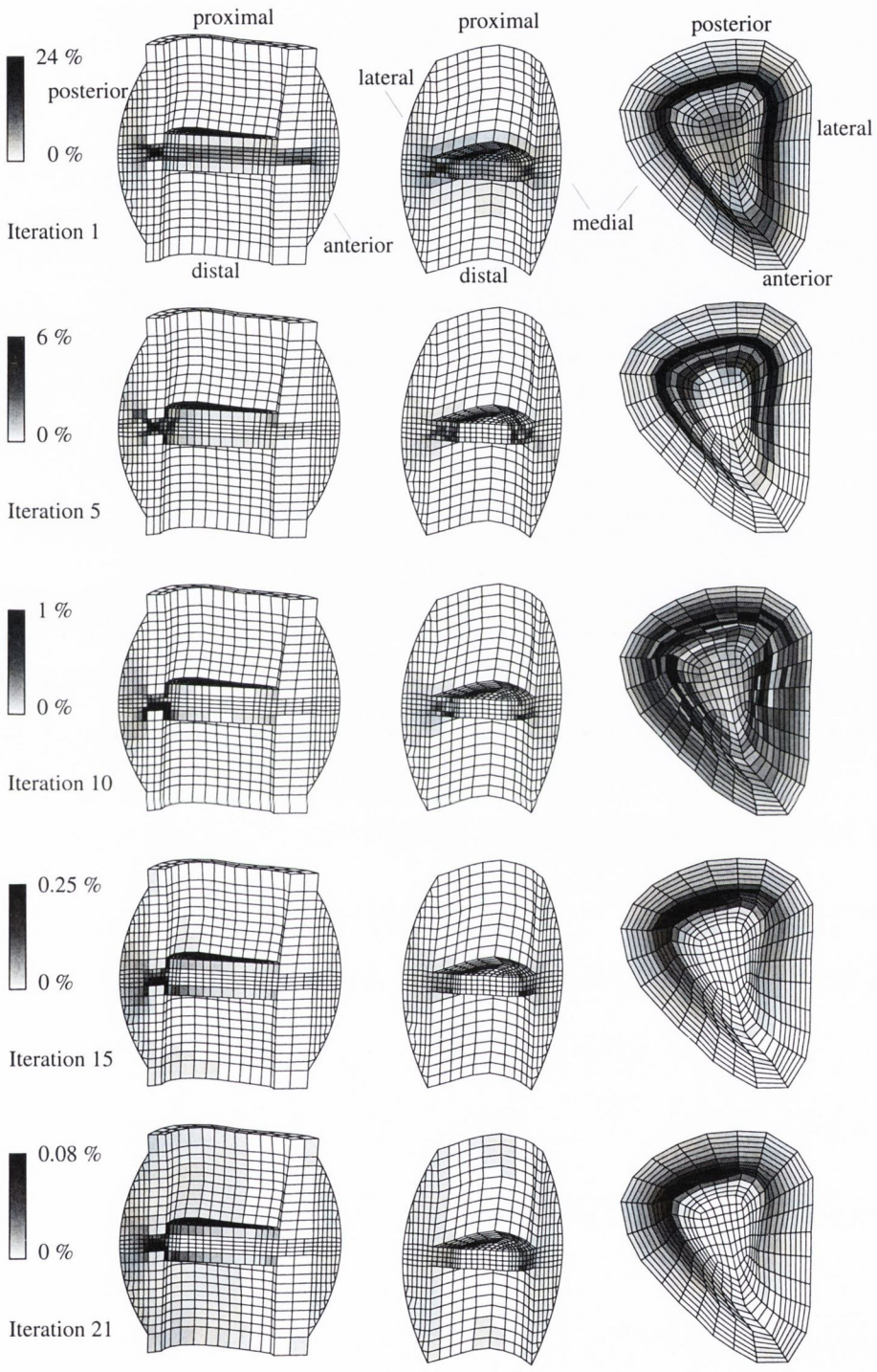

Figure 4.25. Shear strain distribution in the anterior-posterior direction, medio-lateral direction, and fracture gap cross section for the 300 N loading case. The results are shown at iterations 1, 5, 10, 15, and 21.

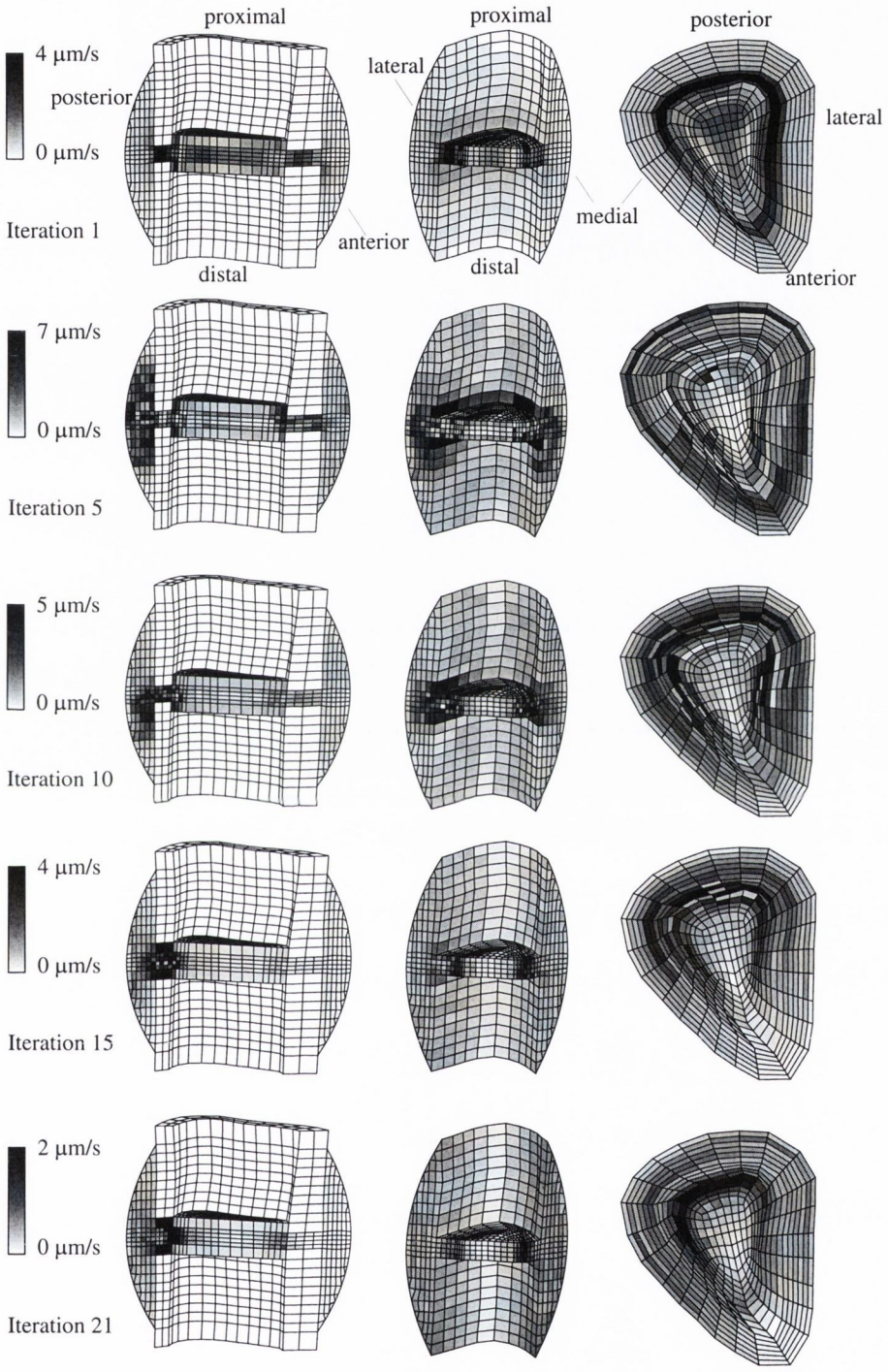

Figure 4.26. Fluid flow distribution in the posterior-anterior direction, medial-lateral direction, and fracture gap cross section for the 300 N loading case. The results are shown at iterations 1, 5, 10, 15, and 21.

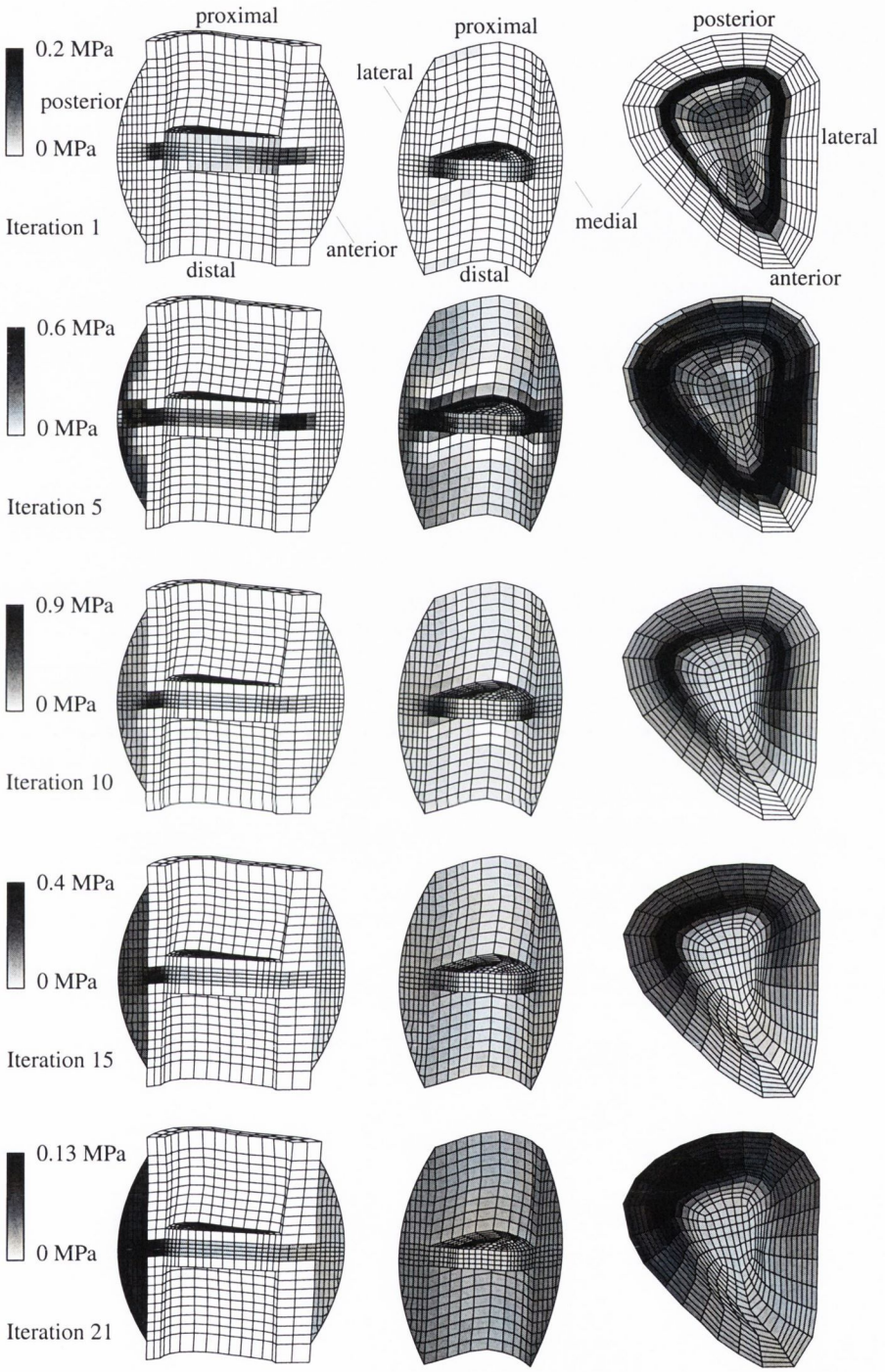

Figure 4.27. Pressure distribution in the posterior-anterior direction, medial-lateral direction, and fracture gap cross section for the 300 N loading case. The results are shown at iterations 1, 5, 10, 15, and 21.

4.7 Fracture healing monitoring

4.7.1 Loading transition

The loading was hypothesized to increase as a function of the reduction of interfragmentary strain for the axisymmetric model with a fracture gap size of 3 mm. Initially, a large amount of fibrous tissue is predicted in the fracture gap and in the medullary cavity (Fig. 4.28). Bone is predicted further from the fracture site and cartilage is predicted in the rest of the external callus. As opposed to the constant load model, fibrous tissue is predicted to resorb quickly to be replaced by cartilage. However, the predicted tissue phenotypes do not change much until bony bridging occurs in the far side of the external callus. Once bridging of the external callus occurs, there is bone formation in the interfragmentary gap. This provides greater stability and healing is achieved. Then, resorption of the external callus begins and all the external callus is resorbed.

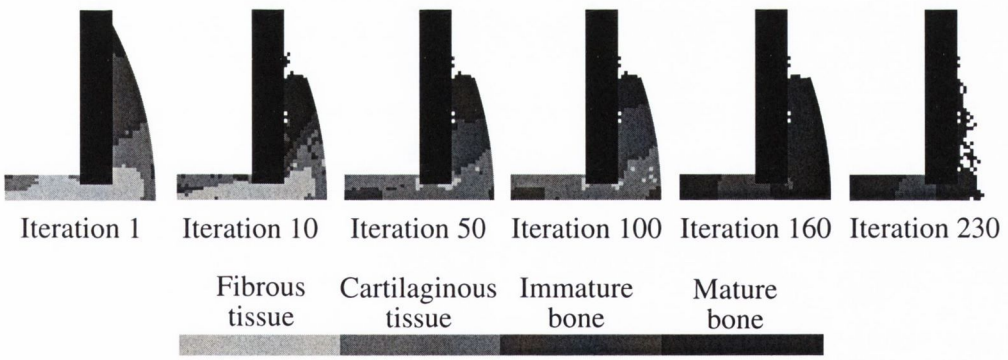

Figure 4.28. Predicted tissue type for the loading transition case.

As healing occurs, the interfragmentary strain decreases and therefore so does the interfragmentary movement. Five phases can be observed (Fig. 4.29). It is predicted that (i) the interfragmentary movement reduces very quickly initially. This corresponds to the phase where fibrous tissue resorbs into cartilage. Due to an interfragmentary strain reduction, the loading is increased. However, the increase in loading may create an increase in interfragmentary

strain in the following iteration and therefore may decrease the loading at the next iteration, and so on. Thus, between iterations 10 and 30, there is a competition between increasing or decreasing the loading, which is shown by the jagged peaks in Fig. 4.29 (phase (ii)). At iteration 30 enough stabilisation is achieved and the interfragmentary strain reduces gradually (phase (iii)). Finally, once bony bridging occurs, there is no more movement and healing is successful (phase (iv)). The last phase (v) is resorption of the external callus.

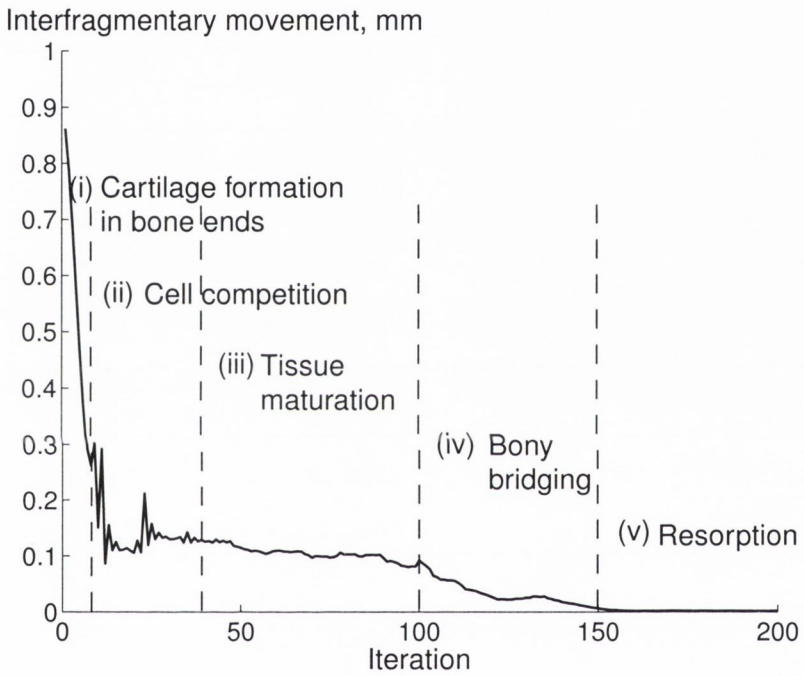

Figure 4.29. Predicted interfragmentary movement as loading is increased and healing occurs. The corresponding phases are shown.

4.7.2 Bending stiffness during fracture healing

The bending stiffness is very low (0.64 Nm/deg) when there is only granulation tissue in the fracture gap (Fig. 4.30). As healing occurs, the bending stiffness increases very rapidly within the first 10 iterations. For a loading of 300 N, the bending stiffness keeps increasing gradually to reach its maximum (61.4 Nm/deg) at about iteration 20. On the other hand for a 500 N loading,

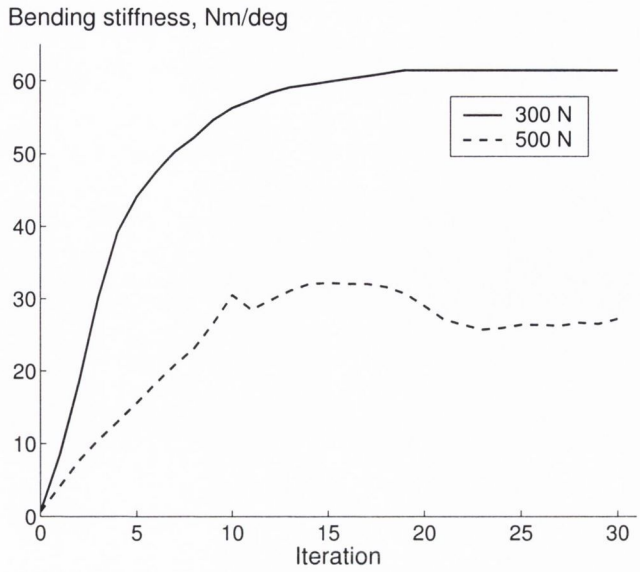

Figure 4.30. Predicted bending stiffness for the 3D model at 300 N and 500 N loading.

the bending stiffness increases until iteration 10 but remains more or less stable to a value of 30 Nm/deg.

4.8 Conclusion

Based on two mechanical stimuli, octahedral shear strain and fluid flow, simulations of fracture healing can be executed successfully. The main phases of fracture healing were predicted and the simulation is sufficiently valid that many factors, viz. gap size, loading, fracture type, can be discriminated. A 3D model showed the important differences in mechanical stimuli between a 2D and a 3D model. Finally, the model used for clinical applications has shown potential for use in a clinical environment, in so far as clinical measures can be determined from it. Those results will be discussed in the next chapter.

Chapter 5

Discussion

Contents

5.1 Introduction

Simulations of fracture healing for various fracture gap sizes and loading conditions have been presented in the previous chapter. In this chapter, these results are discussed in the context of attempting to better understand the influence of mechanical loading during fracture healing. New developments of the mechano-regulation concept presented by Prendergast *et al.* [74] are considered first. Next, the insights that the model can give regarding the effect of clinical factors on fracture healing are discussed, and comparisons with previous biomechanical analyses are made. Due to the complexity of the fracture healing process, simplifications had to be made to facilitate modelling; the limitations of these are discussed. Finally, the application of this model to a clinical environment is investigated and the contributions that the model can make to a better understanding of the mechano-regulation of tissue differentiation are evaluated.

5.2 Algorithm development

5.2.1 An iterative process

Some published biomechanical analyses of fracture healing [22, 23, 62, 65, 67, 94] have calculated the mechanical stimuli at specific time-points of fracture healing and have proposed a mechano-regulation concept of tissue differentiation during fracture healing from the obtained results. However, these concepts have not been applied in an iterative simulation. The approach used in this study is proposed as an advance on these previous studies since only the initial geometry and material properties are needed to simulate the time-course of fracture healing.

The simulations performed in this thesis predicted that fibrous tissue forms first between the bone ends due to a high shear strain and/or fluid flow. Intramembranous bone is predicted further from the fracture site. Cartilaginous tissue is predicted in the remaining external callus and in the medullary cal-

lus. As cells migrate to the fracture ends, bone formation progresses in the external callus through endochondral ossification. Some stability is achieved, thereby reducing the interfragmentary strain and enabling cartilaginous tissue to form in the fracture gap. Due to the higher stiffness of cartilage, the interfragmentary strain reduces even further allowing bony bridging of the external callus. Once bridging of the callus has occured, a greater stability is achieved and successful healing is predicted through ossification of the fracture gap and callus. The thesis objective of simulating tissue differentiation during fracture healing was successfully reached since the fundamental healing patterns were predicted.

From these results, the author proposes five main biomechanical phases during fracture healing (Fig. 5.1). Phase (i) is when intramembranous bone formation reduces the interfragmentary strain. Phase (ii) corresponds to mat-

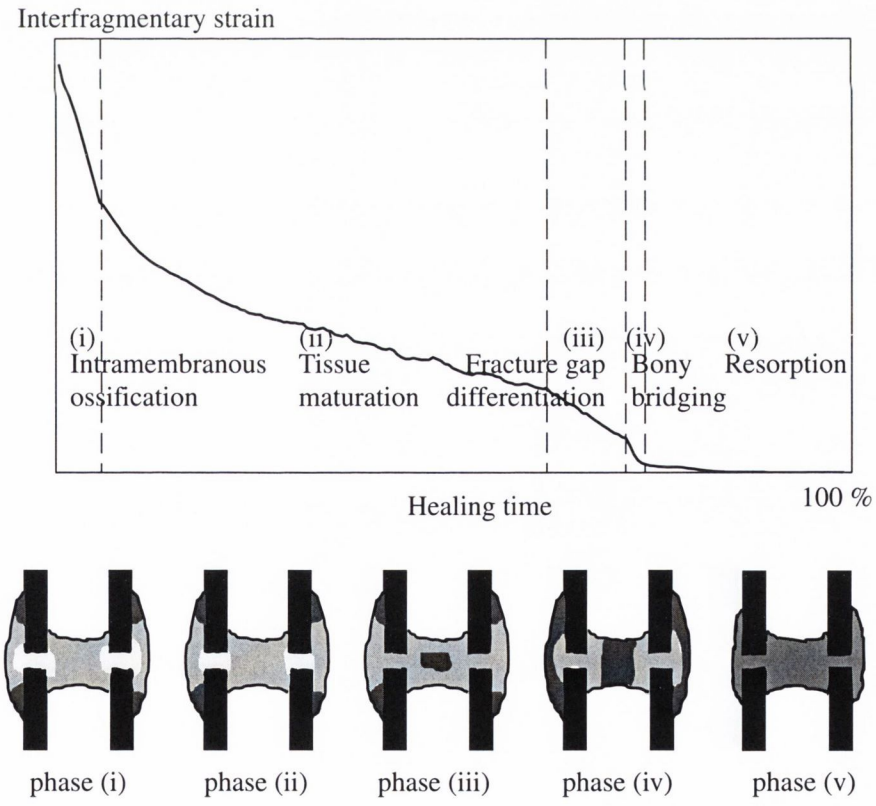

Figure 5.1. Predicted biomechanical phases during fracture healing.

uration of the cartilaginous tissue thereby corresponding to a slow decrease of the interfragmentary strain. Phase (iii) corresponds to replacement of the fibrous tissue in the fracture gap by cartilage. In phase (iv), bony bridging of the external callus creates a sharp reduction of the interfragmentary strain. Finally, once complete stability has been achieved and bone has formed in the external callus, resorption occurs in phase (v).

5.2.2 Resorption concept

Resorption of the external and internal callus were investigated. There was a gradual resorption of the external callus starting from the region far from the fracture and progressively moving towards the fracture ends. As expected, the resorption of the external callus increased the interfragmentary movement (see between iteration 160 and 180 on Fig. 5.2). However, since bone has formed in the fracture gap, the fracture is well able to withstand the load applied on the cortical bone without the interfragmentary displacement increasing considerably.

No resorption is predicted in the medullary cavity, contrary to the clinical observation. However, the internal callus is not meant to provide any support during fracture healing, which has lead Einhorn [27] and McKibbin [32] to argue that tissue differentiation in the medullary cavity does not depend on mechanical stimuli but is rather guided by biological factors. If this is true, then a mechano-regulation procedure should not predict resorption of the internal callus. In this study, it is found that the shear strain in the medullary cavity is low enough to allow resorption, but the fluid flow remains too high. The high fluid flow may be due to the high value of permeability used for bone, or to the definition of the material properties of the marrow. As seen in the material parametric study, varying the stiffness of the marrow had a significant effect on the strain and fluid flow in the medullary cavity. Alternatively, the lack of resorption of the internal callus may be attributed to the magnitude of the boundary of the resorption field in the mechano-regulation diagram.

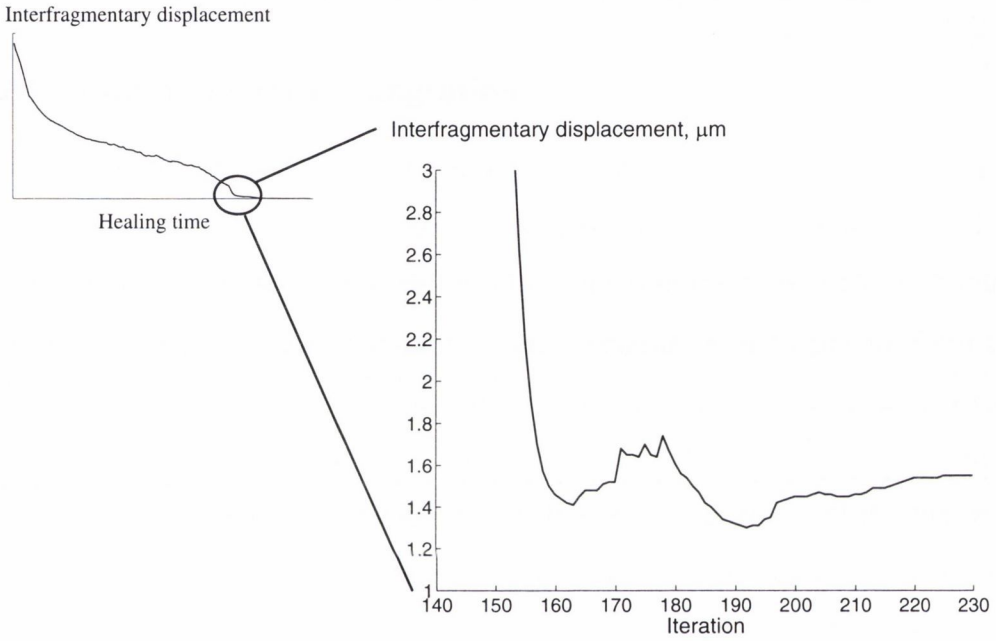

Figure 5.2. Interfragmentary displacement for the 3 mm gap at 500 N loading during the resorption phase. Note that the interfragmentary displacement decreases until iteration 160 where resorption of the external callus starts, thereby increasing the interfragmentary displacement. However, more mineralisation causes the interfragmentary displacement to decrease until it reaches its lowest at iteration 190. Finally, the interfragmentary displacement increases due to further resorption.

Resorption may occur at higher fluid flow levels than permitted in this study. Finally, it is observed clinically [44], that resorption of the medullary cavity happens in the late stages of modelling. This may be due to the reorganization of the woven bone into lamellar cortical bone with reduced permeability and porosity. The fluid flow would thus be reduced and resorption may have been predicted if this modelling phase had been simulated in this study.

5.2.3 Cell proliferation/migration

It has been recognized that progenitor cells play an important role during fracture healing. Particularly, their origin seems to be fundamental. This study is the first one to include cell proliferation/migration in a biomechanical analysis. As was stated in Chapter 2, three origins seem to prevail from the literature: (i) periosteum layer, (ii) surrounding tissues, and (iii) bone marrow. The effect of each cell origin was investigated in this study using a simple representation of cell proliferation/migration by calculating cell density with a diffusion equation. Even though cell movement has attributes that are not fully captured by a diffusion equation, a diffusion equation can be used to give a first order approximation [79]. In this study, it was shown that the time gradient of cell density can represent the advance of front cells observed in histological studies [38].

5.2.4 3D simulation

This study is the first study in three-dimensions of a fractured tibia including a fracture callus. An algorithm was developed and coded to carry out the 3D simulation of fracture healing using the poroelasticity theory capabilities of DIANA. This took some time and it is put forward here as one of the substantial achievements of this research work.

Resorption was also included in the 3D model; however, no resorption was predicted in the internal or external callus. The strain predictions were low enough to allow resorption to occur but a relatively high fluid flow in the callus

inhibited resorption. The fluid flow in the medullary cavity or external callus varied between 0.04 and 0.4 μm/s. This may indicate that either the fluid flow prediction is too high (due to a too high bone permeability) or the limit value of fluid flow between bone resorption and bone formation is too low.

Fracture healing was predicted for 300 N loading whereas, for a 500 N loading, healing was not achieved but rather soft tissue persisted. The reason is that the loading produced considerable bending in the external callus, and therefore soft tissues were maintained. This suggests that the loading conditions need further definition. Physiologically, all the muscles acting together counteract the action of each one by stabilising the bone to avoid too much bending [92]. Nonetheless, the results clearly establish that the 3D mechanoregulation model can capture the effect of loading.

5.3 Investigations of aspects of fracture healing

5.3.1 Influence of progenitor cells

It was predicted that the origin of the cells has a significant influence on the healing patterns. When cells originate from the periosteum layer or from the periosteum cortical interface, healing is predicted to occur through ossification of the external callus. The difference between these two origins is mainly on the healing rate and on the location of the bony bridging.

Entirely different healing patterns are obtained when cells originate from the bone marrow. In that case, only ossification of the internal callus is necessary to obtain successful healing. These results may indicate that the variability of healing patterns obtained for the same loading conditions in experimental studies may be attributed to a difference in the origin of the cells depending on the amount and quality of (i) the soft tissues surrounding the periosteum, (ii) the cells lying under the inner cambial of periosteum, or (iii) the cells provided by the bone marrow. It is possible that cells originate from a combination of these three origins but that the combination varies from one fracture to an-

other. When combining these three origins equally, the main patterns observed during fracture healing and described above are predicted.

This approach can be compared with the conventional way of modelling fracture healing [20, 21, 22, 23, 62, 65, 67] which assumes that all the cells are distributed instantly and differentiate all at the same time. It is predicted that, even though the healing patterns are similar, the healing rate is different. This is because computer time is used when cells are instantly distributed in the fracture whereas, when the origin of the cells is simulated, real time may be accounted for in the diffusion equation to allow for a prediction of the healing period. Moreover, the conventional approach always assumes differentiation of cells evenly in the regenerating tissue. However, in some fracture cases, such as fracture healing through primary healing, there is little contribution from the external callus; or in intramedullary nailing there is hardly any contribution from the bone marrow. This can be predicted using the approach described in this study by limiting the cell origin as required.

5.3.2 Influence of fracture gap size

Less fibrous tissue for smaller gap sizes was predicted between the bone ends. Due to a lower strain throughout the reparative phase, stabilisation is achieved earlier, and ossification in the external callus progresses more rapidly. On the other hand, when the gap size is increased, a large amount of fibrous tissue is predicted between the bone ends. Due to the large formation of fibrous tissue, it is more difficult to obtain stabilisation. The stabilisation is only achieved through gradual ossification of the external callus on its far side. Thus, the effect of fracture gap size is predicted to be very important on the healing patterns. The results of this study correlate well with the results from Claes and co-workers [15, 58].

The calculated interfragmentary movement can be compared with the ones measured by Claes *et al.* [58]. Results for the 6 mm - 300 N case are within the range of the measured displacements in the Claes *et al.* study (Fig. 5.3). The

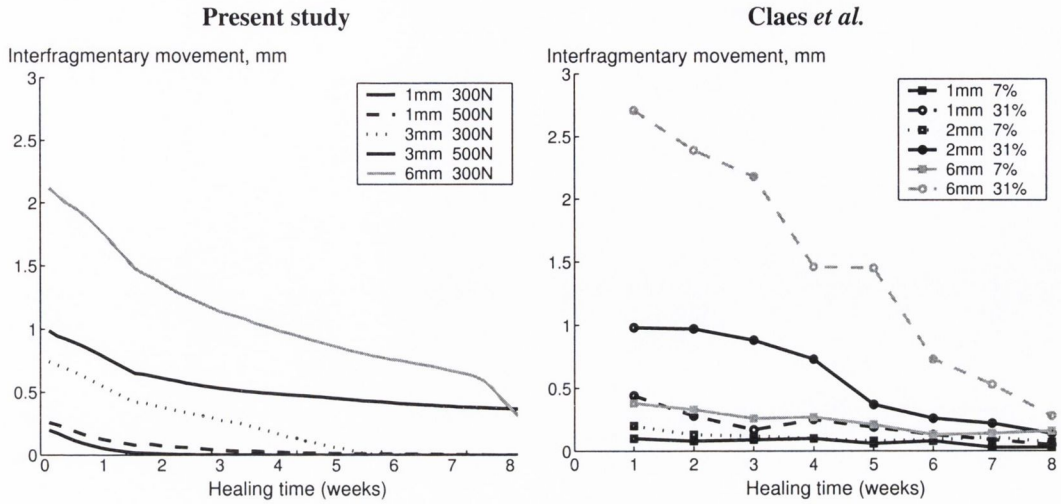

Figure 5.3. Predicted interfragmentary movements in this study compared with the ones measured by Claes *et al.* [58].

results are similar for the 1 mm fracture gap, although reduction of movement is predicted to be faster in this study. As found by Claes *et al.*, the interfragmentary movement decreases more rapidly for large than small fracture gap size.

Perren [60] advocated the interfragmentary strain theory as a possible regulator of tissue differentiation during fracture healing. This study brings some new insight to Perren's ideas by predicting the healing patterns and interfragmentary strain for several gap sizes. This study shows that the reduction of interfragmentary strain correlates well with the progress towards successful healing. However, the interfragmentary strain is not used here as a mechano-regulator of fracture healing – it is only calculated at each healing stage. It is suggested that if other regulators are used successfully to predict fracture healing, the interfragmentary strain may be a good clinical measure to assess the progress of fracture healing.

Based on clinical results, Perren [60] suggested that for a very small fracture gap, the interfragmentary strain would be very high, and thus the osteoclasts would resorb part of the cortical ends to increase the gap size and reduce the

interfragmentary strain. This was later confirmed by Cheal *et al.* [94] and Gardner *et al.* [65] who calculated high strains/stresses at the cortical ends suggesting tissue damage. This was not studied here; however, it seems that there is an optimal fracture gap size to produce the quickest healing. A very small gap size tends to get bigger; whereas for above a threshold gap size, the smaller the gap size the earlier successful healing. It might be proposed that an optimal gap size will generate the appropriate volume of external callus [16], and therefore a more effective secondary healing. It may be suggested that a gap size between 0.5 and 1 mm gives the most satisfactory results.

5.3.3 Influence of axial loading

The effect of loading was investigated using an axisymmetric model with three different gap sizes. The difference between 300 N and 500 N was evident on the healing patterns and interfragmentary strain. A higher loading increased the initial amount of fibrous tissue and cartilage formation. It also increased the interfragmentary strain considerably. Earlier healing was predicted for a low loading.

Even though there is an important effect of the loading on fracture motion, it is predicted that the effect is not as great as the fracture gap size. As expected, the interfragmentary movement reduces when the load is reduced from 500 N to 300 N, but the movement reduction is greater from a 3 mm gap size to a 1 mm gap size with the same loading. These results agree with the findings of Augat *et al.* [15]. It is also predicted that the influence of loading decreases as the fracture gap size decreases. There are less temporal differences between fracture healing at 300 N and 500 N with a 1 mm gap size than for fracture healing at 300 N and 500 N with a 3 mm gap size (Fig. 5.4). This again is in good agreement with Augat *et al.* [15].

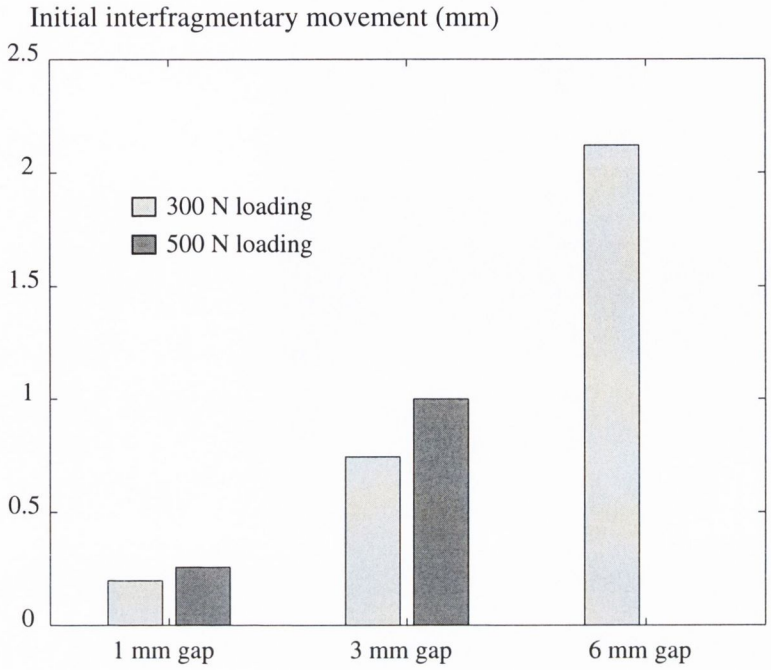

Figure 5.4. Predicted initial interfragmentary displacement for a fracture gap size of 1, 3, and 6 mm at 300 N and 500 N loading.

5.3.4 Influence of asymmetric loading

The loading applied on the plane strain model was chosen to give the same interfragmentary displacement as the axisymmetric model at 500 N loading. The octahedral shear strains were very similar in the external callus and in the medullary cavity. However, the initial strain was much lower in the plane strain model than in the axisymmetric model (25 % compared with 95 %). This is due to the third component of the principal strain (circumferential strain) which is not accounted for in the plane strain model but which is very high for the axisymmetric model due to the high compression in the fracture gap.

Lower fluid flows were also calculated for the plane strain model compared to the axisymmetric model. However, since the strain and fluid flow are high enough in both cases to predict fibrous tissue formation, the healing patterns are similar but it takes longer for the axisymmetric model to reduce the inter-

fragmentary strain. Thus, a plane strain model can be used to predict realistic fracture healing patterns. However, the exact value of the mechanical stimuli should be taken with caution since this is only a two-dimensional model that underestimates the octahedral shear strain and fluid flow.

There is a clear difference in the healing patterns between the axial and bending loadings. As expected, more deformation occured on the side more highly loaded and therefore more fibrous tissue is predicted on that side. In the bending case, it takes longer for the bone to heal byconsiderably delaying both sides. Thus, this model predicts that fracture healing is sensitive to a bending load. It is interesting to note that even the less loaded side is delayed in the resorption phase compared to the axial loading. Nevertheless, resorption occurs earlier and faster on the less loaded side compared to the more loaded side, indicating that a smaller volume of external callus is needed. This would suggest that the assymetry in external callus volume observed clinically may be attributable to the bending load acting in the tibia.

In 3D, more fibrous tissue and cartilage are predicted in the posterior side than in the anterior side. On the other hand, the healing patterns are symmetric in the coronal plane. Thus, the results indicate that it is more important to predict healing patterns in the sagittal plane than in the coronal plane when using 2D models.

For a loading of 300 N, there is little change of healing patterns between iterations 10 and 15. Since for the 3D model, one iteration corresponded to one week, the results seem to agree with Gardner *et al.* [65] who found little change in tissue differentiation from weeks 8 to 12, attributable to a maturation stage.

5.3.5 Influence of fracture type

It was intended to apply the same load for both oblique and transverse models. However, the amount of deformation was too great and no convergence was obtained after the first iteration. Thus, different mechanical behaviours are predicted between transverse and oblique fractures. Due to the geometry of

oblique fractures, the soft tissue is not only compressed by the cortical ends, but a large amount of shearing also occurs.

Even though the loading was considerably reduced in the oblique fracture, the mechanical stimuli are still predicted to be very high, and a large amount of fibrous tissue is predicted in the medullary cavity and the bone fragments. A major difference with the transverse model is that the external callus is not symmetrically strained. Thus, the ossification of the external callus does not occur at the same speed between the proximal and the distal parts. Therefore, some resorption is predicted in the stabilised proximal or distal part depending on the side of the fracture, which may indicate that, in an oblique fracture, different amounts of callus are formed depending on the orientation of the fracture.

Due to the reduced loading, the healing rate is more rapid than in the transverse fracture. This indicates that the initial granulation tissue deforms too much under shearing conditions but once cartilage or bone forms, its stiffness is high enough to rapidly reduce the interfragmentary strain. The low loading predicts a slight resorption of the fracture gap. This obviously is not seen clinically and is explained in this study by the constant low load applied on the cortical bone. As with a transverse fracture, a bending loading with an oblique fracture delays fracture healing by increasing the shear strain on the more loaded side.

5.4 Limitations of the present study

5.4.1 Simplifications in loading

A constant loading was applied on the cortical bone. However, the clinical reality is that weight bearing of the patient increases as healing occurs [92, 95]. In this study, an attempt to model this was made by hypothesizing that loading depends on interfragmentary strain. It was shown that differences in healing times were predicted and that fibrous tissue in the fracture gap was replaced

by cartilage in the initial stages of the reparative phase.

There were limitations on the loading conditions in the 3D model. To the author's knowledge, no muscle and joint data in a fractured tibia are available in the literature. Thus, an axial loading in the proximal part was applied and the distal part was restrained from moving. This had the disadvantage of giving a high bending in the mid-diaphysis of the tibia where the fracture was modelled; however, it was considered the simplest way of modelling the loading conditions in the absence of more detailed information.

5.4.2 Constitutive modelling of tissues

The tissues were represented as biphasic poroelastic materials. Large strain field was accounted for and is necessary considering the initial high strain in a fracture [94]. An infinitesimal stress-strain relationship was used when the interfragmentary strain was lower than 5 %.

In the 3D model, due to computational cost, the full mesh was solved using linear elastic material and the predicted displacements on the fracture callus were used to calculate the biophysical stimuli in the fracture callus represented as biphasic poroelastic tissue. This has the disadvantage of overestimating the displacement at the fracture callus and therefore of overestimating the octahedral shear strain and interstitial fluid flow. In the 3D model, the cortical bone was represented as linear elastic to save computational cost. Even though interstitial fluid flow influences bone adaptation, the parametric study on the permeability of cortical bone indicates that its value does not affect the mechanical stimuli in the fracture.

5.4.3 Material properties

Uncertainties in the material properties given in the algorithm remain in this study. Since, the material properties were not measured but were taken from the literature, a material parametric study was performed on all the material parameters.

The material properties that had greatest effect on the outcome of the analyses were the stiffness and permeability of granulation tissue. These properties are also uncertain as no one has ever measured the stiffness or permeability of granulation tissue. The Young's modulus used in this study (0.2 MPa) has the same value as that used by Gardner *et al.* [65]. However, Gardner *et al.* used a linear elastic model which, probably overestimates the peak displacement and therefore would overestimate the stiffness of the granulation tissue. In this study, the value of 0.2 MPa was obtained with a loading of 500 N which is a rather high initial load. Thus, this value may be considered as an upper bound value. When the loading was reduced to 100 N, the corresponding interfragmentary displacement gave a Young's modulus of 0.02 MPa, which is probably a more realistic value. The permeability value of granulation tissue was taken to be the same as fibrous tissue since both tissues are rather similar in appearance.

In general, the parametric study indicated that a reduced stiffness leads to a reduced healing period or non-healing, whereas an increased stiffness results in earlier or similar healing period. Similarly, a reduced permeability reduces the fluid flow and therefore reduces the healing period, whereas an increased permeability value increases fluid flow and increases the healing period.

5.4.4 Limitations in representing the biological system

The model includes a description of cell proliferation/migration – it is the first model to do so. However, the cell proliferation/migration rate was independant of biophysical stimuli whereas, it may be the case that mechanical environment not only stimulate cell differentiation but also cell proliferation.

Two hypotheses have prevailed in the literature for tissue replacement. First, cells are hypothesized to transdifferentiate from one cell type to another to form another tissue type. This is achieved by a structural change of the cell. Second, cells are hypothesized to terminate their life following a programmed cell death (apoptosis) [96]. In that case, new progenitor cells replace the

existing tissue cells and differentiate following the lineage pathway guided by mechanical stimuli [5]. The regulatory model used here is compatible with both hypotheses. If cell transdifferentiation is to be true, then the model is based in the replacement of one tissue type to another depending on the mechanical stimuli. If cell apoptosis is to be true, then the model would assume that progenitor cells are recruited in some way and differentiate immediately into the new tissue phenotype.

As described previously, earlier studies in fracture healing do not account for a 'real' time to predict tissue differentiation; instead, a 'computer time' is used. In this study, a more physiological timing to predict fracture healing is possible. It is based on the time used for cells to proliferate and to differentiate. The proliferation constant (Equ. 3.16) was calculated so that no more proliferation would occur after 16 weeks, considered as the usual time for a human tibia to heal [56].

Even though angiogenesis is believed to play an essential role in the replacement of cartilage into bone, it was not simulated explicitly in this study. When the blood supply is poor, oxygen tension is low and persistance of cartilaginous tissue is observed [40]. An explanation for persistance of cartilaginous tissue in some fractures may be the high strain breaking off the new blood vessels that try to reestablish the blood circulation. Oxygen tension may only play an indirect role in fracture healing. Healing of a fracture may be delayed because the mechanical stimuli may be too high to allow bone formation *and* to allow blood vessel growth (Fig. 5.5). In this way, the proposed model implicitly accounts for the influence of oxygen tension.

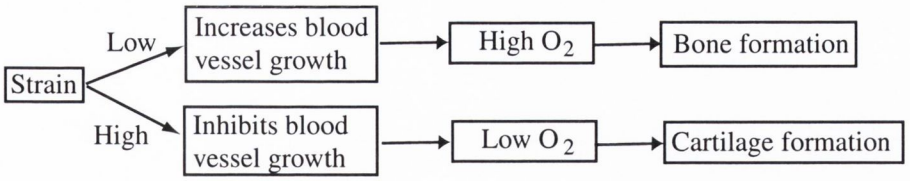

Figure 5.5. Hypothesized angiogenesis influence on tissue differentiation.

5.5 Clinical applications

5.5.1 Cell origin

It was found that cell origin may have a real importance in the healing patterns. This has several clinical implications. When cells originate from the periosteum layer and the periosteum cortical interface, it is predicted that the fracture heals mainly through ossification of the external callus. Clinically, this may correspond to the use of an intramedullary pin, which blocks the medullary cavity and therefore eliminates the bone marrow as a source of cells. For fractures with an intramedullary pin, a larger external callus is generally seen [56], which may be due to a recrudescence of progenitor cells from the external callus. On the other hand, when using an external fixator or a plaster, none of the origins are blocked and therefore each of them may contribute to fracture healing in some way. When plates are used, Perren [60] observed fractures to heal by primary healing. This may be due to the cells originating mainly from the bone marrow, depending on the tightness of the plates. In that case, this study indicates that the healing period would be very slow, which is confirmed by the clinical results [44]. Thus, depending on the type of fixation used, the origin of the cells could vary and consequently so too would the healing patterns.

The cell origin may also be a function of the amount of surrounding tissues. For example, there is very little soft tissue in the anterior part of the tibia. It is believed to be a factor in the delayed union of tibial fractures [40]. This

could be taken into account by reducing the amount of cells originating from the particular source. The same would apply for fractures with high energy impact that usually lead to oblique fractures but also cause damage to the surrounding tissues and therefore delayed healing.

5.5.2 Bending stiffness predictions

A clinical application of this study is the prediction of bending stiffness during fracture healing. It was proposed by Richardson *et al.* [55] that the external fixator could be removed when the bending stiffness of the tibia in the sagittal plane had achieved a value of 15 Nm/deg. It was further suggested by Marsh [56] that if a fracture had not achieved a bending stiffness of 7 Nm/deg after 20 weeks, healing was considered as delayed. In this study, it was found that, for a 300 N loading a bending stiffness of 15 Nm/deg was achieved at iteration 2 corresponding to week 2. The initial bending stiffness when the fracture was only made of granulation tissue was 0.64 Nm/deg and the final bending stiffness when healing was successful was 61.4 Nm/deg (Fig. 2.9). These two values are consistent with the results given by Marsh and Richardson *et al.* However, the predicted bending stiffness as healing occurs is higher than the measured one from the clinical studies of Marsh or Richardson *et al.* During the first few weeks of healing, the reparative tissues are very soft and display a non-linear load-displacement relationship. Since tissues were modelled as linearly elastic in this study for the full 3D model, this may have contributed to the high predicted bending stiffness. It is also possible that the stiffness value of 0.2 MPa for granulation tissue is too high and that a value close to 0.02 MPa is closer to reality.

5.6 Mechano-regulation of tissue differentiation

5.6.1 Motion and force control

The load transfer within the fracture can be simplified using spring models (Fig. 5.6). The load applied on the fracture is shared between the external callus and the fracture gap. It is this transfer mechanism that regulates tissue differentiation during fracture healing.

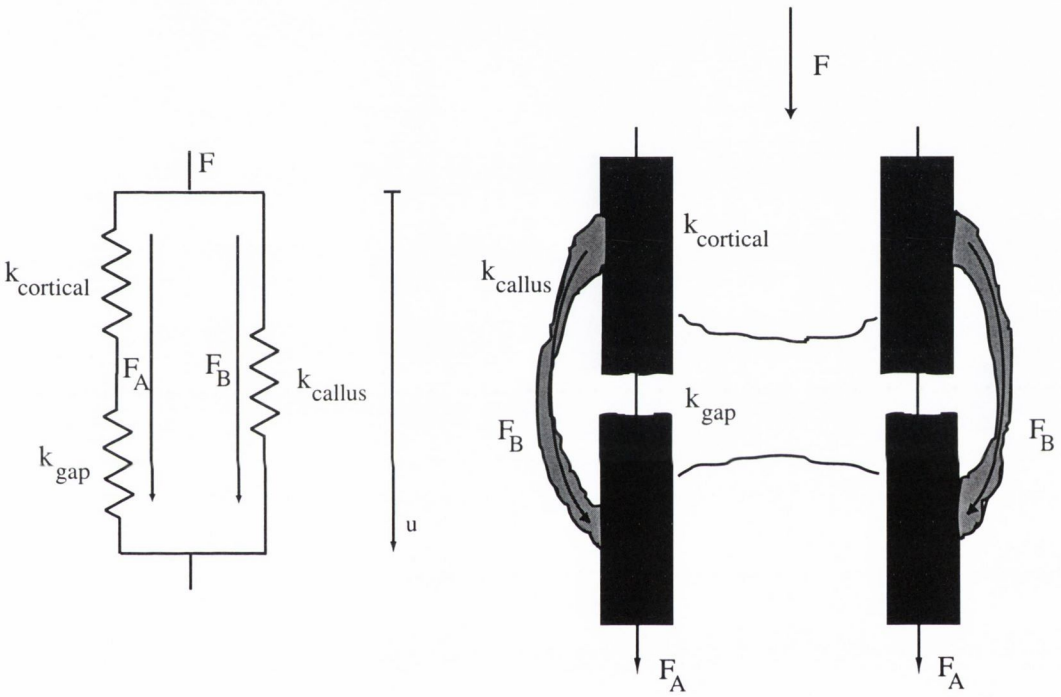

Figure 5.6. Schematic of the load sharing transfer mechanism in a fracture.

The stiffness of the fracture can be represented as three springs of different stiffness k for (i) the cortical bone ($k_{cortical}$), (ii) the fracture gap (k_{gap}), and (iii) the external callus (k_{callus}). The force, F, applied on the fracture is divided into two forces as follows

$$F = F_A + F_B \tag{5.1}$$

where $F_A = 1/[(1/k_{cortical} + 1/k_{gap})]u$, and $F_B = k_{callus}u$. The equivalent

stiffness of the fracture bone is defined as $F = k_{fracture}u$, where

$$k_{fracture} = \frac{k_{cortical}k_{gap}}{k_{cortical} + k_{gap}} + k_{callus} \tag{5.2}$$

The cortical bone stiffness is fixed and has a relatively high value. The fracture gap and external callus stiffnesses vary over time as healing occurs. The following stages take place during the healing process:

- Initially $k_{gap} \ll k_{cortical}$, therefore $k_{cortical}k_{gap}/(k_{cortical} + k_{gap}) \simeq k_{gap}$. Thus, the stiffness of the fracture is equivalent to the sum of the stiffness of the fracture gap and the stiffness of the external callus. Since both of them are very small, the fracture is controlled by the maximum displacement allowed by the tissues or the fixation device. This results in a low load and the fracture is in 'motion-control' because a set amount of motion occurs across the regenerating tissue [74], see Fig. 5.7.

- As healing occurs and tissues in the external callus differentiate into cartilage, the stiffness of the external callus increases. Thus, there is a transition period where load increases and interfragmentary strain decreases. The stiffness of the external callus begins to dominate the stiffness of the fracture gap.

- As further differentiation occurs and cartilage or bone forms in the fracture gap, the load is shared between the fracture gap and the external callus by an equal amount.

- As bone matures in the fracture gap, the stiffness of the fracture gap and external callus are not negligeable anymore when compared to the cortical stiffness. Thus, $k_{cortical}k_{gap}/(k_{cortical} + k_{gap}) \simeq k_{cortical}/2$ and the initial stiffness is restored. The fracture is under 'load-control' because it is the force across the fracture, and not the displacement, that is being prescribed as the patient reaches full weight bearing.

- With further increase in fracture gap stiffness, the external callus is resorbed to restore the non-fractured initial stiffness.

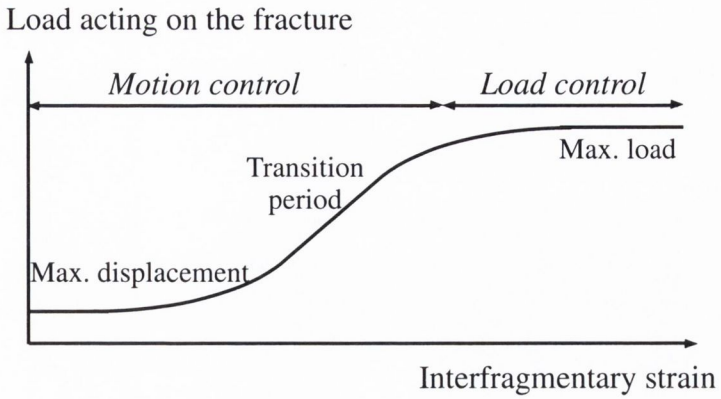

Figure 5.7. Hypothesized mechanical control during fracture healing.

5.6.2 Mechanical stimuli

In this study, two mechanical stimuli were proposed as regulators of tissue differentiation during fracture healing. This was first suggested by Prendergast *et al.* [74] for tissue differentiation at bone-implant interfaces and was simulated by Huiskes *et al.* [26] and van Driel *et al.* [77]. Prendergast *et al.* [75] have shown that at bone-implant interfaces, the fluid pressure or hydrostatic stress did not change much when varying the material properties of tissues. They therefore concluded that such a mechanical stimulus is not suitable for regulating tissue differentiation. A recent study by Yuan *et al.* [88], looking at the bone-implant interfaces under high compression, suggested octahedral shear strain and fluid flow to be regulators of tissue differentiation. They also concluded that fluid pressure was not a regulator because it did not change significantly during tissue differentiation. Several experimental studies have suggested that a strain stimulus be used as a possible regulator of tissue differentiation but also tissue adaptation [97, 98]. Moreover, other studies have suggested that interstitial fluid flow plays an important role in the stimulation and differentiation of osteoblast and chondrocyte cells [99, 100, 101].

Carter and colleagues have proposed hydrostatic stress as a regulator of cartilage formation. They stated that "in developing soft tissues, the hydrostatic stress consists mainly of pressure in the fluid phase" [24]. In the present

study, it is predicted that the fluid pressure is very high in the medullary cavity and in the fracture gap as found by Blenman *et al.* [22], and Claes and Heigele [67]. However, a higher fluid pressure level is predicted here. This result contradicts the view adopted by Carter *et al.* [24] and indicates that a linear model cannot predict accurately the mechanical stimuli regulating tissue differentiation. Moreover, in this study fluid pressure is predicted to increase in the external callus as ossification progresses. These results do not agree with the concept advocated by Carter and colleagues [22, 24], or Claes and Heigele [67].

A different concept and approach was used by Ament and Hofer [20]. They used a fuzzy logic model with a set of rules to predict tissue differentiation. Strain-energy density was used as a mechanical regulator. However, since the strain-energy density is similar for any tissue, its value did not determine the tissue type. Instead, an osteogenic index determined bone formation from cartilage formation. It was suggested in this study that osteogenesis may only play an indirect role during fracture healing and that mechanical stimuli control the differentiation process. Thus, it is questionable whether the approach taken by Ament and Hofer [20] would be successful under different loading conditions.

Fluid shear stress has been proposed by Kuiper *et al.* [72] to regulate tissue differentiation. It represents the action of interstitial fluid in shearing the cells. Since fluid shear stress and fluid flow are related to pressure gradient, it is possible that similar results would have been obtained using the mechano-regulation concept proposed by Kuiper *et al.* [72].

As described above, there are five potential mechanical regulators in the literature: tissue shear strain, fluid pressure, fluid flow, fluid shear stress, and strain energy density (Table 5.1). This study suggests that fluid flow and tissue shear strain are both regulators of tissue differentiation during fracture healing. It also suggests that fluid pressure is not.

In this study, the fluid flow is predicted to be very inhomogeneous spatially and temporally. The spatial inhomogeneity is a direct result of different permeability for each element. This introduces some high discontinuity from

Authors	Mechanical stimuli	Analysis type
Carter et al. [24]	Max. princ. strain	2D and axisymmetric
	Hydrostatic stress	Linear solid elastic
Claes and Heigele [67]	Local strains	Axisymmetric
	Hydrostatic pressure	Non-linear solid elastic
Ament and Hofer [20]	Strain energy density	Axisymmetric
		Linear elastic solid
Kuiper et al. [21]	Shear strain	Axisymmetric
	Fluid shear stress	Linear poroelastic
This study	Octahedral shear strain	2D, axisymmetric, and 3D
	Fluid flow	Non-linear poroelastic

Table 5.1. Hypothesized mechanical stimuli regulating tissue differentiation during fracture healing.

one element to another that may also be responsible for the temporal inhomogeneity. It is doubtful that this state fully reflects a physiological situation. There is reason to think that the interstitial fluid flow would vary as fluid flows through cells of different sizes and of different density. So far no study has measured fluid flow during fracture healing [1].

A new field of tissue differentiation was added to the mechano-regulation diagram proposed by Prendergast *et al.* [74], *i.e.* a resorption field. It was proposed that when the mechanical stimuli were very low, resorption of the tissues would occur. The fracture healing simulations have shown that the resorption phase of the external callus was predicted for all models except the 3D model. It was suggested that resorption did not occur in the 3D model due to an inadequate definition of the loading, and that resorption of the endosteal

[1] It is also possible that this heterogenous fluid flow is due to numerical instabilities [78]. The high discontinuity of material properties from one element to another can create some numerical instabilities as it breaches the fundamental assumption of continuity of the FE method.

callus did not occur due to a too high fluid flow prediction. It is concluded that the new field introduced in the model can simulate the resorption phase during fracture healing.

One of the strengths of this study is that the input parameters (material properties and boundary fields in the mechano-regulation diagram) were kept the same for all the simulations. Since fracture healing was predicted for many different loading and geometrical conditions, it is believed that this confirms the hypothesis of fluid flow and shear strain as mechanical stimuli regulating tissue differentiation.

5.7 Conclusion

Fracture healing has been successfully simulated for various fracture gap sizes and loading conditions. Simulations were based on a mechanano-regulation concept developed by Prendergast *et al.* [74] and Huiskes *et al.* [26], whose concept is based on the calculation of two mechanical stimuli: tissue shear strain and interstitial fluid flow. The successful simulation of several clinical factors with the same input parameters in the mechano-regulation diagram indicates that the concept gives realistic healing patterns for various fracture cases.

The study indicates that the two mechanical stimuli investigated can predict tissue differentiation during fracture healing. As the concept has been used previously for tissue differentiation at implant interfaces [26, 74, 77, 88], these new results have wide implications to the broad area of tissue differentiation. Such a model could be developed for embryogenesis, growth plate, wound healing or tissue engineering. The possibility of discovering the mechanical stimuli regulating tissue differentiation opens up many clinical and scientific applications.

It is believed that studies like this one will be more and more frequent with the advance of the 'third culture' [6]. Computer simulations will be a tool to

gain understanding of the biological and biomechanical processes. There will come a time where knowledge of the information contained within the genes and knowledge of the influence of external environments will be combined together to form a predictive model of the different stages of human growth.

Chapter 6

Conclusion

Contents

6.1 Main results

A model to predict tissue differentiation during fracture healing was presented in this thesis. The following points are the main conclusions of this study:

- Realistic healing patterns during the regenerative phase of fracture healing were predicted based on a mechano-regulation concept developed previously.
- The resorption phase of fracture healing was predicted by adding a resorption field in the mechano-regulation diagram.
- A new approach to model cell proliferation/migration was used based on the diffusion equation.
- The regenerative phase of fracture healing was predicted in a three-dimensional human tibia.
- The origin of progenitor cells was predicted to have an important effect on the healing patterns.
- Fracture gap size had a large influence on healing patterns; the larger the gap, the more difficult it was predicted to heal.
- The loading magnitude had a large influence on healing patterns; a higher loading increased considerably the interfragmentary strain.
- The interfragmentary strain could be used to monitor fracture healing. As healing occured, a gradual decrease of the interfragmentary strain was predicted.
- A fracture loaded in bending is predicted to give non-uniform healing and non-uniform resorption of the external callus.
- An oblique fracture gives much more motion than a transverse fracture. An oblique fracture is therefore predicted to take longer to heal for the same gap size and loading conditions than a transverse fracture.

- A geometrically realistic model of a human tibia gives unphysiologic deformation when only joint loading is used. Additional muscle data are needed to simulate fracture healing.

- The octahedral shear strain and fluid flow are predicted to regulate tissue differentiation, whereas the fluid pressure is predicted not to be able to regulate tissue differentiation.

- Fracture healing is predicted to be under displacement-control during the initial reparative phase. As differentiation occurs, a transition period is predicted where the interfragmentary strain decreases and loading increases. Once complete bone formation has occured, the fracture is under load-control.

- The bending fracture stiffness was predicted to increase gradually as healing occurs.

- It was suggested that angiogenesis does not need to be explicitly modelled to predict delayed healing.

6.2 Perspectives

The main objective of this thesis was achieved, *i.e.* to predict the regenerative and resorption phases during fracture healing. Some uncertainties remain on the definition of the material properties and on a more realistic loading conditions corresponding to the load experienced clinically as healing occurs. It is therefore in these areas that further work should be done. A more accurate definition of the material properties used for the granulation tissue, the fibrous tissue and the woven bone would be particularly useful to derive precise calculations of shear strain and fluid flow. Finally, an automation of the mesh generation would enable the study of patient specific fractures to predict the sensitivity of the model from patient to patient and to compare the effect of one fixator device with another.

It was shown that the model can be used to predict tissue differentiation during fracture healing. However, this concept could be applied in other biomechanical areas to give a wider understanding of mechano-regulation of tissues. The confirmation of tissue strain and interstitial fluid flow as mechanical regulators of tissue differentiation would open prospects to uncover a united theory on the processes regulating tissue differentiation.

Bibliography

[1] Aristotle. *Parts of animals.* The Loeb Classical Library. Harvard University Press, 1937. Translated by A.L. Peck.

[2] J. Wolff. *Das Gesetz der Transformation der Knochen (Translated by P. Manquet and R. Furlong as The law of bone remodelling in 1986).* Springer, Berlin, 1892.

[3] W. Roux. *Der züchtende Kampf der Theile, oder die 'Theilauslese' im Organismus (The struggle of the components within organisms).* W. Englemann, Leipzig, 1881.

[4] F. Pauwels. *Gesammelte Abhandlungen zur Funktionellen Anatomie des Bewegungsapparates (Translated by P. Maquet and R. Furlong as Biomechanics of the locomotor apparatus).* Springer-Verlag, 1980.

[5] A.I. Caplan. Mesenchymal stem cells. *J. Orthop. Res.*, 9:641–650, 1991.

[6] K. Kelly. The third culture. *Science*, 279:292–293, 1998.

[7] R. Huiskes and E.Y.S. Chao. A survey of finite element analysis in orthopaedic biomechanics: the first decade. *J. Biomech.*, 16:385–409, 1983.

[8] P.J. Prendergast. Finite element models in tissue mechanics and orthopaedic implants design. *Clin. Biomech.*, 12:343–366, 1997.

[9] B. van Rietbergen, H. Muller, D. Ulrich, P. Ruegsegger, and R. Huiskes. Tissue stresses and strain in trabeculae of a canine proximal can be quantified from computer resonstructions. *J. Biomech.*, 32:443–451, 1999.

[10] P.J. Prendergast, W.D. van Driel, and J.H. Kuiper. A comparison of finite element codes for the solution of biphasic poroelastic problems. *Proc. Instn Mech. Engrs.*, 210:131–136, 1996.

[11] J.Z. Wu, W. Herzog, and M. Epstein. Evaluation of the finite element software abaqus for biomechanical modelling of biphasic tissues. *J. Biomech.*, 31:165–169, 1998.

[12] R. Huiskes, R. Ruimerman, G.H. van Lenthe, and J.D. Janssen. Effects of mechanical forces on maintenance and adaptation of form in trabecular bone. *Nature*, 405:704–706, 2000.

[13] P.B. Chang, B.J. Williams, T.J. Santner, W.I. Notz, and D.L. Bartel. Robust optimization of total joint replacements incorporating environmental variables. *J. Biomech. Eng.*, 121:304–310, 1999.

[14] H.T. Aro and E.Y.S. Chao. Bone-healing patterns affected by loading, fracture fragment stability, fracture type, and fracture site compression. *Clin. Orthop. Rel. Res.*, 293:8–17, 1993.

[15] P. Augat, K. Margevicius, J. Simon, S. Wolf, G. Suger, and L. Claes. Local tissue properties in bone healing: influence of size and stability of the osteotomy gap. *J. Orthop. Res.*, 16:475–481, 1998.

[16] L.E. Claes, C.A. Heigele, C. Neidlinger-Wilke, D. Kaspar, W. Seidl, K.J. Margevicius, and P. Augat. Effects of mechanical factors on the fracture healing process. *Clin. Orthop. Rel. Res.*, 355S:S132–S147, 1998.

[17] A.E. Goodship and J. Kenwright. The influence of induced micromovement upon the healing of experimental tibial fractures. *J. Bone Joint Surg.*, 67B:650–655, 1985.

[18] A.E. Goodship, J.L. Cunningham, and J. Kenwright. Strain rate and timing of stimulation in mechanical modulation of fracture healing. *Clin. Orthop. Rel. Res.*, 355S:S105–S115, 1998.

[19] J. Kenwright and T. Gardner. Mechanical influences on tibial fracture healing. *Clin. Orthop. Rel. Res.*, S355:S179–S190, 1998.

[20] Ch. Ament and E.P. Hofer. A fuzzy logic model of fracture healing. *J. Biomech.*, 33:961–968, 2000.

[21] J.H. Kuiper, B.A. Ashton, and J.B. Richardson. Computer simulation of fracture callus formation and stiffness restoration. In P.J. Prendergast, T.C. Lee, and A.J. Carr, editors, *Proc. 12th Europ. Soc. Biomech.*, page 61. R. Acad. Med. Ire., 2000.

[22] P.R. Blenman, D.R. Carter, and G.S. Beaupré. Role of mechanical loading in the progressive ossification of a fracture callus. *J. Orthop. Res*, 7:398–407, 1989.

[23] D.R. Carter, P.R. Blenman, and G.S. Beaupré. Correlations between mechanical stress history and tissue differentiation in initial fracture healing. *J. Orthop. Res*, 6:736–748, 1988.

[24] D.R. Carter, G.S. Beaupré, N.J. Giori, and J.A. Helms. Mechanobiology of skeletal regeneration. *Clin. Orthop. Rel. Res.*, 355S:S41–S55, 1998.

[25] J.D. Currey. The validation of algorithms used to explain adaptive remodeling in bone. In A. Odgaard and H. Weinans, editors, *Bone structure and remodeling*, volume 2 of *Recent advances in human biology*, pages 9–14. World Scientific, 1995.

[26] R. Huiskes, W.D. van Driel, P.J. Prendergast, and K. Søballe. A biomechanical regulatory model for periprosthetic fibrous tissue differentiation. *J. Mat. Sci.: Mat. in Med.*, 8:785–788, 1997.

[27] T.A. Einhorn. The cell and molecular biology of fracture healing. *Clin. Orthop. Rel. Res.*, 355S:S7–S21, 1998.

[28] H.M. Frost. The biology of fracture healing, part I. *Clin. Orthop. Rel. Res.*, 248:283–293, 1989.

[29] A.I. Caplan and B.D. Boyan. *Bone Volume 8, Mechanism of bone development and growth*, chapter Endochondral bone formation: the lineage cascade, pages 1–46. CRC Press, 1994.

[30] R.A. Brand and C.T. Rubin. Fracture healing. *Surg. Musc. Syst.*, 1:93–114, 1990.

[31] M.C. van der Meulen, A. Bailón-Plaza, and W.L. Hunter. Long bone fracture healing in bone morphogenetic protein-5 deficient mice. *J. Bone Miner. Res.*, 13:S352, 1998.

[32] B. McKibbin. The biology of fracture healing in long bones. *J. Bone Joint Surg.*, 60B:150–162, 1978.

[33] M. Owen. The origin of bone cells in the postnatal organism. *Arthritis and Rheumatism*, 23:1073–1079, 1980.

[34] D.J. Simmons. Fracture healing perspectives. *Clin. Orthop. Rel. Res.*, 200:100–113, 1985.

[35] C.T. Brighton and R.M. Hunt. Early histological and ultrastructural changes in medullary fracture callus. *J. Bone Joint Surg.*, 73-A:832–847, 1991.

[36] J. Glowacki. Angiogenesis in fracture repair. *Clin. Orthop. Rel. Res.*, 355S:S82–S89, 1998.

[37] J.U. Yoo and B. Johnstone. The role of osteochondral progenitor cells in fracture repair. *Clin. Orthop. Rel. Res.*, 355S:S73–S81, 1998.

[38] A. Iwaki, S. Jingushi, Y. Oda, T. Izumi, J.I. Shida, M. Tsuneyoshi, and Y. Sugioka. Localization and quantification of proliferating cells during rat fracture repair: detection of proliferating cell nuclear antigen by immunochemistry. *J. Bone Min. Res.*, 12:96–102, 1997.

[39] M. Sandberg, H. Aro, P. Multimaki, H. Aho, and E. Vuorio. In situ localization of collagen production by chondrocytes and osteoblasts in fracture callus. *J. Bone Joint Surg.*, 1989.

[40] F.W. Rhinelander. Tibial blood suply in relation to fracture healing. *Clin. Orthop. Rel. Res.*, 105:35–81, 1974.

[41] J. Trueta. Blood supply and the rate of healing of tibial fractures. *Clin. Orthop. Rel. Res*, 105:11–26, 1974.

[42] C.T. Brighton and A.G. Krebs. Oxygen tension of healing fractures in the rabbit. *J. Bone Joint Surg.*, 54-A:323–332, 1972.

[43] R.B. Heppenstall, G. Grislis, and T.K. Hunt. Tissue gas tension and oxygen consumption in healing bone defects. *Clin. Orthop. Rel. Res*, 106:357–365, 1975.

[44] C.N. Cornell and J.M. Lane. Newest factors in fracture healing. *Clin. Orthop. Rel. Res.*, 277:297–311, 1992.

[45] J. Kenwright and A.E. Goodship. Controlled mechanical stimulation in the treatment of tibial fractures. *Clin. Orthop. Rel. Res.*, 241:36–47, 1989.

[46] J. Kenwright, J.B. Richardson, A.E. Goodship, M. Evans, D.J. Kelly, A.J. Spriggins, J.H. Newman, S.J. Burrough, J.D. Harris, and D.I. Rowley. Effect of controlled axial micromovement on healing of tibial fractures. *The Lancet*, 1986.

[47] E.L. Egger, F. Gottsauner-Wolf, J. Palmer, H.T. Aro, and E.Y.S. Chao. Effects of aial dynamization on bone healing. *J. Trauma*, 34:185–192, 1993.

[48] H.T. Aro, P.J. Kelly, D.G. Lewallen, and E.Y.S. Chao. The effects of physiologic dynamic compression on bone healing under external fixation. *Clin. Orthop. Rel. Res.*, 256:260–273, 1990.

[49] L.E. Claes, H.J. Wilke, P. Augat, S. Rübenacker, and K.J. Margevicius. Effect of dynamisation on gap healing of diaphyseal fractures under external fixation. *Clin. Biomech.*, 10:227–234, 1995.

[50] M.E. O'Sullivan, E.Y.S. Chao, and P.J. Kelly. Current concepts review – the effects of fixation on fracture-healing. *J. Bone. Joint Surg.*, 71-A:306–310, 1989.

[51] P. Antich-Adrover, D. Martí-Garin, J. Murias-Alvarez, and C. Puente-Alonso. External fixation and secondary intramedullary nailing of open tibial fractures. *J. Bone Joint Surg.*, 79-B:433–437, 1997.

[52] E.Y.S. Chao, H.T. Aro, D.G. Lewallen, and P.J. Kelly. The effect of rigidity on fracture healing in external fixation. *Clin. Orthop. Rel. Res.*, 241:24–35, 1989.

[53] P.J. Prendergast and D. Taylor. Design of intramedullary prostheses to prevent bone loss – predictions based on damage-stimulated remodeling. *J. Biomed. Eng.*, 14:499–506, 1992.

[54] A. Barquet, J. Masaferro, A. Dubra, C. Milans, and O. Castiglioni. The dynamic ASIF-BM tubular external fixator in the treatment of open fractures of the shaft of the tibia. *Injury*, 23:461–466, 1992.

[55] J.B. Richardson, J.L. Cunningham, B.T. O'Connor, and J. Kenwright. Measuring stiffness can define healing of tibial fractures. *J. Bone Joint Surg.*, 76B:389–394, 1994.

[56] D. Marsh. Concepts of fracture union, delayed union, and nonunion. *Clin. Orthop. Rel. Res.*, 355S:S22–S30, 1998.

[57] O.O.A. Oni, J. Dunning, R.J. Mobbs, and P.J. Gregg. Clinical factors and the size of the external callus in tibial shaft fractures. *Clin. Orthop. Rel. Res.*, 273:278–283, 1991.

[58] L. Claes, P. Augat, G. Suger, and H-J. Wilke. Influence of size and stability of the osteotomy gap on the success of fracture healing. *J. Orthop. Res.*, 15:577–584, 1997.

[59] H. Weinans and P.J. Prendergast. Tissue adaptation as a dynamical process far from equilibrium. *Bone*, 19:143–149, 1996.

[60] S.M. Perren. Physical and biological aspects of fracture healing with special reference to internal fixation. *Clin. Orthop. Rel. Res.*, 138:175–196, 1979.

[61] S.M. Perren and J. Cordey. The concept of interfragmentary strain. In H.K. Uhthoff, editor, *Current concepts of internal fixation of fractures*, pages 63–77. Spinger-Verlag, Berlin, 1980.

[62] D.R. Carter, J.A. Helms, B.K. Tay, and G.S. Beaupré. Stress and strain distributions predict tissue differentiation patterns in distraction osteogenesis. In *Trans. 44th Orthop. Res. Soc.*, page 234, New Orleans, L., 1998.

[63] E.G. Loboa Polefka, G.S. Beaupré, and D.R. Carter. Stress and strain distributions are correlated with pseudarthosis development. In *Trans. 46th Orthop. Res. Soc.*, page 861, Orlando, FL., 2000.

[64] D.R. Carter, M. Wong, and T.E. Orr. Musculoskeletal ontogeny, phylogeny and functional adaptation. *J. Biomech.*, 24(S1):3–16, 1991.

[65] T.N. Gardner, T. Stoll, L. Marks, S. Mishra, and M. Knothe Tate. The influence of mechanical stimulus on the pattern of tissue differentiation in a long bone fracture – an FEM study. *J. Biomech.*, 33:415–425, 2000.

[66] T.N. Gardner, J. Hardy, M. Evans, and J. Kenwright. Temporal changes in dynamic interfragmentary motion and callus formation in fractures. *J. Biomech.*, 30:315–321, 1997.

[67] L.E. Claes and C.A. Heigele. Magnitudes of local stress and strain along bony surfaces predict the course and type of fracture healing. *J. Biomech.*, 32:255–266, 1999.

[68] V.C. Mow, S.C. Kuei, W.M. Lai, and C.G. Armstrong. Biphasic creep and stress relaxation of articular cartilage in compression: theory and experiments. *J. Biomech. Eng.*, 102:73–84, 1980.

[69] M.A. Biot. General theory of three-dimensional consolidation. *J. Appl. Phys*, 12:155–164, 1941.

[70] B.R. Simon. Multiphase poroelastic finite element models for soft tissue structures. *Appl. Mech. Rev.*, 45:191–218, 1992.

[71] J.H. Kuiper, J.B. Richardson, and B.A. Ashton. Mechanical signals in early fracture callus. In J. Vander Sloten, G. Lowet, R. Van Audekercke, and G. Van der Perre, editors, *Proc. 10th Europ. Soc. Biomech.*, page 154, Leuven, 1996.

[72] J.H. Kuiper, J.B. Richardson, and B.A. Ashton. Computer simulation to study the effect of fracture site movement on tissue formation and fracture stiffness restoration. In *Europ. Congress on Comput. Meth. in Appl. Sci. and Eng. (ECCOMAS2000)*, pages 1–6, 2000.

[73] J.M. Kay and R.M. Nedderman. *Fluid mechanics and transfer processes.* Cambridge University Press, 1985.

[74] P.J. Prendergast, R. Huiskes, and K. Søballe. Biophysical stimuli on cells during tissue differentiation at implant interfaces. *J. Biomech.*, 30:539–548, 1997.

[75] P.J. Prendergast and R. Huiskes. Finite element analysis of fibrous tissue morphogenesis – a study of the osteogenic index using a biphasic approach. *Mech. Comp. Mat.*, 32:209–218, 1996.

[76] P.J. Prendergast and M.C.H. van der Meulen. Mechanics of bone regeneration. Chapter 32 in Handbook of Bone Mechanics, Edited by S.C. Cowin.

[77] W.D. van Driel, R. Huiskes, and P.J. Prendergast. A regulatory model for tissue differentiation using poroelastic theory. In Thimus et al., editor, *Poromechanics, A tribute to Maurice A. Biot*, pages 409–413. A.A. Balkema Publishers, 1998.

[78] D. Lacroix and P.J. Prendergast. A homogenization procedure to prevent numerical instabilities in poroelastic tissue differentiation models. In *Eighth Ann. Symp.: Comp. Meth. Orthop. Biomech.*, Orlando, FL., 2000.

[79] J.D. Murray. *Mathematical biology.* Springer-Verlag, 1989.

[80] S.C. Cowin. Bone poroelasticity. *J. Biomech.*, 32:217–238, 1999.

[81] M.B. Schaffler and D.B. Burr. Stiffness of compact bone: effects of porosity and density. *J. Biomech.*, 21:13–16, 1988.

[82] D. Zhang, S. Weinbaum, and S.C. Cowin. Estimates of the peak pressure in bone pore water. *J. Biomech. Eng.*, 120:697–703, 1998.

[83] E.A. Neuman, K.E. Fong, and T.M. Keaveny. Dependence of intertrabecular permeability on flow direction and anatomic site. *Ann. Biomed. Eng.*, 27:517–524, 1999.

[84] M.J. Grimm and J.L. Williams. Measurements of permeability in human calcenal trabecular bone. *J. Biomech.*, 30:746–745, 1997.

[85] J.A. Ochoa and B.M. Hillberry. Permeability of bovine cancellous bone. In *Trans. 38th Orthop. Res. Soc.*, page 162, 1992.

[86] C.G. Armstrong and V.C. Mow. Variations in the intrinsic mechanical properties of human articular cartilage with age, degeneration and water content. *J. Bone Joint Surg.*, 64A:88–94, 1982.

[87] J.S. Jurvelin, M.D. Buschmann, and E.B. Hunziker. Optical and mechanical determination of poisson's ratio of adult bovine humeral articular cartilage. *J. Biomech.*, 30:235–241, 1997.

[88] X. Yuan, L. Ryd, and R. Huiskes. Wear particle diffusion and tissue differentiation in TKA implant fibrous interfaces. *J. Biomech.*, 33:1279–1286, 2000.

[89] R.Y. Hori and J.L. Lewis. Mechanical properties of the fibrous tissue found at the bone-cement interface following total joint replacement. *J. Biomed. Mater. Res.*, 16:911–927, 1982.

[90] C.B. Anderson. Mechanics of fluids. In T. Baumeister, editor, Marks' Saturated Handbook for Mechanical Engineers , pages 3.48–3.76. 1967.

[91] S. Tepic, T. Macirowski, and R.W. Mann. Mechanical properties of articular cartilage elucidated by osmotic loading and ultrasound. *Proc. Natl. Acad. Sci. USA*, 80:3331–3333, 1983.

[92] G.N. Duda, K. Eckert-Hübner, R. Sokiranski, A. Kreutner, R. Miller, and L. Claes. Analysis of inter-fragmentary movement as a function of musculoskeletal loading conditions in sheep. *J. Biomech.*, 21:201–210, 1998.

[93] D. Lacroix, P.J. Prendergast, G. Li, and D. Marsh. The effect of cell origin on tissue differentiation during fracture healing: an investigation using computer simulation (Accepted in J. Eng. in Med.).

[94] E.J. Cheal, K.A. Mansmann, A.M. DiGioia III, W.C. Hayes, and S.M. Perren. Role of interframentary straiin in fracture healing: ovine model of a healing osteotomy. *J. Orthop. Res.*, 9:131–142, 1991.

[95] P.J. Aranzulla, D.S. Muckle, and J.L. Cunningham. A portable monitoring system for measuring weight-bearing during tibial fracture healing. *Med. Eng. Phy.*, 20:543–548, 1998.

[96] F.Y.I. Lee, Y.W. Choi, F.F. Behrens, D.O. DeFouw, and T.A. Einhorn. Programmed removal of chondrocytes during endochondral fracture healing. *J. Orthop. Res.*, 16:144–150, 1998.

[97] J.R. Mosley and L.E. Lanyon. Strain rate as a controlling influence on adaptative modeling in response to dynamic loading of the ulna in growing male rats. *Bone*, 23:313–318, 1998.

[98] C.H. Turner, V. Anne, and R.M.V. Pidaparti. A uniform strain criterion for trabecular bone adaptation: do continuum-level strain gradients drive adaptation? *J. Biomech.*, 30:555–563, 1997.

[99] H.J. Donahue. Gap junctions and biophysical regulation of bone cell differentiation. *Bone*, 26:417–422, 2000.

[100] C.R. Jacobs, C.E. Yellowley, B.R. Davis, Z. Zhou, J.M. Cimbala, and H.J. Donahue. Differential effect of steady versus oscillating flow on bone cells. *J. Biomech.*, 31:969–976, 1998.

[101] L. Wang, S.P. Fritton, S.C. Cowin, and S. Weinbaum. Fluid pressure relaxation depends upon osteonal microstructure: modeling an oscillatory bending experiment. *J. Biomech.*, 32:663–672, 1999.

Appendix A

Model geometry

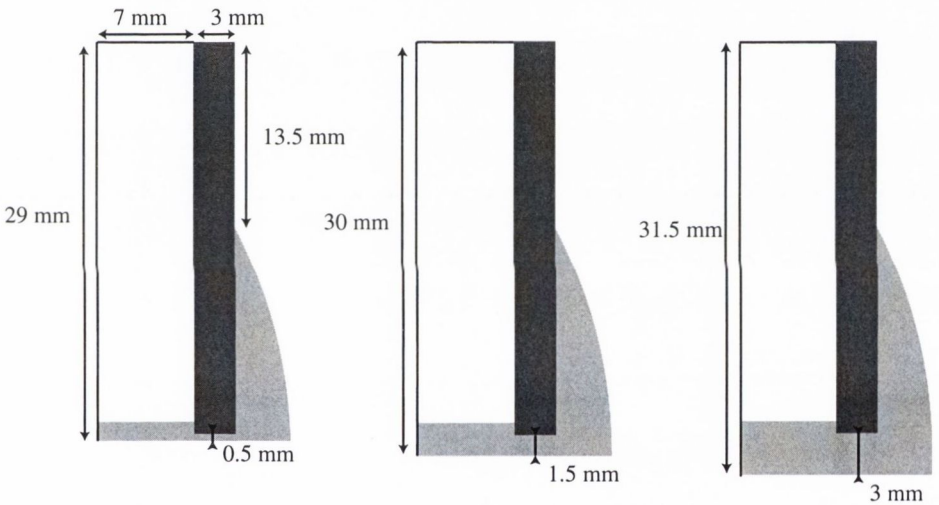

Figure A.1. Dimensions of axisymmetric fracture models.

Appendix B

Fixator geometry

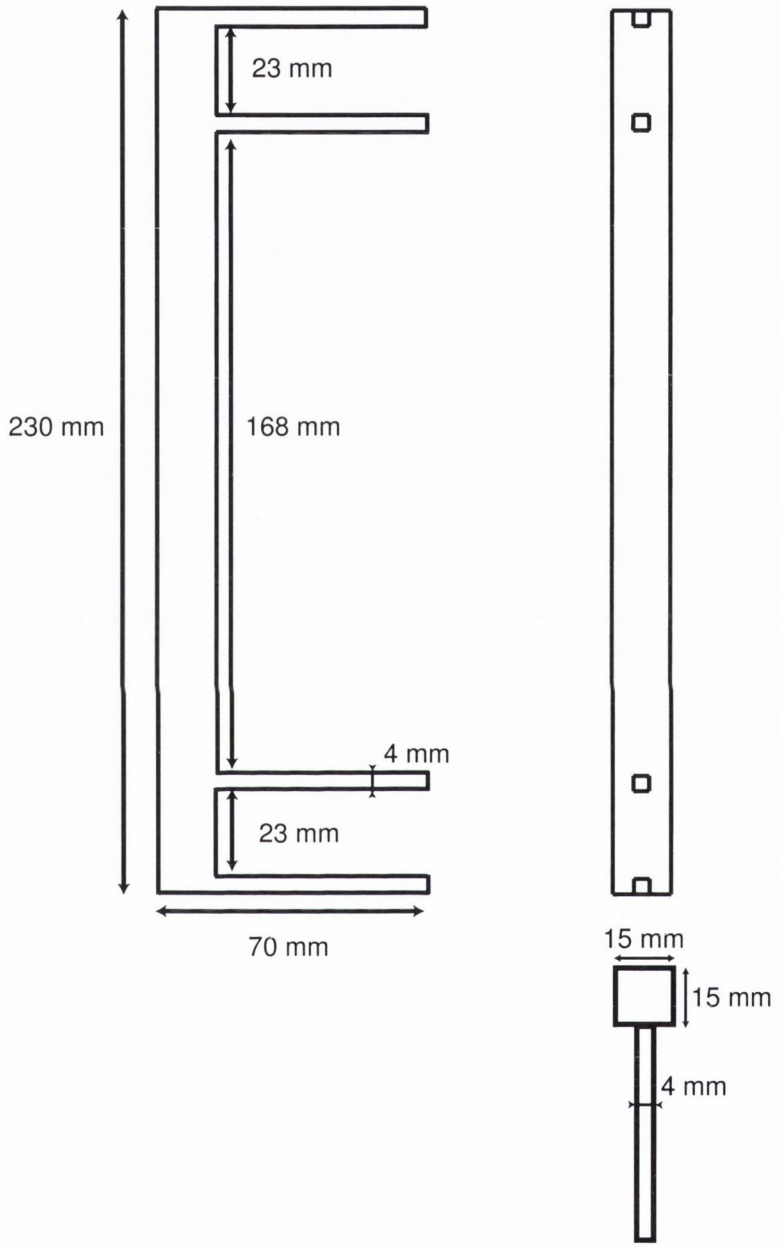

Figure B.1. Dimensions of the external fixator used in this study.

Appendix C

Young's modulus parametric study

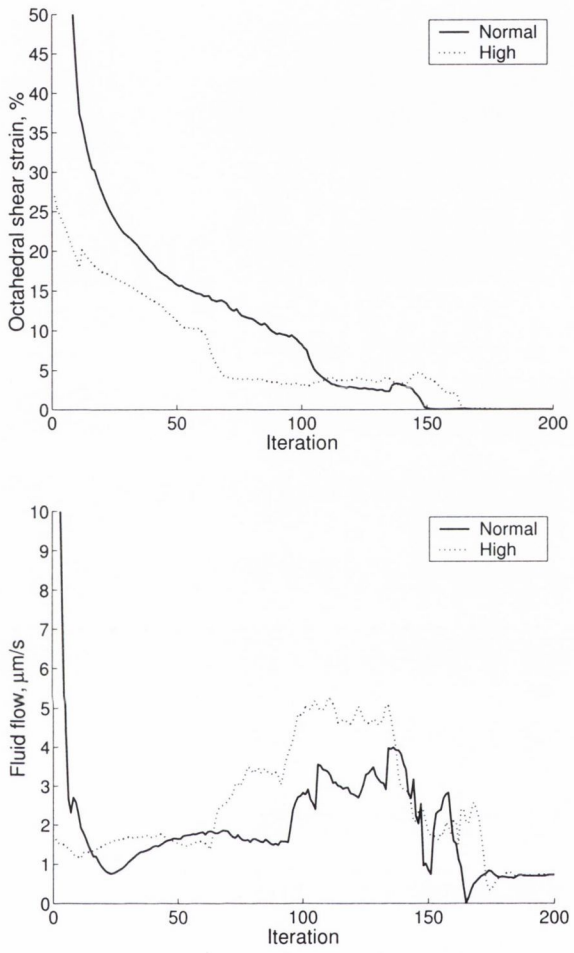

Young's modulus (MPa)	Cortical bone	Marrow	Granulation tissue	Fibrous tissue	Cartilage	Immature bone	Mature bone
Normal	20000	2	0.2	2	10	1000	6000
Low			0.01				
High			1				

Figure C.1. Young's modulus parametric study on granulation tissue. Octahedral shear strain and fluid flow in the interfragmentary gap.

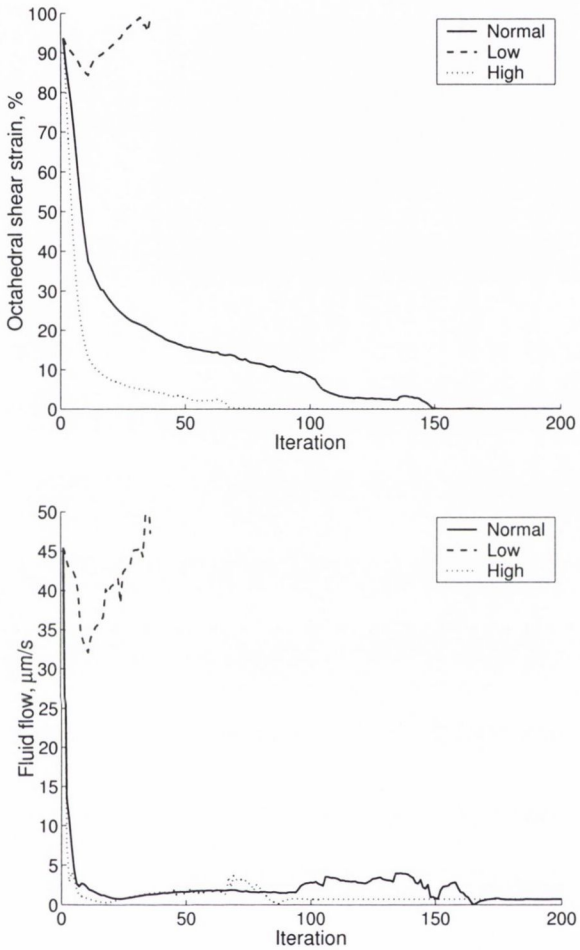

Young's modulus (MPa)	Cortical bone	Marrow	Granulation tissue	Fibrous tissue	Cartilage	Immature bone	Mature bone
Normal	20000	2	0.2	2	10	1000	6000
Low				0.1			
High				10			

Figure C.2. Young's modulus parametric study on fibrous tissue. Octahedral shear strain and fluid flow in the interfragmentary gap.

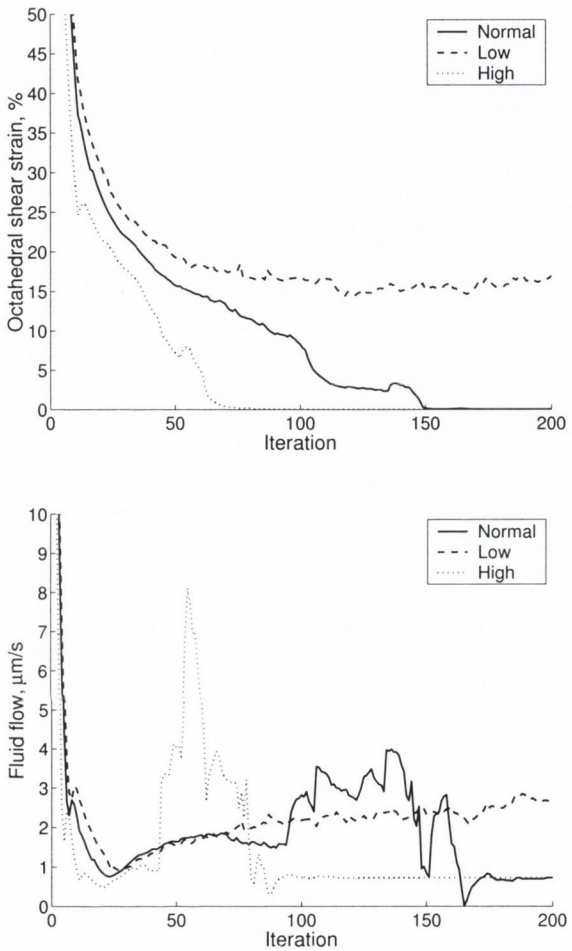

Young's modulus (MPa)	Cortical bone	Marrow	Granulation tissue	Fibrous tissue	Cartilage	Immature bone	Mature bone
Normal	20000	2	0.2	2	10	1000	6000
Low					1		
High					100		

Figure C.3. Young's modulus parametric study on cartilage. Octahedral shear strain and fluid flow in the interfragmentary gap.

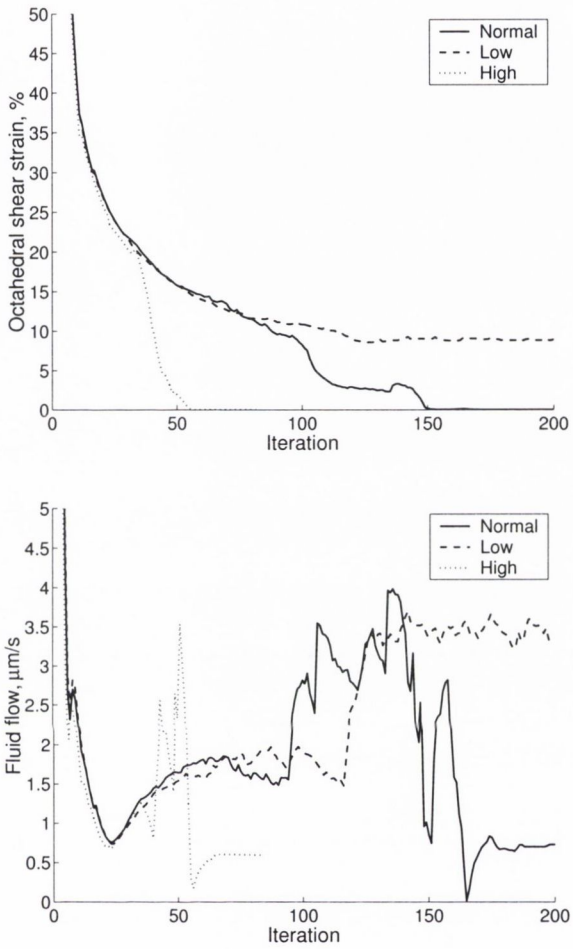

Young's modulus (MPa)	Cortical bone	Marrow	Granulation tissue	Fibrous tissue	Cartilage	Immature bone	Mature bone
Normal	20000	2	0.2	2	10	1000	6000
Low						300	
High						6000	

Figure C.4. Young's modulus parametric study on immature woven bone. Octahedral shear strain and fluid flow in the interfragmentary gap.

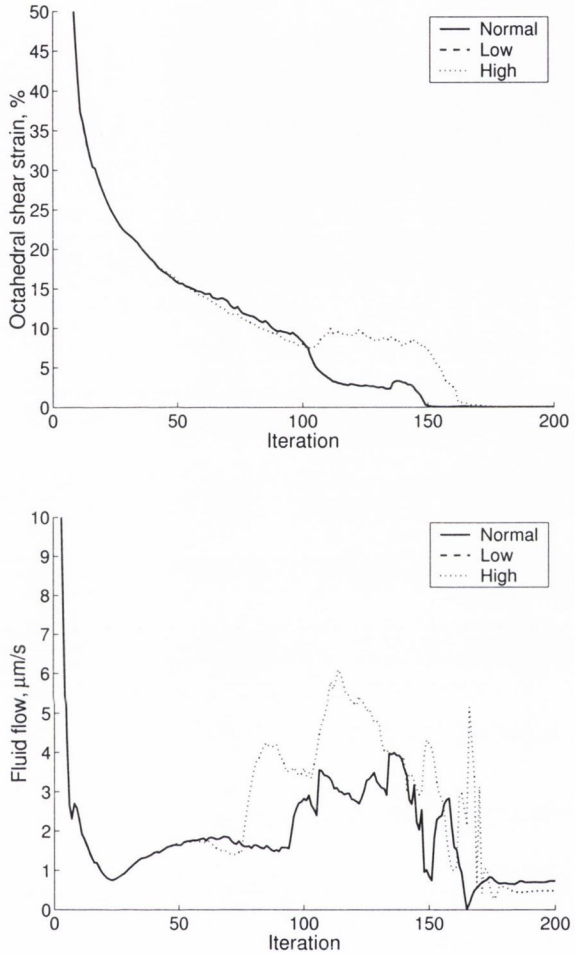

Young's modulus (MPa)	Cortical bone	Marrow	Granulation tissue	Fibrous tissue	Cartilage	Immature bone	Mature bone
Normal	20000	2	0.2	2	10	1000	6000
Low							1000
High							10000

Figure C.5. Young's modulus parametric study on mature woven bone. Octahedral shear strain and fluid flow in the interfragmentary gap.

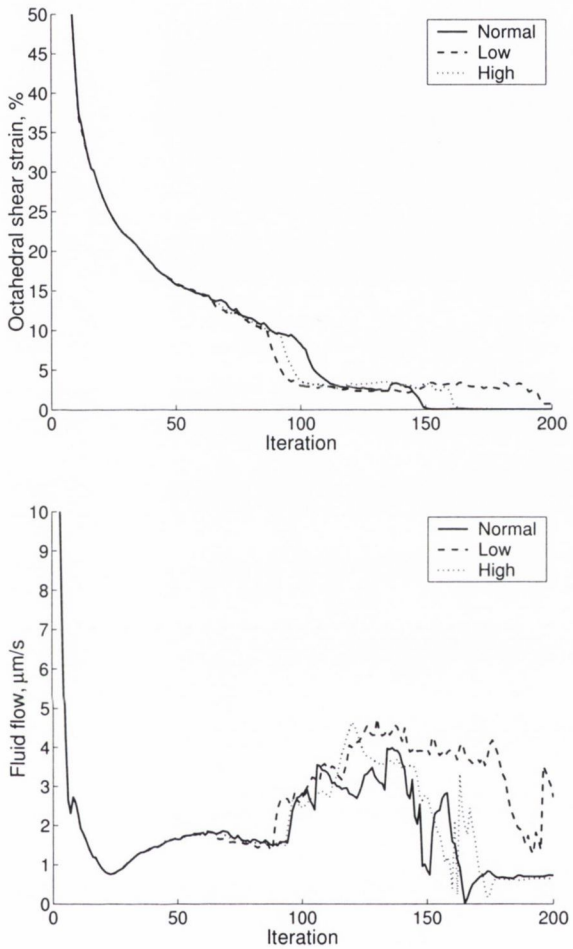

Young's modulus (MPa)	Cortical bone	Marrow	Granulation tissue	Fibrous tissue	Cartilage	Immature bone	Mature bone
Normal	20000	2	0.2	2	10	1000	6000
Low	15000						
High	25000						

Figure C.6. Young's modulus parametric study on cortical bone. Octahedral shear strain and fluid flow in the interfragmentary gap.

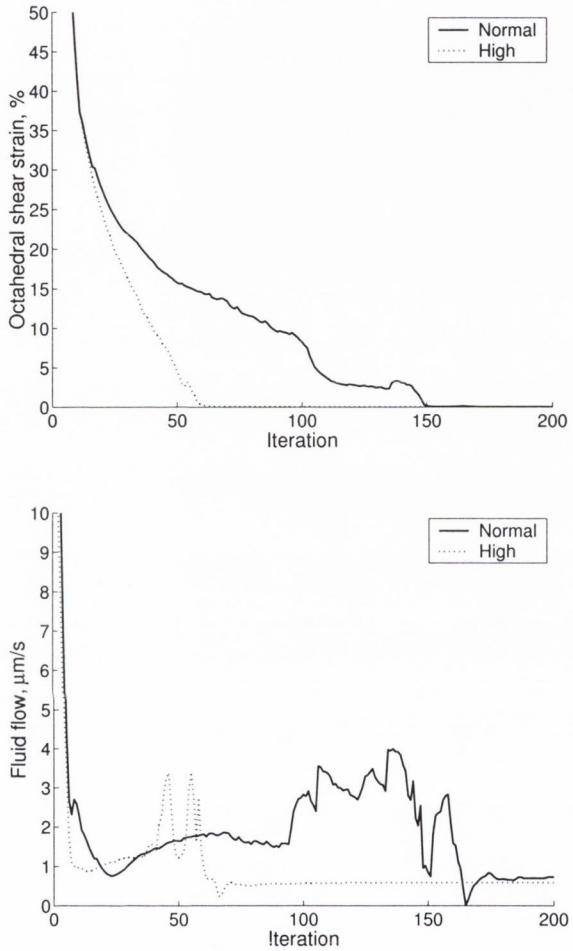

Young's modulus (MPa)	Cortical bone	Marrow	Granulation tissue	Fibrous tissue	Cartilage	Immature bone	Mature bone
Normal	20000	2	0.2	2	10	1000	6000
Low		0.1					
High		10					

Figure C.7. Young's modulus parametric study on bone marrow. Octahedral shear strain and fluid flow in the interfragmentary gap.

Appendix D

Permeability parametric study

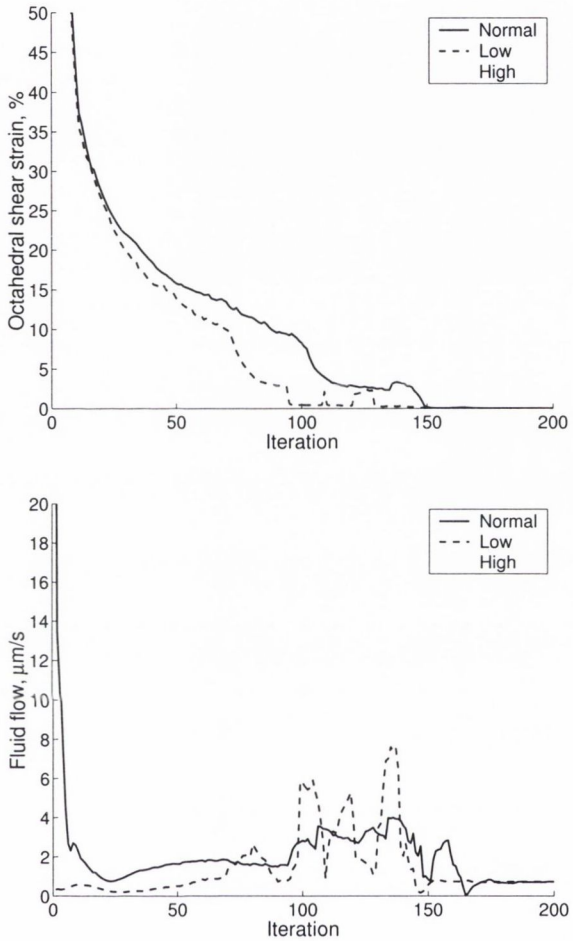

Permeability (m^4/N s)	Cortical bone	Marrow	Granulation tissue	Fibrous tissue	Cartilage	Immature bone	Mature bone
Normal	1E-17	1E-14	1E-14	1E-14	5E-15	1E-13	3.7E-13
Low			1E-16				
High			5E-13				

Figure D.1. Permeability parametric study on granulation tissue. Octahedral shear strain and fluid flow in the interfragmentary gap.

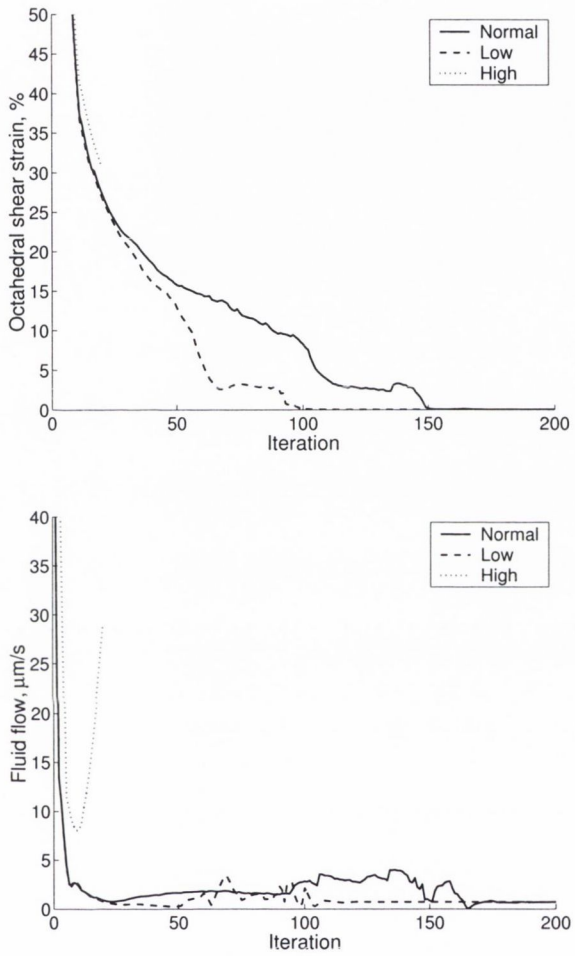

Permeability (m^4/N s)	Cortical bone	Marrow	Granulation tissue	Fibrous tissue	Cartilage	Immature bone	Mature bone
Normal	1E-17	1E-14	1E-14	1E-14	5E-15	1E-13	3.7E-13
Low				1E-16			
High				5E-13			

Figure D.2. Permeability parametric study on fibrous tissue. Octahedral shear strain and fluid flow in the interfragmentary gap.

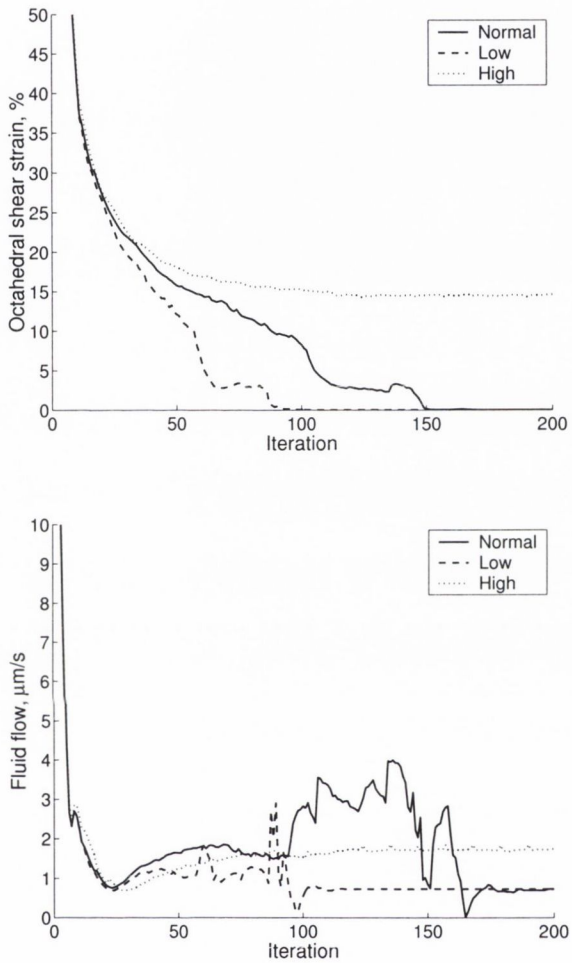

Permeability (m^4/N s)	Cortical bone	Marrow	Granulation tissue	Fibrous tissue	Cartilage	Immature bone	Mature bone
Normal	1E-17	1E-14	1E-14	1E-14	5E-15	1E-13	3.7E-13
Low					1E-16		
High					5E-13		

Figure D.3. Permeability parametric study on cartilage. Octahedral shear strain and fluid flow in the interfragmentary gap.

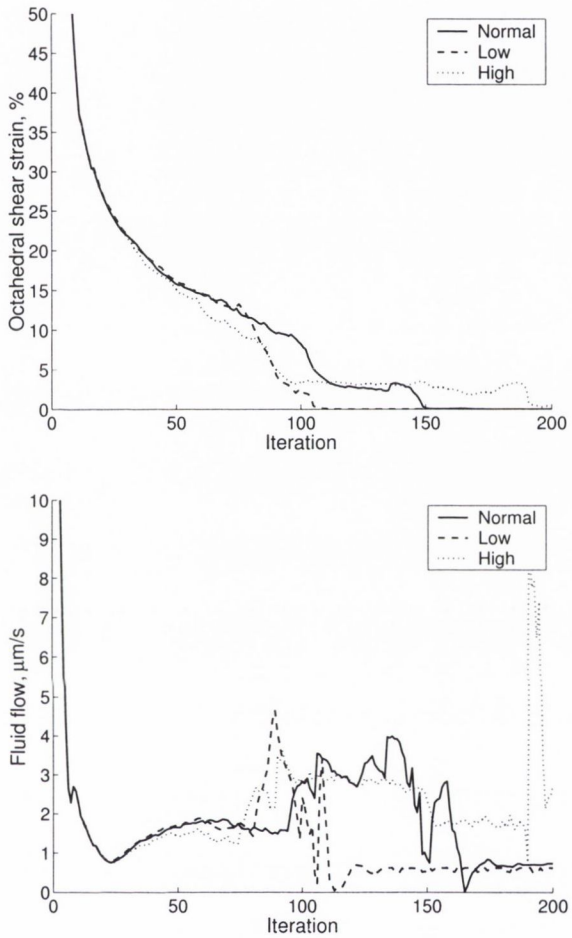

Permeability (m^4/N s)	Cortical bone	Marrow	Granulation tissue	Fibrous tissue	Cartilage	Immature bone	Mature bone
Normal	1E-17	1E-14	1E-14	1E-14	5E-15	1E-13	3.7E-13
Low						1E-14	
High						3.7E-13	

Figure D.4. Permeability parametric study on immature woven bone. Octahedral shear strain and fluid flow in the interfragmentary gap.

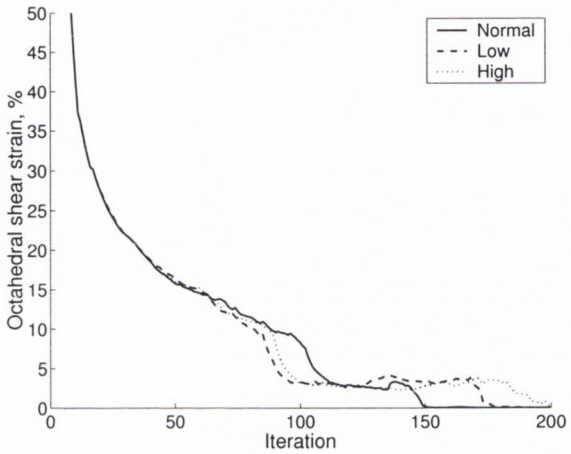

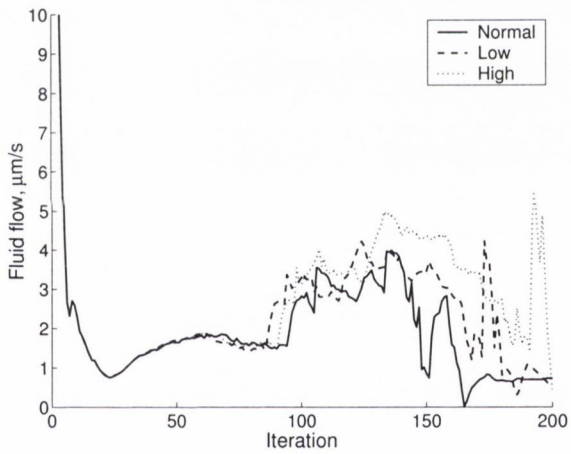

Permeability (m^4/N s)	Cortical bone	Marrow	Granulation tissue	Fibrous tissue	Cartilage	Immature bone	Mature bone
Normal	1E-17	1E-14	1E-14	1E-14	5E-15	1E-13	3.7E-13
Low							1E-14
High							5E-13

Figure D.5. Permeability parametric study on mature woven bone. Octahedral shear strain and fluid flow in the interfragmentary gap.

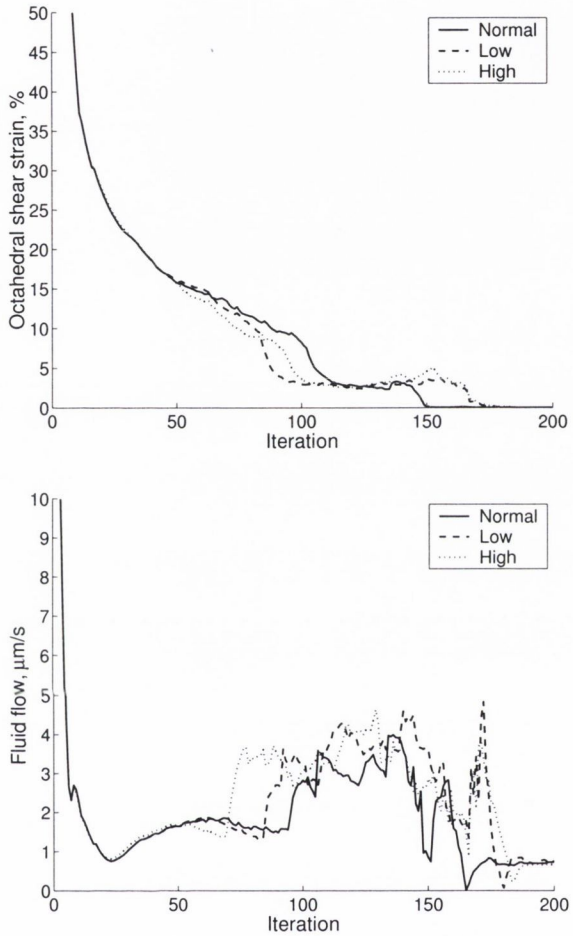

Permeability ($m^4/N\ s$)	Cortical bone	Marrow	Granulation tissue	Fibrous tissue	Cartilage	Immature bone	Mature bone
Normal	1E-17	1E-14	1E-14	1E-14	5E-15	1E-13	3.7E-13
Low	1E-19						
High	1E-15						

Figure D.6. Permeability parametric study on cortical bone. Octahedral shear strain and fluid flow in the interfragmentary gap.

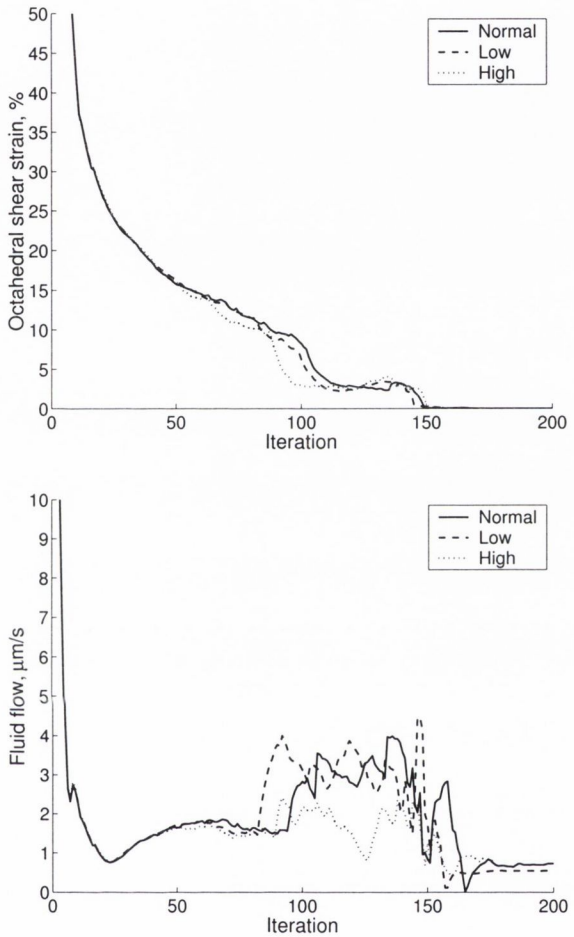

Permeability (m^4/N s)	Cortical bone	Marrow	Granulation tissue	Fibrous tissue	Cartilage	Immature bone	Mature bone
Normal	1E-17	1E-14	1E-14	1E-14	5E-15	1E-13	3.7E-13
Low		1E-16					
High		5E-13					

Figure D.7. Permeability parametric study on bone marrow. Octahedral shear strain and fluid flow in the interfragmentary gap.

Appendix E

Poisson's ratio parametric study

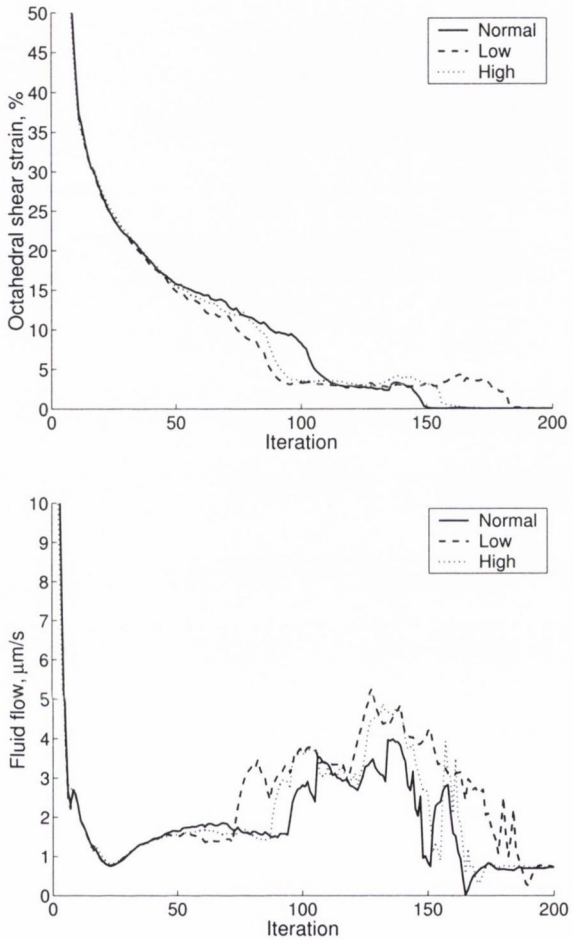

Poisson's ratio	Cortical bone	Marrow	Granulation tissue	Fibrous tissue	Cartilage	Immature bone	Mature bone
Normal	0.3	0.1667	0.1667	0.1667	0.1667	0.3	0.3
Low			0.1				
High			0.3				

Figure E.1. Poisson's ratio parametric study on granulation tissue. Octahedral shear strain and fluid flow in the interfragmentary gap.

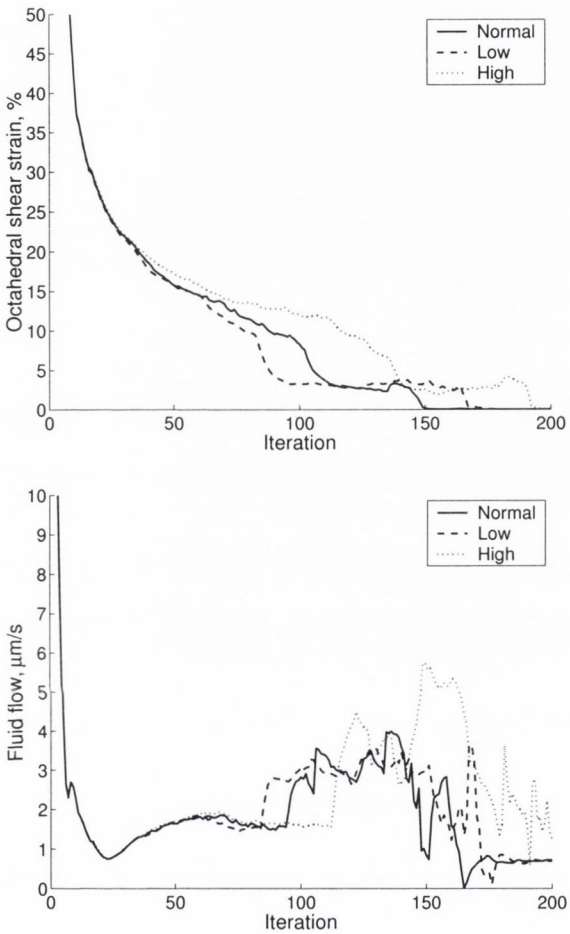

Poisson's ratio	Cortical bone	Marrow	Granulation tissue	Fibrous tissue	Cartilage	Immature bone	Mature bone
Normal	0.3	0.1667	0.1667	0.1667	0.1667	0.3	0.3
Low				0.1			
High				0.3			

Figure E.2. Poisson's ratio parametric study on fibrous tissue. Octahedral shear strain and fluid flow in the interfragmentary gap.

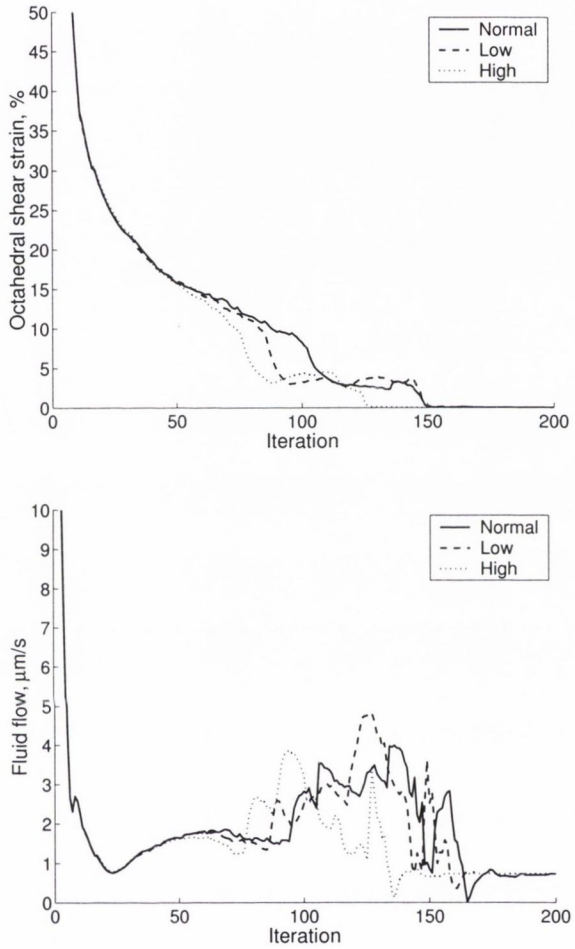

Poisson's ratio	Cortical bone	Marrow	Granulation tissue	Fibrous tissue	Cartilage	Immature bone	Mature bone
Normal	0.3	0.1667	0.1667	0.1667	0.1667	0.3	0.3
Low					0.1		
High					0.3		

Figure E.3. Poisson's ratio parametric study on cartilage. Octahedral shear strain and fluid flow in the interfragmentary gap.

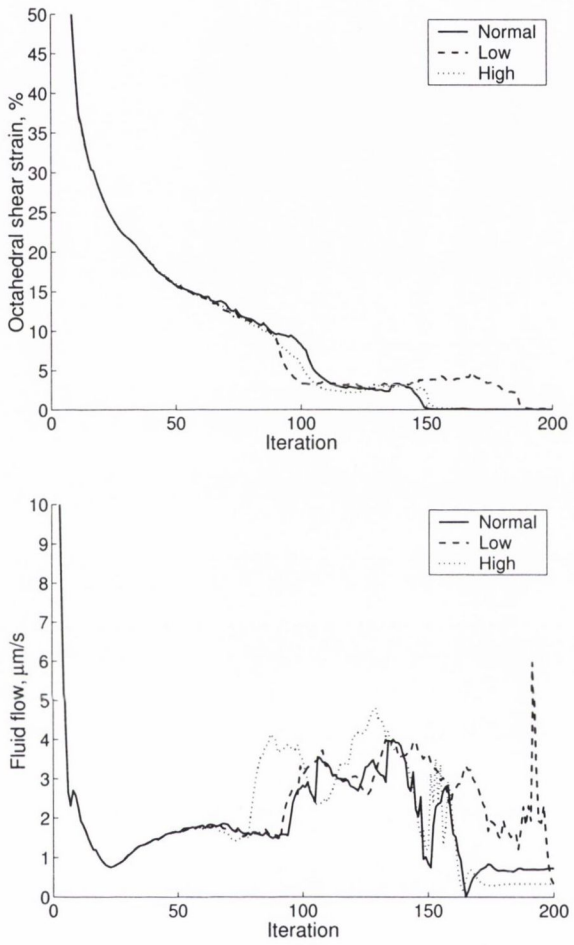

Poisson's ratio	Cortical bone	Marrow	Granulation tissue	Fibrous tissue	Cartilage	Immature bone	Mature bone
Normal	0.3	0.1667	0.1667	0.1667	0.1667	0.3	0.3
Low						0.2	0.2
High						0.35	0.35

Figure E.4. Poisson's ratio parametric study on woven bone. Octahedral shear strain and fluid flow in the interfragmentary gap.

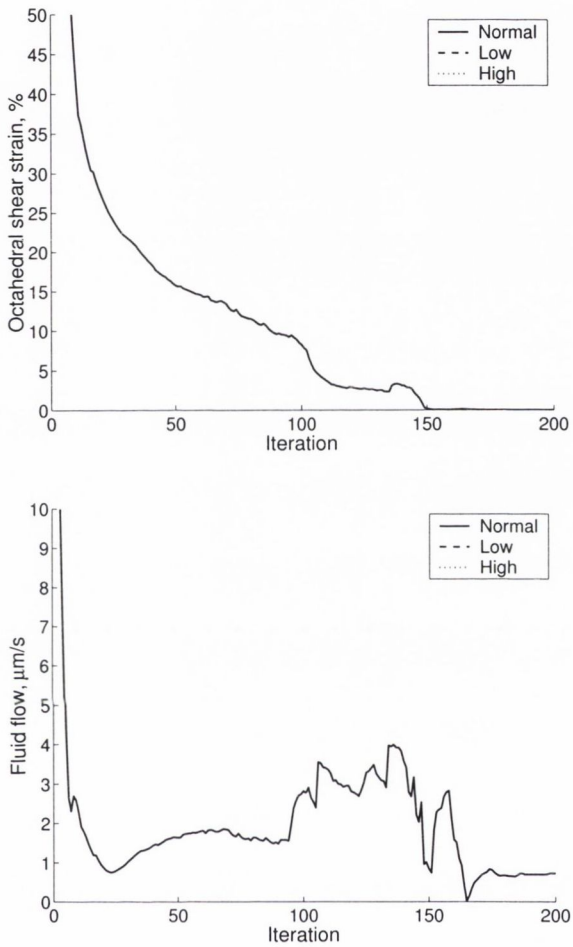

Poisson's ratio	Cortical bone	Marrow	Granulation tissue	Fibrous tissue	Cartilage	Immature bone	Mature bone
Normal	0.3	0.1667	0.1667	0.1667	0.1667	0.3	0.3
Low	0.25						
High	0.35						

Figure E.5. Poisson's ratio parametric study on cortical bone. Octahedral shear strain and fluid flow in the interfragmentary gap.

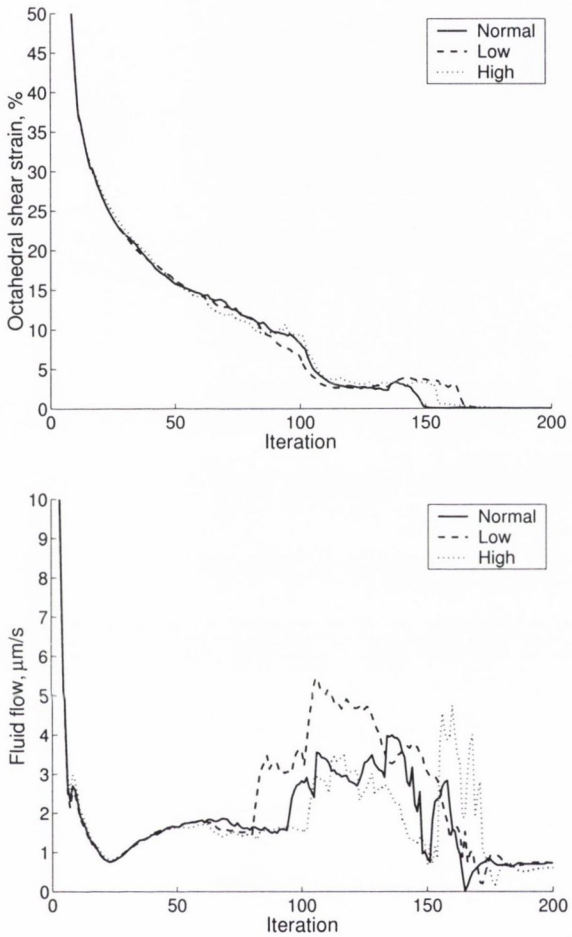

Poisson's ratio	Cortical bone	Marrow	Granulation tissue	Fibrous tissue	Cartilage	Immature bone	Mature bone
Normal	0.3	0.1667	0.1667	0.1667	0.1667	0.3	0.3
Low		0.1					
High		0.3					

Figure E.6. Poisson's ratio parametric study on bone marrow. Octahedral shear strain and fluid flow in the interfragmentary gap.

Appendix F

Porosity parametric study

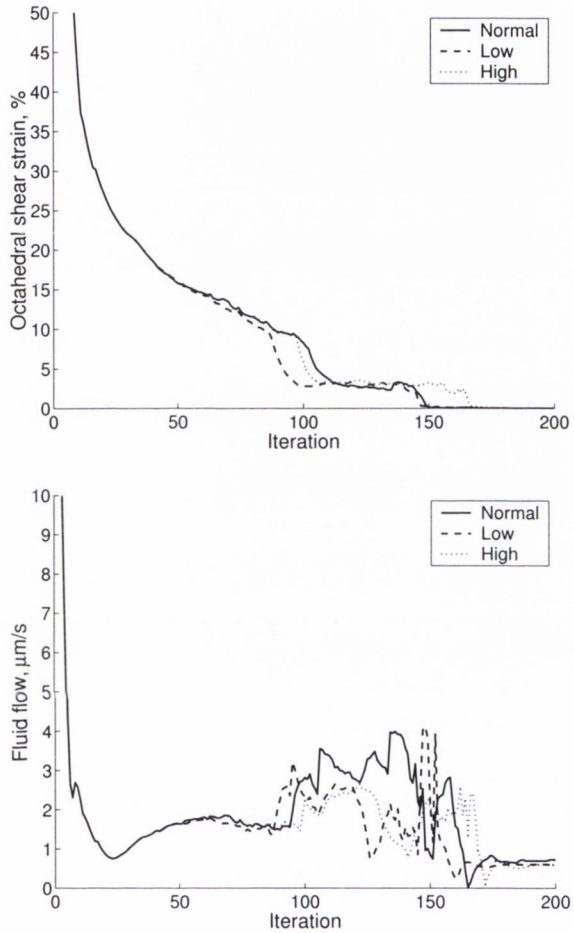

Porosity	Cortical bone	Marrow	Granulation tissue	Fibrous tissue	Cartilage	Immature bone	Mature bone
Normal	0.04	0.8	0.8	0.8	0.8	0.8	0.8
Low			0.4				
High			0.9				

Figure F.1. Porosity parametric study on granulation tissue. Octahedral shear strain and fluid flow in the interfragmentary gap.

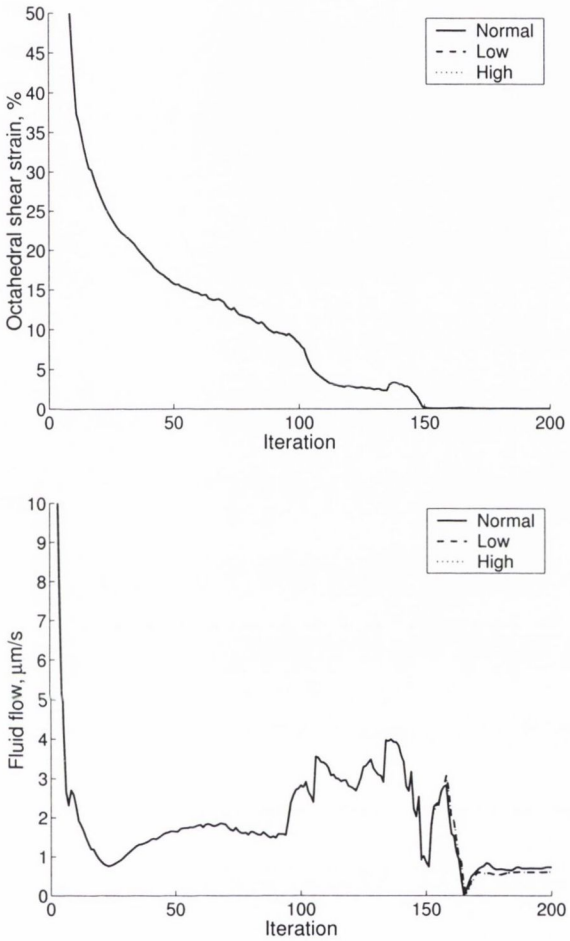

Porosity	Cortical bone	Marrow	Granulation tissue	Fibrous tissue	Cartilage	Immature bone	Mature bone
Normal	0.04	0.8	0.8	0.8	0.8	0.8	0.8
Low				0.4			
High				0.9			

Figure F.2. Porosity parametric study on fibrous tissue. Octahedral shear strain and fluid flow in the interfragmentary gap.

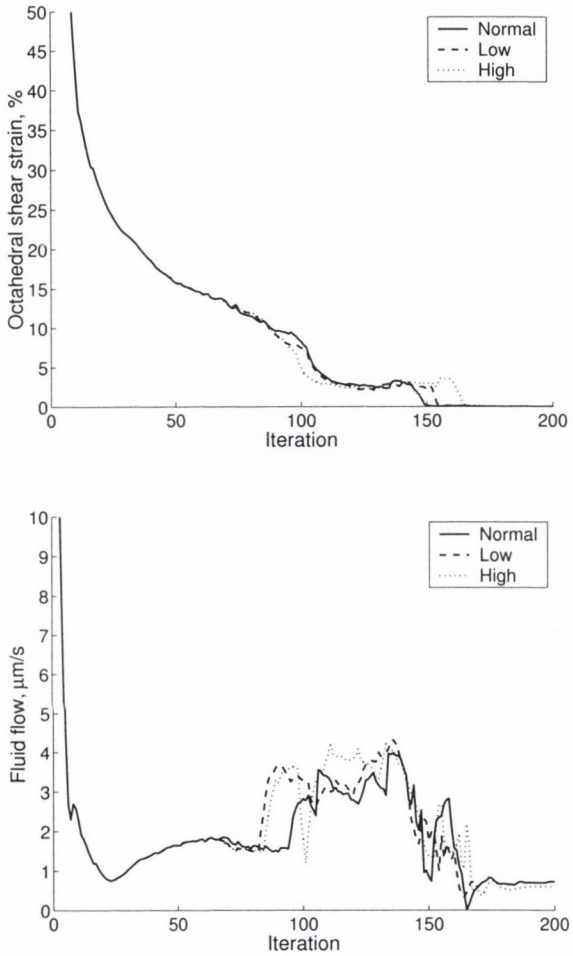

Porosity	Cortical bone	Marrow	Granulation tissue	Fibrous tissue	Cartilage	Immature bone	Mature bone
Normal	0.04	0.8	0.8	0.8	0.8	0.8	0.8
Low					0.4		
High					0.9		

Figure F.3. Porosity parametric study on cartilage. Octahedral shear strain and fluid flow in the interfragmentary gap.

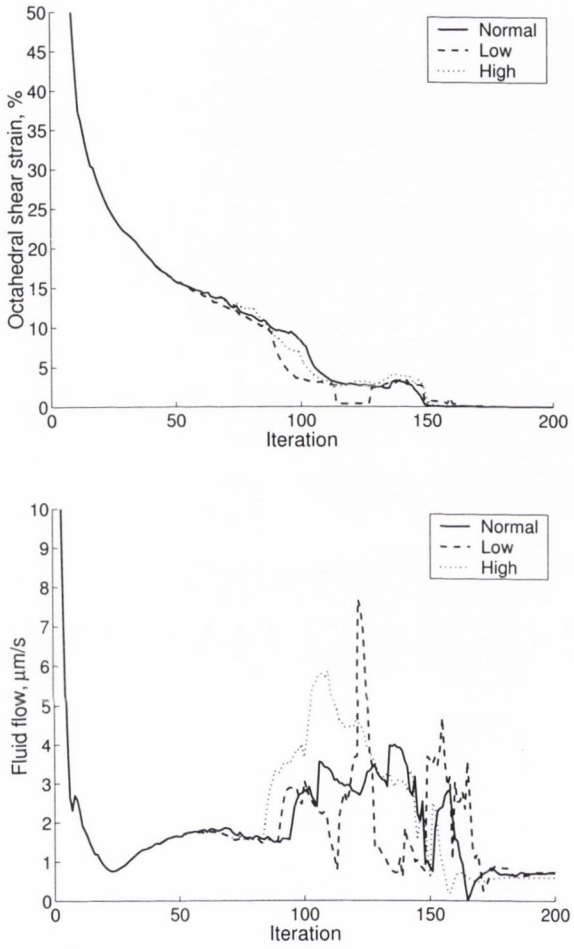

Porosity	Cortical bone	Marrow	Granulation tissue	Fibrous tissue	Cartilage	Immature bone	Mature bone
Normal	0.04	0.8	0.8	0.8	0.8	0.8	0.8
Low						0.4	0.4
High						0.9	0.9

Figure F.4. Porosity parametric study on woven bone. Octahedral shear strain and fluid flow in the interfragmentary gap.

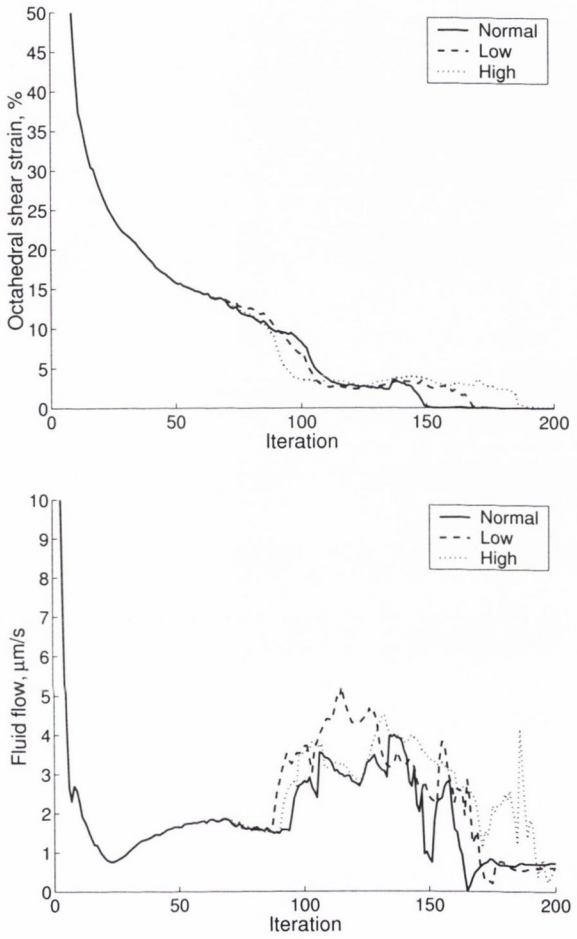

Porosity	Cortical bone	Marrow	Granulation tissue	Fibrous tissue	Cartilage	Immature bone	Mature bone
Normal	0.04	0.8	0.8	0.8	0.8	0.8	0.8
Low	0.01						
High	0.1						

Figure F.5. Porosity parametric study on cortical bone. Octahedral shear strain and fluid flow in the interfragmentary gap.

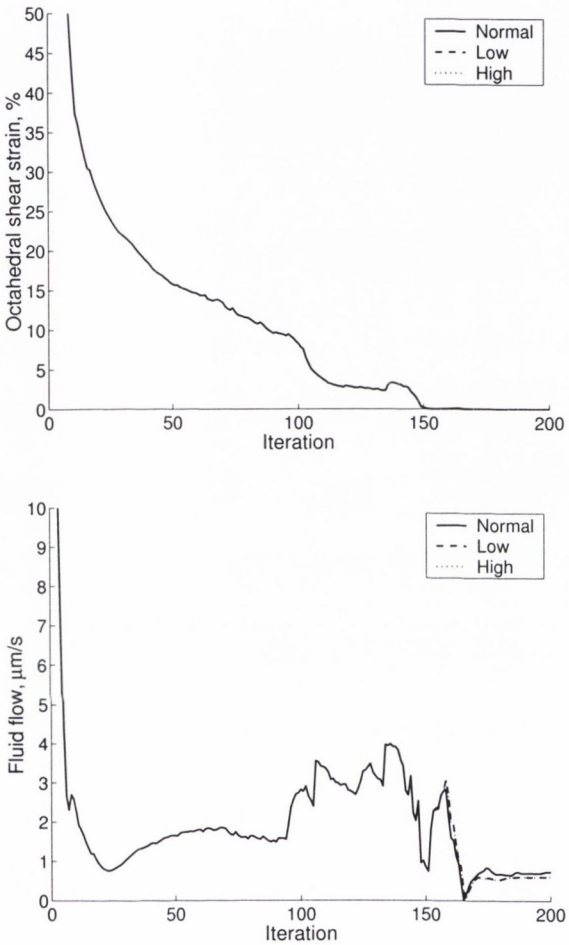

Porosity	Cortical bone	Marrow	Granulation tissue	Fibrous tissue	Cartilage	Immature bone	Mature bone
Normal	0.04	0.8	0.8	0.8	0.8	0.8	0.8
Low		0.4					
High		0.9					

Figure F.6. Porosity parametric study on bone marrow. Octahedral shear strain and fluid flow in the interfragmentary gap.

Appendix G

Solid compression modulus parametric study

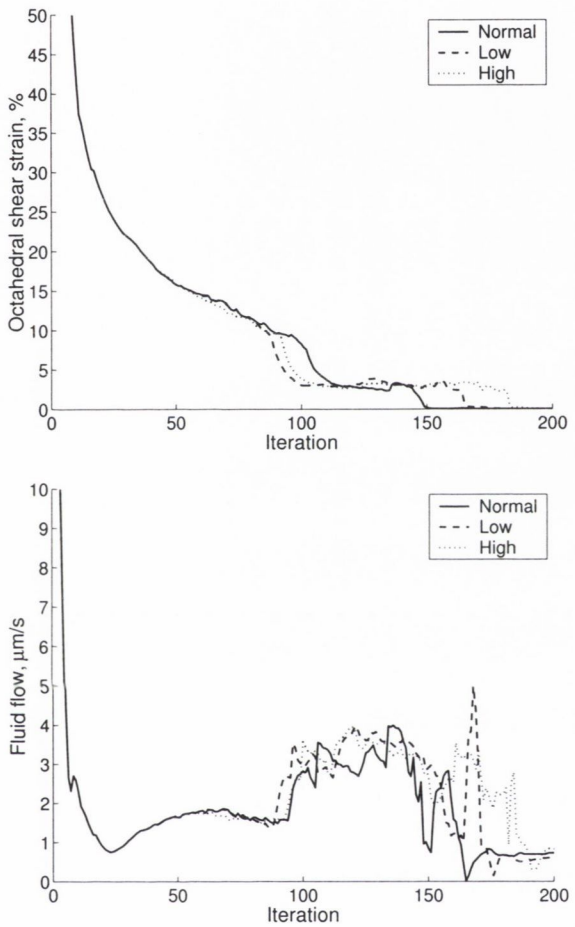

Ks (MPa)	Cortical bone	Marrow	Granulation tissue	Fibrous tissue	Cartilage	Immature bone	Mature bone
Normal	13920	2300	2300	2300	3400	13920	13920
Low	10000					10000	10000
High	15000					15000	15000

Figure G.1. Solid compression modulus parametric study on bone. Octahedral shear strain and fluid flow in the interfragmentary gap.

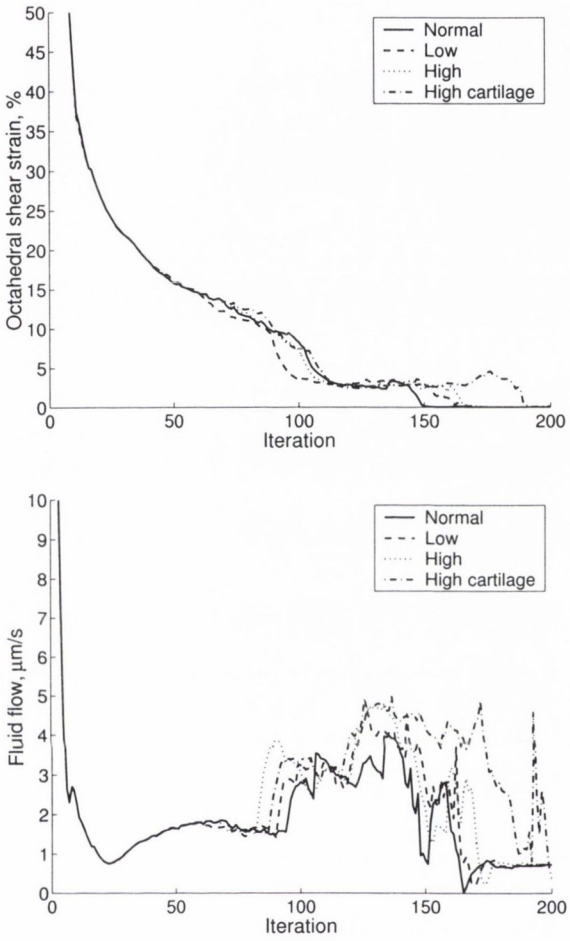

Ks (MPa)	Cortical bone	Marrow	Granulation tissue	Fibrous tissue	Cartilage	Immature bone	Mature bone
Normal	13920	2300	2300	2300	3400	13920	13920
Low		1000	1000	1000	1000		
High		5000	5000	5000	5000		
High cartilage					7000		

Figure G.2. Solid compression modulus parametric study on soft tissues. Octahedral shear strain and fluid flow in the interfragmentary gap.

Appendix H

Fluid compression modulus parametric study

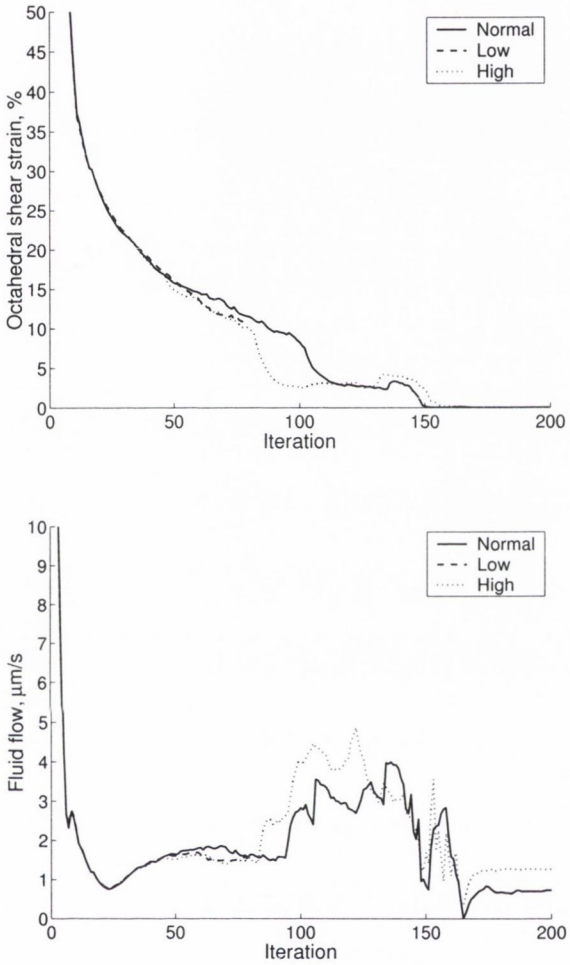

Kf (MPa)	Cortical bone	Marrow	Granulation tissue	Fibrous tissue	Cartilage	Immature bone	Mature bone
Normal	2300	2300	2300	2300	3400	2300	2300
Low	1000	1000	1000	1000	1000	1000	1000
High	5000	5000	5000	5000	5000	5000	5000

Figure H.1. Fluid compression modulus parametric study. Octahedral shear strain and fluid flow in the interfragmentary gap.